

# The Interaction Between Climate Forcing and Feedbacks

Andrew Gettelman<sup>1</sup>, Trude Eidhammer<sup>2</sup>, Margaret L Duffy<sup>3</sup>, Daniel Thompson McCoy<sup>4</sup>,  
Ci Song<sup>4</sup>, and Duncan Watson-Paris<sup>5</sup>

<sup>1</sup>Pacific Northwest National Laboratory

<sup>2</sup>National Center for Atmospheric Research (UCAR)

<sup>3</sup>NCAR

<sup>4</sup>University of Wyoming

<sup>5</sup>University of California, San Diego

January 24, 2024

## Abstract

A Perturbed Parameter Ensemble (PPE) with the Community Atmosphere Model version 6 (CAM6) is used to better understand the sensitivity of simulated clouds to both aerosol forcing and cloud feedbacks and the interactions between them. Aerosol forcing through aerosol-cloud interactions is mostly negative (a cooling) due to shortwave radiation, while feedbacks are positive or negative in different regions due to contrasting longwave and shortwave effects. Both forcing and feedbacks are related to the mean climate state. Higher magnitude cloud radiative effects generally mean larger net forcing and larger net feedback.

Aerosol forcing is broadly related to the susceptibility of clouds to drop number. Feedbacks are less related to susceptibility, and in different regions. Aerosol forcing and cloud feedbacks are anti-correlated in the CAM6 PPE such that stronger negative forcing is associated with stronger positive feedbacks. Even the processes governing forcing and feedback sensitivity in the PPE are similar. These include the warm rain formation process, ice loss processes and deep convective intensity.

# The Interaction Between Climate Forcing and Feedbacks

A. Gettelman<sup>1\*</sup>, T. Eidhammer<sup>2</sup>, M. L. Duffy<sup>2</sup>, D. T. McCoy<sup>3</sup>, C. Song<sup>3</sup>, D.  
Watson-Parris<sup>4</sup>

<sup>1</sup>Pacific Northwest National Laboratory, Richland, WA, USA

<sup>2</sup>NSF National Center for Atmospheric Research, Boulder, CO, USA

<sup>3</sup>Department of Atmospheric Sciences, University of Wyoming, Laramie, WY, USA

<sup>4</sup>University of California San Diego, La Jolla, CA, USA

## Key Points:

- Parametric uncertainty of Aerosol Forcing and Cloud Feedbacks are large
- Aerosol Forcing and Cloud Feedbacks are related through cloud processes and depend on the mean state of clouds
- Warm rain formation and ice processes are critical sensitivities that couple forcing and feedback

---

\*Formerly at NCAR

Corresponding author: Andrew Gettelman, [andrew.gettelman@pnnl.gov](mailto:andrew.gettelman@pnnl.gov)

**Abstract**

A Perturbed Parameter Ensemble (PPE) with the Community Atmosphere Model version 6 (CAM6) is used to better understand the sensitivity of simulated clouds to both aerosol forcing and cloud feedbacks and the interactions between them. Aerosol forcing through aerosol-cloud interactions is mostly negative (a cooling) due to shortwave radiation, while feedbacks are positive or negative in different regions due to contrasting longwave and shortwave effects. Both forcing and feedbacks are related to the mean climate state. Higher magnitude cloud radiative effects generally mean larger net forcing and larger net feedback. Aerosol forcing is broadly related to the susceptibility of clouds to drop number. Feedbacks are less related to susceptibility, and in different regions. Aerosol forcing and cloud feedbacks are anti-correlated in the CAM6 PPE such that stronger negative forcing is associated with stronger positive feedbacks. Even the processes governing forcing and feedback sensitivity in the PPE are similar. These include the warm rain formation process, ice loss processes and deep convective intensity.

**Plain Language Summary**

A climate model is run many times with modified parameters to see how the parameters affect key aspects of climate change. The paper focuses on two aspects of climate change. First, the cloud response to aerosol particles tends to create a cooling, which partially offsets greenhouse gas warming, but the magnitude of the cooling is not well known. It varies a lot in the model when parameters are changed. Second, the paper examines the cloud response to surface temperature increases, called cloud feedbacks, which are the largest uncertainty in estimating the level of future climate change. Cloud feedbacks are also sensitive to parameters. The results show that the cloud feedbacks and aerosol forcing changes are similar but opposite in the model: the cooling and warming generally increase together. This occurs because they are linked to similar parameters, which indicate sensitivity to critical processes, including how rain forms, and how much ice is in the atmosphere.

**1 Introduction**

Uncertainties in predicting the evolution of the Earth’s climate arise from complexity in the response of the system to anthropogenic radiative forcing, and in the actual level of radiative forcing. The largest uncertainty in the fast response of the climate system is due to the response of clouds to changes in the environment: cloud feedbacks (Gettelman & Sherwood, 2016; S. Sherwood et al., 2020). In addition, the largest uncertainty in anthropogenic radiative forcing is the response of clouds to aerosol perturbations (“Summary for Policymakers”, 2021), often termed Aerosol-Cloud Interactions (ACI). These perturbations are significant but complex (Bellouin et al., 2020). More aerosol particles increase cloud drop numbers and lead to brighter clouds (Twomey, 1974) and potentially longer-lived or thicker clouds (Albrecht, 1989). To assess these processes globally, comprehensive Earth System Models (ESMs) with atmospheric components that include a detailed representation of cloud physics, aerosol physics as well as the interactions between them must be used. The scale of these models, typically 100km horizontal, several hundred meter vertical and 10-30 minute time-steps is too coarse to explicitly resolve key cloud and aerosol processes and therefore introduces very large uncertainties in cloud physics representations.

Much has been written about analyzing model and observational analogs for ACI (Bellouin et al., 2020) and cloud feedbacks (S. Sherwood et al., 2020). Many of the processes which control both ACI and cloud feedback responses are the same. For example, extensive decks of bright liquid cloud at the top of the Planetary Boundary Layer (PBL) over the darker ocean significantly cool the planet by reflecting solar radiation

64 back to space. These clouds exist due to an inversion that traps moist ocean air near the  
65 surface. The strength of that inversion has been shown to be important in cloud forma-  
66 tion and maintenance, and how that inversion changes over time is important for how  
67 clouds will respond to climate change: how thick they are and their propensity to rain  
68 (S. C. Sherwood et al., 2014). Similarly, aerosols impact clouds by changing the drop pop-  
69 ulation (more aerosols implies more cloud drops), and how these clouds evolve may also  
70 be determined by the inversion at the top of the boundary layer (Ackerman et al., 2004),  
71 and their propensity to rain.

72 Given the importance of cloud processes at the nexus of forcing and feedback, there  
73 has yet been little work on the interaction between these two effects beyond global means.  
74 Kiehl (2007) noted that in ESMs there was a relationship across models between the total  
75 response to climate change and aerosol forcing. This was updated by Forster et al.  
76 (2013) to show less of an overall relationship. The latest generation of ESMs show no  
77 relationship (Smith et al., 2020), though Watson-Parris & Smith (2022) find a relation-  
78 ship between forcing and feedback when constrained on historical surface temperature.  
79 Gettelman et al. (2016) noted other process level interactions such as an ‘Aerosol Me-  
80 diated Cloud Feedback’ whereby the mechanism for cloud feedbacks occurs by climate  
81 change altering aerosol populations. An example noted by Gettelman et al. (2016) is that  
82 increasing wind speeds over the S. Ocean increase sea spray and cloud drop number, bright-  
83 ening clouds. This negative cloud feedback is mediated by aerosols. This work will seek  
84 to examine the relationship between cloud feedbacks and aerosol forcing of clouds in more  
85 detail by taking advantage of a unique dataset with a modern ESM.

86 Here we will look at the interaction between aerosol forcing and cloud feedbacks  
87 with a large Perturbed Parameter Ensemble (PPE) from the Community Atmosphere  
88 Model version 6 (CAM6). The CAM6-PPE uses parameter perturbations to sample model  
89 structural uncertainty, and produce a wide range of climates resulting from very differ-  
90 ent adjustments to cloud and aerosol processes. Similar PPEs have been used to under-  
91 stand model parametric uncertainty (Qian et al., 2018), constrain aerosol forcing (Re-  
92 gayre et al., 2023; Lee et al., 2016) and low cloud feedbacks (H. Zhang et al., 2018). In  
93 this work, we will use the CAM6-PPE to better understand the interaction between forc-  
94 ing and feedback with the goal of understanding critical process and how they interact.

95 Section 2 describes the data and methods to be used. Section 3 presents detailed  
96 results of forcing sensitivity, feedback sensitivity and their interactions. Discussion is in  
97 Section 4 and conclusions are in Section 5.

## 98 2 Methods

99 The simulations used for this analysis are from the Community Atmosphere Model  
100 version 6 (CAM6) PPE. The CAM6-PPE is described in detail by Eidhammer et al. (2024).  
101 It consists of 263 ensemble members in which latin hypercube sampling is used to mod-  
102 ify 45 parameters in the microphysics, convection, turbulence and aerosol schemes. Note  
103 that one of the simulations did not complete, and that two pairs of parameters are var-  
104 ied together, so effectively 43 parameters are varied. These atmospheric parameters are  
105 typically the most uncertain in many climate models and contain many variables which  
106 alter cloud and aerosol processes. Parameter ranges are chosen to be physically plausi-  
107 ble for each parameter. We also will subset the parameter space based on physically real-  
108 istic climates as described below. Simulations are run with an atmosphere-land con-  
109 figuration for 3 years, for Present Day (PD) climatological boundary conditions, repeat-  
110 ing climatological averaged Sea Surface Temperatures (SSTs) each year. In addition, two  
111 other additional sets of 263 simulations are run with the same parameters. In one set,  
112 SSTs are uniformly increased by 4K to assess the cloud response to warming, following  
113 Cess et al. (1989), termed SST4K. In the other set of 263 simulations, PD SSTs and the

114 same boundary conditions are used, except aerosol emissions are set to 1850 ‘Pre-Industrial’  
 115 levels (hereafter PI simulations).

116 The principle we will exploit is that different parameters modify different specific  
 117 processes in the cloud physics (e.g., frequency or intensity of deep convection, rain for-  
 118 mation processes, freezing and ice nucleation processes, etc). The changing balance of  
 119 processes alters the climate. First, we will use the PPE to understand if forcing and feed-  
 120 backs depend on the base climate state of those simulations. Then we will use the PPE  
 121 to understand which parameters give rise to variations and sensitivity in forcing and feed-  
 122 backs. Finally we will explore the relationship between aerosol forcing and cloud feed-  
 123 backs. The parameters map to the underlying physical mechanisms. While the param-  
 124 eters in the PPE are model specific, the process representations are very similar to (or  
 125 even the same as) other modern ESMs. Thus the results may have more general applica-  
 126 tion since the relationships we elucidate are well founded in processes, not just in pa-  
 127 rameters.

128 As described by Gettelman et al. (2019), the aerosol induced cloud forcing (ACI,  
 129 or just ‘forcing’) is defined as the change in Cloud Radiative Effect (CRE) between sim-  
 130 ulations with Present Day (PD) and Pre-Industrial (PI) aerosol emissions. Typically we  
 131 are concerned with the Shortwave (SW) cloud forcing (SW ACI =  $\Delta\text{SWCRE}$ ), but there  
 132 is also Longwave (LW) forcing (LW ACI =  $\Delta\text{LWCRE}$ ). Cloud feedbacks are defined as  
 133 the kernel adjusted cloud feedbacks (Soden et al., 2008) using the kernels from Zelinka  
 134 et al. (2012) as applied by Duffy et al (2023). The kernels adjust LW and SW CRE to  
 135 remove effects of changes to the atmospheric temperature and water vapor, and the ef-  
 136 fect of a changing surface albedo.

137 To constrain the simulations for fidelity against observations we also compare them  
 138 to observations of radiative fluxes and clouds from the CERES (Clouds and the Earth’s  
 139 Radiant Energy System) satellite Energy Balanced and Filled (EBAF) products (Loeb  
 140 et al., 2018).

141 Finally, for analysis of the simulations and sensitivity to parameters (and hence pro-  
 142 cesses), we use Gaussian process emulators (Watson-Parris et al., 2021) trained on the  
 143 PPE ensemble to determine the sensitivity of forcing and feedbacks to each parameter.

### 144 **3 Results**

145 First we illustrate the parametric uncertainty (i.e. the PPE spread) of feedbacks  
 146 and forcing (Section 3.1). Then we examine how aerosol forcing is related to the mean  
 147 state and to different parameters, which are both indicative of specific processes (Sec-  
 148 tion 3.2). Next we will do the same analysis for cloud feedbacks (Section 3.3) and then  
 149 we will explore the interaction between aerosol forcing and cloud feedbacks (Section 3.4)

#### 150 **3.1 PPE Mean and Spread**

151 Figure 1 illustrates the global mean change in SW (Figure 1A), LW (Figure 1B)  
 152 net TOA radiation (Figure 1C) and change in total cloud fraction (Figure 1D) for the  
 153 263 PPE members. The forcing in Figure 1A and B is the change in CRE, while the feed-  
 154 backs are the kernel-adjusted feedbacks. The spread estimates the parametric uncertainty  
 155 in forcing and feedback.

156 The spread in net ACI forcing is only  $\sim 2\text{Wm}^{-2}$ , because the global mean SW and  
 157 LW are of opposite sign and are strongly anti-correlated, resulting in a fairly narrow range  
 158 in total net TOA change (Figure 1C). The anti-correlation is not as strong for cloud feed-  
 159 backs where the SW and LW components are both positive in most ensemble members.  
 160 Note that the TOA change for feedbacks includes a significant change NOT associated  
 161 with clouds, but rather for the clear sky (due to a warmer surface). There is also far less

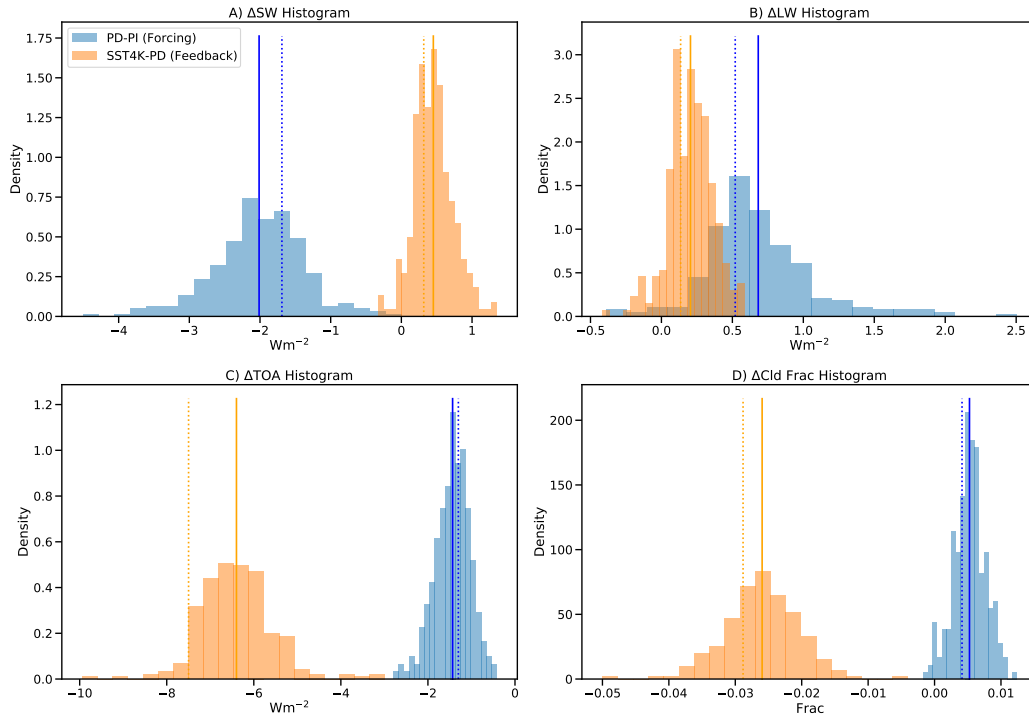


**Figure 1.** Histograms of global A) TOA SW change, B) TOA LW change, C) Net TOA change and D) Cloud Fraction change for Present Day - Pre-Industrial (Aerosol Forcing, Blue) and SST+4K - Present Day (Feedback response, orange). Forcing is change in TOA Cloud Radiative Effect (CRE) and feedbacks are the kernel adjusted cloud feedbacks as described in the text. Solid lines are the mean of the distribution, dotted lines are results with the default CAM6 parameter settings.

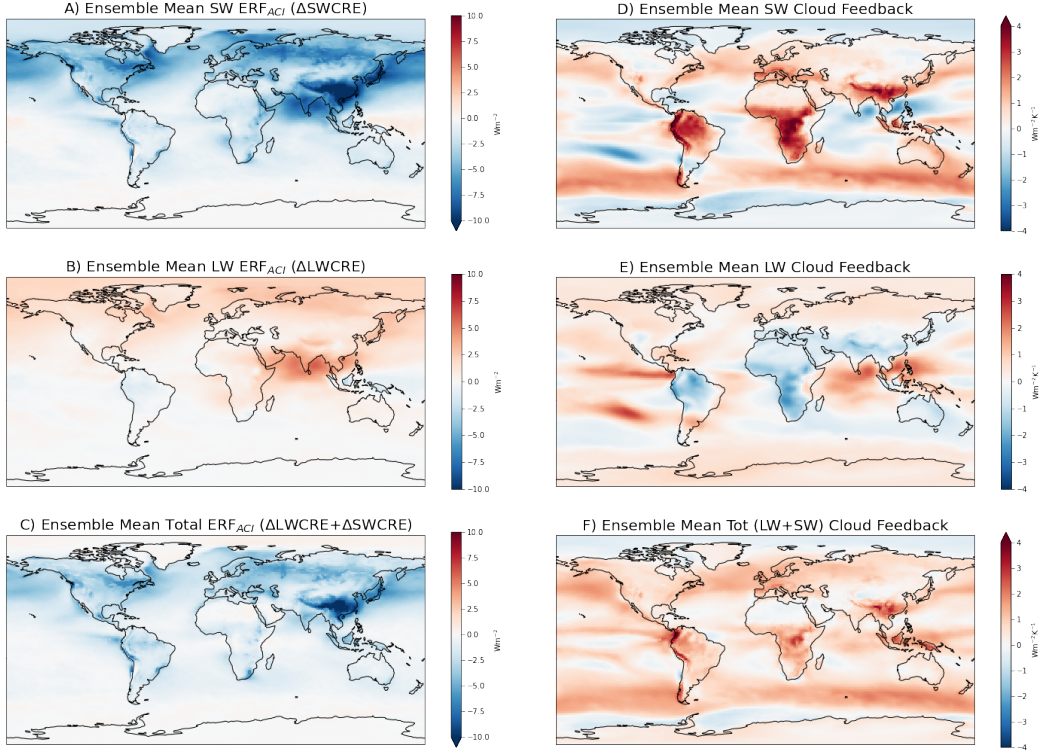


**Figure 2.** PPE ensemble means of Aerosol Cloud Interactions (Forcing) for the A) SW, B) LW and C) Total (LW+SW) as well as Cloud Feedbacks for the D) SW, E) LW and F) Total (LW+SW).

162 cloud fraction change (Figure 1D), both the mean and PPE spread, for aerosol forcing  
 163 than for cloud feedbacks.

164 Figure 2 illustrates the ensemble mean cloud forcing (ACI) as the change in CRE  
 165 between present (PD) and pre-industrial (PI) simulations for the SW (Figure 2A), LW  
 166 (Figure 2B) and Net (Figure 2C). Figure 1A and B indicate that for both forcing and  
 167 feedback, the ensemble mean (solid vertical lines in Figure 1) is similar to the default  
 168 (dotted vertical lines in Figure 1). We have verified that this is qualitatively the case for  
 169 maps as well by mapping the default case individually: the ensemble mean just provides  
 170 better statistics to smooth out noise in the short 3 year simulations. ACI is strongest  
 171 in the SW, concentrated in the N. Hemisphere, with the largest values over oceans down-  
 172 wind of source regions (N. Pacific, N. Atlantic and N. Indian Ocean), and a strong SW  
 173 signal over China. SW is larger than LW, with the largest LW effect near India, due per-  
 174 haps to aerosol effects on tropical ice clouds, which mostly cancel the SW effects. There  
 175 is virtually no aerosol forcing in the S. Hemisphere. SW and LW are of opposite sign  
 176 in most regions, but there is not a 1:1 correlation in the magnitude. Net ACI becomes weakly  
 177 positive over the Arctic ocean due to lack of SW cooling from clouds over a bright ice-  
 178 covered surface.

179 Figure 2 also illustrates the ensemble mean cloud feedbacks for the SW (Figure 2D),  
 180 LW (Figure 2E) and total (Figure 2F). As with forcing, the ensemble mean is qualita-  
 181 tively similar to the default case. There are significant positive (and net) SW Cloud Feed-  
 182 backs over tropical continents in convective regions, as well as in the mid-latitude storm

183 tracks in both hemispheres. In the tropical convecting regions, the two mechanisms con-  
 184 trolling cloud feedbacks are the increase in altitude of high clouds and a reduction in anvil  
 185 cloud area (S. Sherwood et al., 2020). The increase in the altitude of high clouds is a pos-  
 186 itive LW cloud feedback (the red area over the tropical west Pacific/Indian ocean). The  
 187 reduction in anvil cloud area should have competing LW positive and SW negative ef-  
 188 fects as illustrated in Figure 2D and Figure 2E. The net cloud feedbacks are positive,  
 189 except over polar regions with frequent sea-ice coverage.

### 190 3.2 Forcing

191 We start by focusing on the aerosol forcing, again defining ACI as the change in  
 192 CRE between PD and PI simulations (either LW, SW or Net=SW+LW). First we at-  
 193 tempt to understand whether ACI is related to properties of the mean state climate. Aerosol  
 194 forcing is a series of processes that might be reflected in correlations between the forc-  
 195 ing and the mean state. Increases in emissions increase aerosols (largely sulfate) which  
 196 increase the Cloud Condensation Nuclei (CCN) and Ice Nuclei (IN), and hence cloud drop  
 197 and ice crystal number. This might affect cloud fraction and/or cloud mass (Ice Water  
 198 Path [IWP] and Liquid Water Path [LWP]). The mean state might make the clouds more  
 199 or less ‘susceptible’ to these changes. For example: higher base state sulfur and higher  
 200 CCN and/or drop number for PI conditions might make a perturbation to sulfur less im-  
 201 portant. Or having more clouds (either larger negative SW CRE or higher cloud frac-  
 202 tion) might result in more ‘marginal’ clouds that could be affected by ACI.

203 We focus on the mean state climate of the PI simulations. In the present day, some  
 204 of the correlation between mean state and aerosols is due to anthropogenic aerosol forc-  
 205 ing, and we are interested in the ‘unaffected’ state. We start with correlations of global  
 206 mean state properties with global mean ACI. Figure 3 illustrates that the magnitude of  
 207 globally averaged Net ACI is correlated with several properties of the mean state: To-  
 208 tal Cloud Fraction (Figure 3A), Sulfate ( $\text{SO}_4$ ) Burden (Figure 3B), CCN at 0.2% super-  
 209 saturation (Figure 3C) and Cloud Top Drop Number ( $N_c$ , Figure 3D). We looked at sev-  
 210 eral PI mean state properties not strongly correlated with global mean forcing: LWP and  
 211 IWP. Column drop number is similar to cloud top drop number (Figure 3D).

212 The orange points are the sub-set of simulations whose mean annual value of SW  
 213 CRE is within  $\pm 5 \text{ Wm}^{-2}$  of the observed CERES EBAF annual global mean ( $-45.3 \text{ Wm}^{-2}$ ).  
 214 This constraint is a gross measure of whether the ‘climate’ in any simulation (specifically  
 215 the cloud climatology) is similar to present day observations. The slopes (orange lines)  
 216 are qualitatively similar (with lower correlation) if we consider only the constrained data  
 217 rather than all the data for most of the variables except cloud coverage. The red dot is  
 218 the ‘default’ parameter set for CAM6.

219 Figure 3A indicates that as total mean state cloud fraction increases, net ACI in-  
 220 creases in magnitude (negative). This implies more cloudiness may mean more marginal  
 221 or thin clouds that are more susceptible to changes. As mean PI sulfate burden increases,  
 222 net ACI forcing is reduced (lower magnitude) (Figure 3B) with a similar relationship for  
 223 CCN (Figure 3C). These both indicate that PI environments with higher sulfur and more  
 224 CCN are less sensitive to additional sulfur, a result noted in other models (Carslaw et  
 225 al., 2013). There is also a relationship between cloud top drop number and Net ACI forc-  
 226 ing (Figure 3D) whereby higher PI drop numbers give rise to larger forcing, which seems  
 227 to work in the opposite way to more PI CCN. In general, these correlations using global  
 228 means are quite low. SW ACI only correlations are a little stronger (not shown). The  
 229 CERES constrained simulations have similar correlations to all simulations, with lower  
 230 magnitude (except for total cloud coverage, where constrained simulations have a smaller  
 231 correlation of the opposite sign).

232 To understand these relationships better, we can map the correlations at each point  
 233 to determine what regimes are important. Figure 4 illustrates the same relationships as



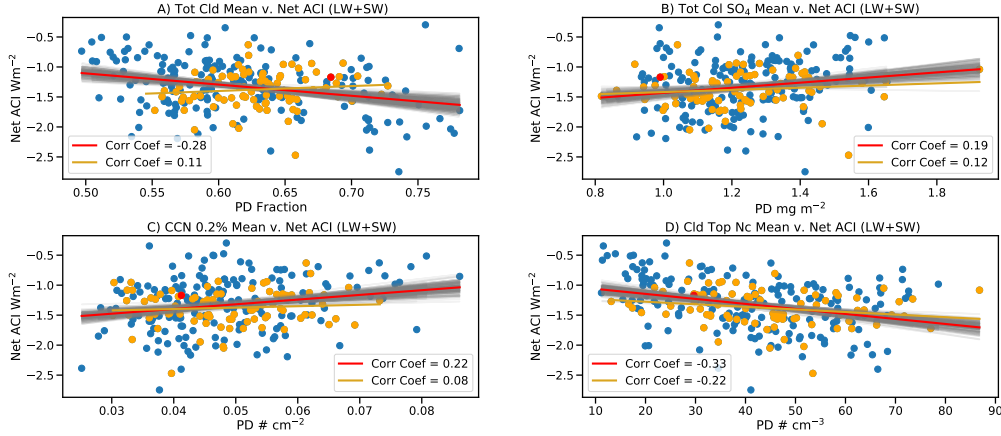


**Figure 3.** Global correlations between mean state for A) Total Cloud Fraction, B) Total Column Sulfate, C) CCN at 0.2% supersaturation and D) Cloud top drop number with Pre-Industrial aerosols (horizontal axis and the Net ACI forcing (PD-PI, vertical axis). Blue points: all simulations, red line, linear regression. Orange indicates those 87 simulations whose global mean PD Shortwave Cloud Radiative Effect is within  $\pm 5 \text{ Wm}^{-2}$  of the CERES EBAF global annual mean. Orange line is the linear regression of these points. Default CAM6 parameters shown as the red dot.

234 Figure 3 using PI mean climate and aerosol net forcing (PD - PI change in SW+LW CRE)  
 235 but now as a map at each point. An expanded set of mean state indicators are illustrated.  
 236 The linear correlation coefficient at each point is plotted, with the stippling indicating  
 237 regions which are NOT significant based on a bootstrap fit. Maps are similar if only the  
 238 simulations constrained by the observed satellite SW CRE climatology are used, but with  
 239 less significance (similar to Figure 3). We have examined the LW and SW components  
 240 separately, and in general net ACI forcing is dominated by the SW as seen in Figure 2.

241 The weak global correlations in Figure 3 belie stronger regional correlations, which  
 242 can be of different sign between regions and hence cloud types. In many cases there are  
 243 opposite sign correlations over the Arctic ocean where the SW ACI goes to zero (Fig-  
 244 ure 2A) and the positive LW ACI component dominates (Figure 2C). The opposite sign  
 245 correlation is due to the local ACI being dominated by the LW and changing sign. There  
 246 is a strong positive correlation between the net ACI forcing (net ACI =  $\Delta \text{SWCRE} +$   
 247  $\Delta \text{LWCRE}$ ) and the PI SW Cloud Radiative Effect (SW CRE, Figure 4G) at low lati-  
 248 tudes over the ocean. Stronger negative PI mean state SW CRE in the subtropics is as-  
 249 sociated with stronger negative ACI. Similar patterns of opposite sign (since SW CRE  
 250 is negative) are seen for total cloud coverage (Figure 4A), LWP (Figure 4B), LW CRE  
 251 (Figure 4F), cloud top liquid number (Figure 4I) and column drop number (Figure 4J).  
 252 Column drop number is integrated to the top of the atmosphere. CCN effects (fewer CCN  
 253 in PI result in stronger magnitude ACI) are mostly positive throughout the N. Hemi-  
 254 sphere. (Figure 4E). Stronger positive ACI at high latitudes (dominated by the LW) is  
 255 associated with more ice fraction at high latitudes (Figure 4H).

256 Figure 3 indicates that stronger magnitude net ACI is associated with PI climates  
 257 that have radiatively thicker sub-tropical liquid clouds. These ‘radiatively thicker’ clouds  
 258 have larger magnitude cloud radiative effect due to being more extensive, with higher  
 259 drop number and LWP. Stronger net ACI can also be associated with less PI CCN at  
 260 middle and high latitudes and less sulfate over the land regions in mid-latitudes. To some  
 261 extent these effects will offset (higher PI CCN should lead to higher Nc), but the effects

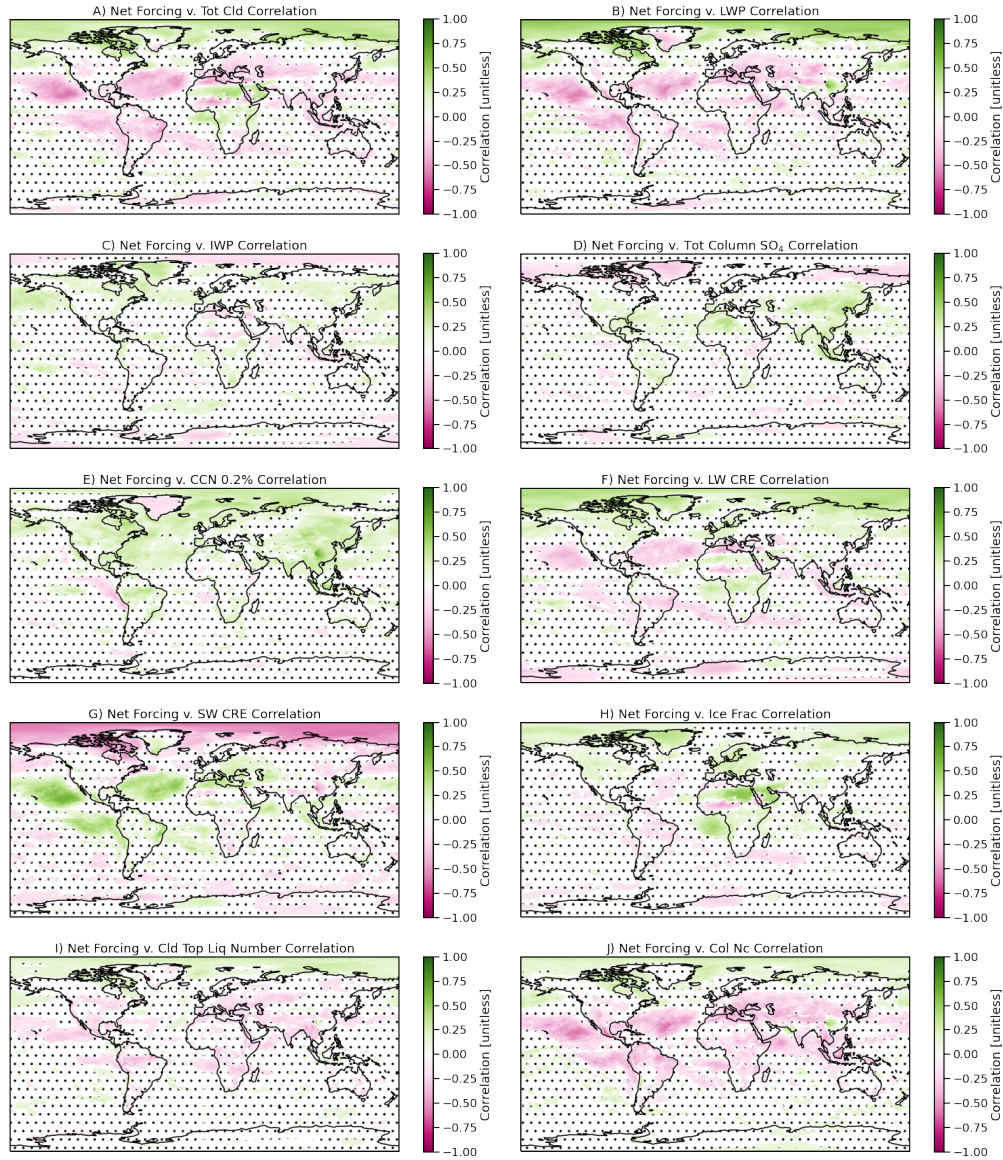


**Figure 4.** Map of linear correlation coefficient at each point between mean state in PI and the ACI forcing (PD-PI) for different variables. Non-significant points are stippled. Significance is determined by a bootstrap fit.

262 occur in different regions (subtropical clouds, and more mid-latitude for CCN). The sub-  
 263 tropical regions noted are regions where there is very little cloud, so simulations with more  
 264 extensive cloud in these marginal regions, along with less PI CCN (and sulfur) to main-  
 265 tain clouds in mid-latitudes, yield larger net ACI response. The strong opposite sign of  
 266 the high latitude correlations as noted are likely due more to the change in ACI com-  
 267 ponents over the Arctic than changes in the mean state.

268 We can also look for which parameters give rise to the largest sensitivity in changes  
 269 between pre-industrial and present day. Parameters affect particular processes, so we can  
 270 use parameter sensitivity as a means to focus on particular processes or sets of processes.  
 271 Since the PPE spans parametric uncertainty, this analysis identifies the sensitivity of pro-  
 272 cesses to parametric uncertainty, and the impact of those processes on forcing and feed-  
 273 back. For example, parameters for auto-conversion and accretion alter the rain forma-  
 274 tion process which is the main sink for cloud water (regulating LWP).

275 Following Eidhammer et al. (2024), we examine changes in model state (PD - PI)  
 276 as a function of parameter in Figure 5. The parameter values (y-axis) are normalized  
 277 (scaled by the minimum and maximum parameter values) while the differences in the  
 278 outputs (x-axis) are standardized (scaled by the mean and standard deviation of the out-  
 279 put values) and then regression slopes are calculated for global and regionally averaged  
 280 values. Figure 5 illustrates the slopes for the normalized regression. The normalization  
 281 and standardization helps show which parameters drive PD-PI changes in each output.  
 282 Parameters are listed by parameterization and the regressions are calculated for differ-  
 283 ent latitude bands as well as global. There are many commonalities across regions, with  
 284 the exception being that cold cloud parameters are more important in the tropics and  
 285 mixed phase cloud parameters are important in the Arctic. Given that ACI forcing is  
 286 mostly in the N. Hemisphere, we do not expect any strong relationships over the South-  
 287 ern Ocean.

288 Important parameters for ACI changes (PD - PI mean quantities) are concen-  
 289 trated, not surprisingly, in the cloud microphysics and aerosol activation parame-  
 290 terizations since ACI processes trace aerosol changes, effects on cloud drop number  
 291 and cloud microphysical adjustments to drop number perturbations. Total aerosol  
 292 forcing (ACI and direct radiative effects of aerosols) is expressed in the residual  
 293 TOA flux (RESTOM) difference, and the cloud forcing (SW CRE and LW CRE are  
 294 the PD - PI change in these quantities). Important parameters alter both accretion  
 295 (*micro\_mg\_accr\_enhan\_fact*) and auto-conversion (*micro\_mg\_autocon\_lwp\_exp* and  
 296 *micro\_mg\_autocon\_nd\_exp*): the main loss process for cloud liquid water. In the Ar-  
 297 ctic, the threshold size of ice crystals for conversion of ice to snow (*micro\_mg\_dcs*) is  
 298 important for ice cloud effects, including changes in ice cloud mass and the changes  
 299 in both LW and SW CRE (LWCF, SWCF). Ice fall speed (*micro\_mg\_vtrmi\_factor*)  
 300 is also important globally. The scaling of the sub-grid vertical velocity for ice nu-  
 301 cleation (*microp\_aero\_wsubi\_scale*) is important in the tropics and globally for gov-  
 302 erning the ice number and hence the LW and SW radiation. Note that it does not  
 303 impact the net TOA balance change because of the offsetting SW and LW effects.  
 304 The sub-grid vertical velocity for liquid drop activation (*microp\_aero\_wsub\_scale*) is  
 305 also important. Liquid drop activation affect CCN formation. In the mid-latitudes,  
 306 including the regions over the ocean where thicker PI clouds increase ACI magni-  
 307 tude, several of the turbulence parameters from CLUBB are important.

308 To take this a bit further, we can break down some of the key correlations  
 309 in Figure 5 by correlating parameter values and net ACI forcing at each point.  
 310 As in Figure 4, we estimate significant correlations with a bootstrap fit. We then  
 311 determine the global average mean absolute correlation from only the location of  
 312 significant correlations. Figure 6 illustrates the mean absolute correlation for each  
 313 parameter for 6 different forcing and feedback components (different colors): To-  
 314 tal, LW and SW for ACI and Cloud Feedback. The squares in Figure 6 show the

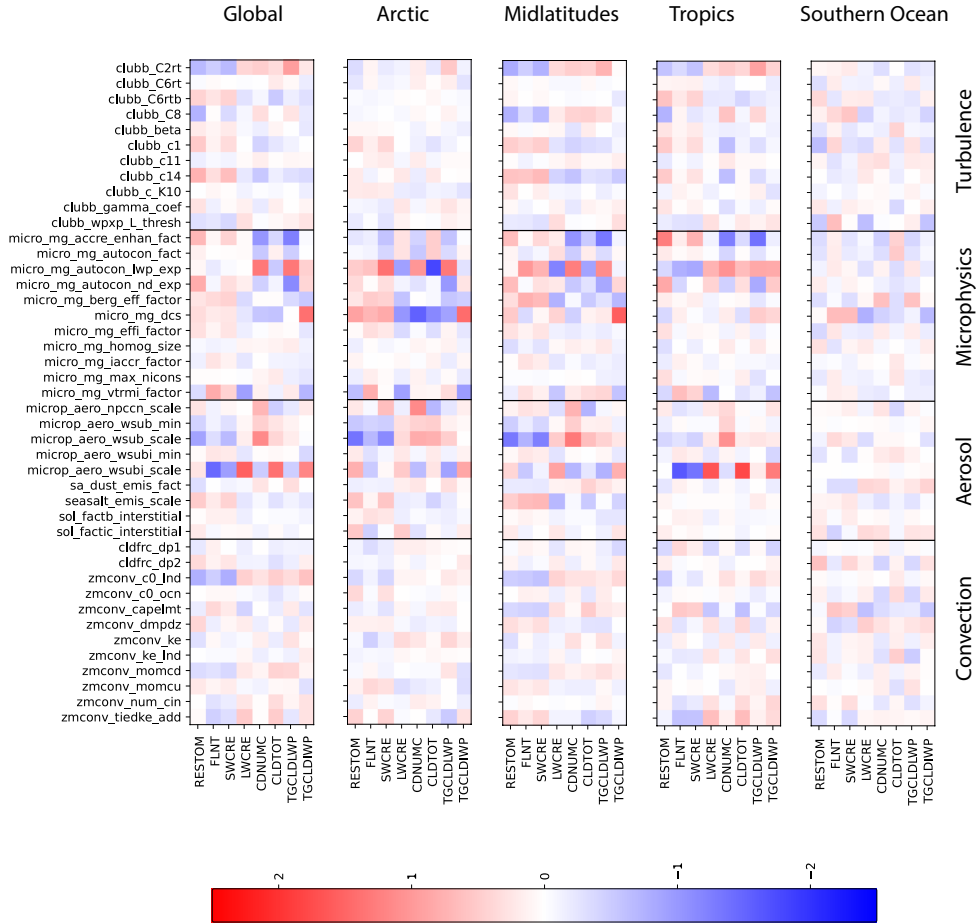


**Figure 5.** Normalized linear regression slope for the difference between PD and PI in 8 different model outputs (x axis) against all parameter values (y axis). The global mean results as well as four different regions are shown; Arctic ( $|lat| > 60^\circ$ ), Midlatitudes ( $30^\circ < |lat| < 60^\circ$ ), Tropics ( $|lat| < 30^\circ$ ) and the Southern Ocean ( $60^\circ S > lat > 30^\circ S$ ). The parameters are grouped into deep convection, aerosol, microphysics and turbulence parameters.

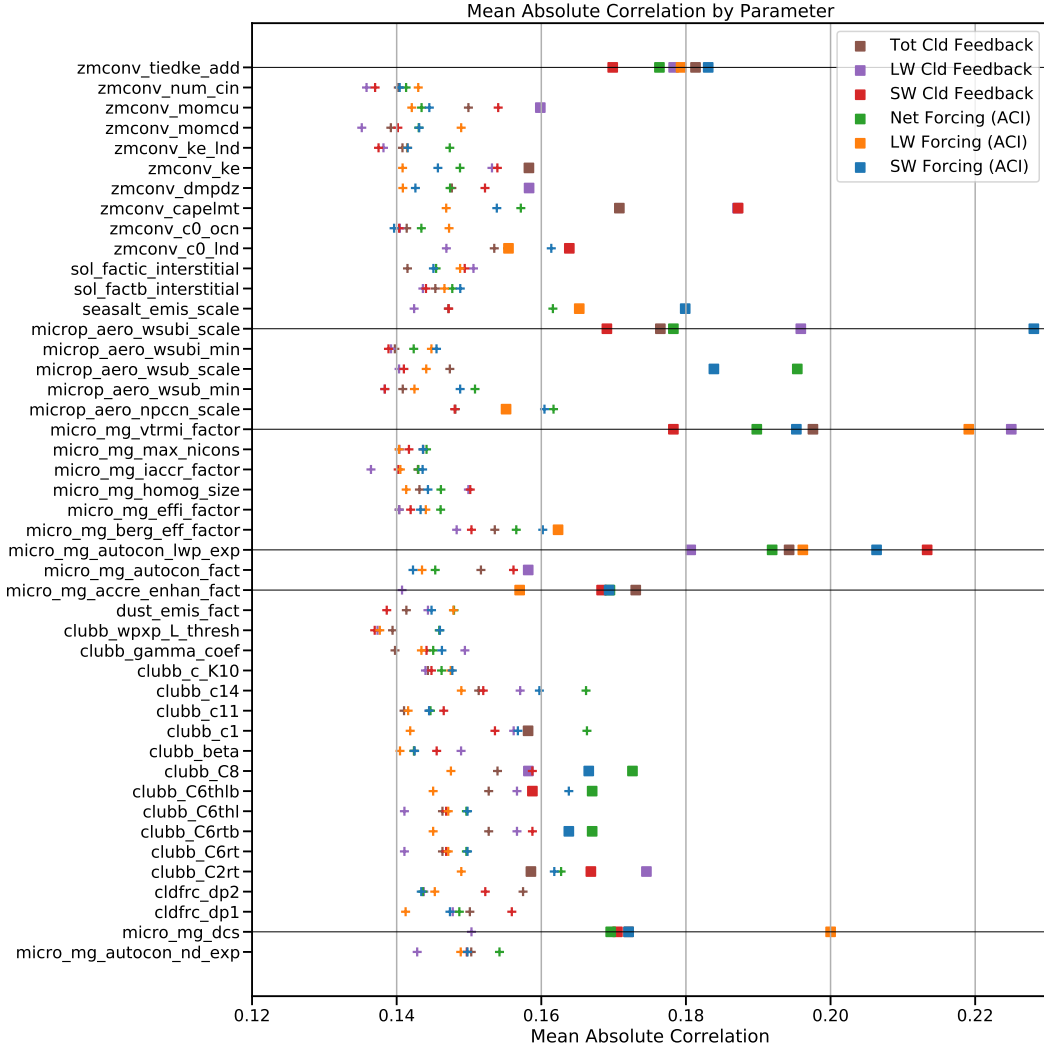


**Figure 6.** Global mean absolute correlation by parameter for ACI Forcing and Cloud Feedbacks. LW, SW and Net are different colors as noted in the legend (e.g. net ACI forcing is green). Parameters with the 10 highest absolute correlations for each component are shown as colored solid squares. The rest of the parameters are plus signs (+). The horizontal lines show the 6 parameters which are in the top 10 correlations for both total cloud feedback (brown) and net forcing (green).

315 parameters with the 10 highest correlations for each component. We will focus on  
 316 the common important parameters across forcing and feedback (horizontal lines)  
 317 in Section 3.4.

318 Focusing on the net ACI Forcing (green in Figure 6), we highlight the param-  
 319 eters with the 10 highest mean absolute correlations (green squares). In general  
 320 the LW (orange) and SW (blue) forcing components also have strong correlations  
 321 with these parameters. Figure 7 illustrates maps of these correlations, ranked as in  
 322 Figure 6 in order of correlation from highest (A) to 10th highest (J).

323 Figure 7 reinforces the global and regional correlations in Figure 5, with a  
 324 bit more insight into processes. Several parameters are related to ice, including the

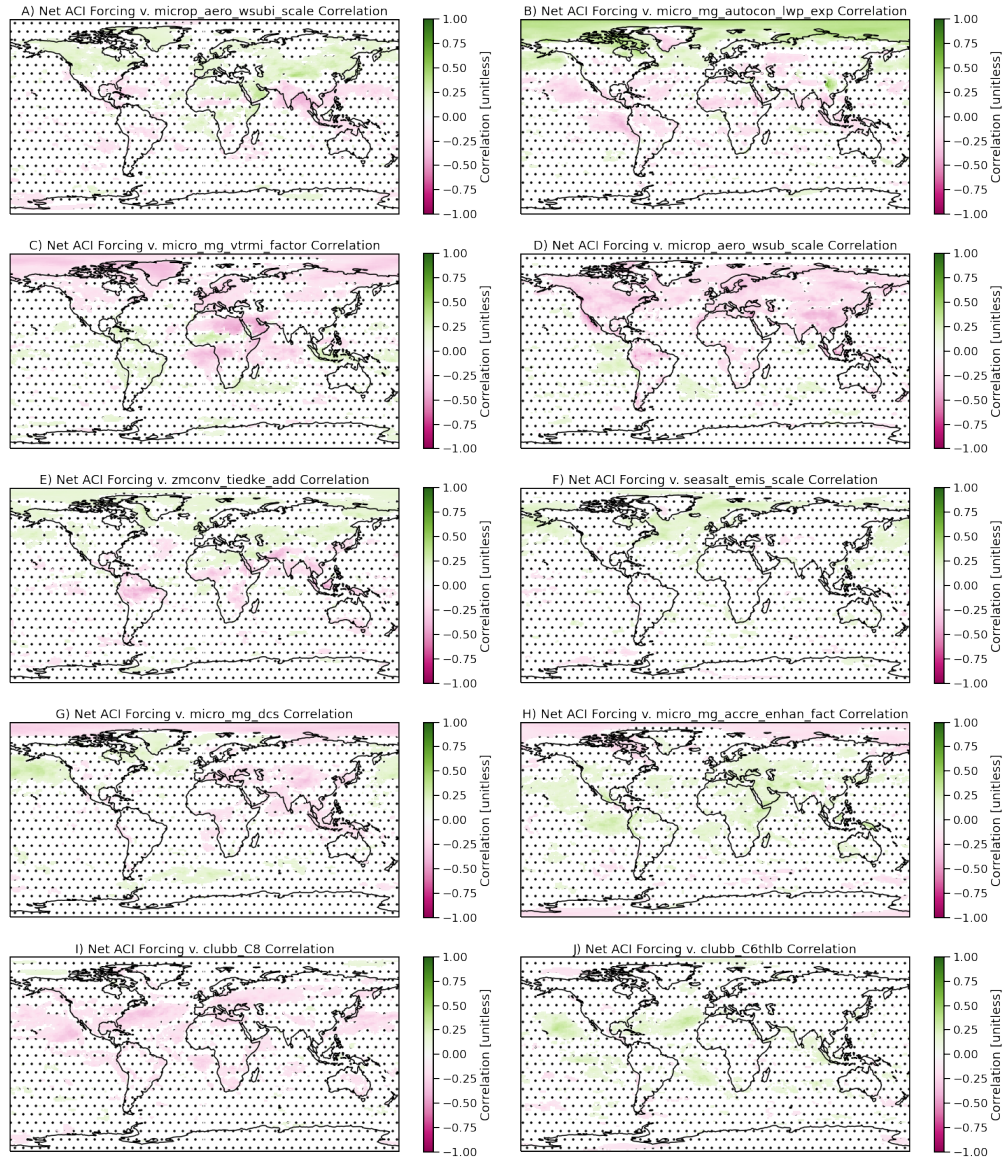


**Figure 7.** Map of linear correlation coefficient at each point between the SW ACI forcing (PD-PI) and selected model parameters varied in the PPE. Non-significant points are stippled. Significance is determined by a bootstrap fit.

325 sub-grid velocity for ice activation (*micro\_aero\_wsubi\_scale*: Figure 7A), the ice  
 326 fall speed scaling (*micro\_mg\_vtrmi\_scale*: Figure 7C) and the ice auto-conversion  
 327 size threshold (*micro\_mg\_dcs*: Figure 7G). The temperature perturbation for deep  
 328 convective triggering (*zmconv\_tiedke\_add*, Figure 7E) likely also plays a role in  
 329 supplying ice to the upper troposphere. Increasing the sub-grid velocity for ice nu-  
 330 cleation will increase ice number (which seems to weaken ACI over land). The ice  
 331 fall speed scaling results in less ice and snow in the atmosphere (associated with  
 332 stronger ACI), while increasing the ice auto-conversion size threshold will increase  
 333 the ice mass, which seems to weaken ACI in mid-latitudes but increase it at high  
 334 latitudes (so more ice will result in stronger ACI at high latitudes, consistent with  
 335 the PI mean state IWP relationship in Figure 4C).

336 Liquid cloud processes are also important. The auto-conversion LWP expo-  
 337 nent (*micro\_mg\_autocon\_lwp\_exp*: Figure 7B) and accretion enhancement factor  
 338 (*micro\_mg\_accr\_enhan\_fact*: Figure 7H) control rain formation and depletion of  
 339 liquid. They have similar patterns and opposite sign. Increasing the LWP exponent  
 340 for auto-conversion results in more sensitivity of cloud water loss to LWP: higher  
 341 auto-conversion sensitivity in the subtropics in results in stronger (more negative)  
 342 ACI, while higher auto-conversion sensitivity in the Arctic results in weaker (less  
 343 negative) ACI. Accretion is also a sink for cloud water, and the enhancement is a  
 344 linear scaling for the loss. In the sub-tropics, more accretion leads to reduced (neg-  
 345 ative) ACI, and would be associated with thinner clouds. The accretion scaling is  
 346 consistent with the sensitivity of ACI to PI mean state sensitivity of clouds in Fig-  
 347 ure 4, while the auto-conversion exponent is more related to the changes in the state  
 348 between PI and PD.

349 Two parameters are related to liquid aerosol activation: increasing  
 350 *microp\_aero\_wsub\_scale* (Figure 7D) is associated with larger negative ACI. Higher  
 351 scaling would increase CCN in PI, but also the sensitivity to changes between PI  
 352 and PD ( $\Delta\text{CCN}$ ). Given that the correlation with ACI in Figure 7D is opposite to  
 353 the mean state effect of PI CCN in Figure 4E, it would appear that it affects ACI  
 354 more through  $\Delta\text{CCN}$ . Increasing sea salt emission (*seasalt\_emis\_scale*), will in-  
 355 crease CCN in the base state, and has a similar correlation with ACI as PI CCN  
 356 (Figure 4E) over the oceans.

357 The last two parameters are related to the unified shallow turbulence  
 358 (CLUBB) and act over the sub-tropical oceans. *clubb\_C8* (Figure 7I) is the coeffi-  
 359 cient of the skewness in the vertical velocity while *clubb\_C6thlb* (Figure 7J) affects  
 360 the high skewness of the liquid water potential temperature. They tend to act in op-  
 361 posite ways. Increasing *clubb\_C8* tends to increase cloud fraction, so the correlation  
 362 matches the total cloud response in Figure 4A.

363 Looking beyond the mean state, we can also try to understand how ACI is  
 364 related to the sensitivity or susceptibility of cloud radiative effects to changes  
 365 in cloud properties. To look at this we examine the susceptibility of cloud ra-  
 366 diative effect (or cloud albedo) to changes in cloud drop number ( $N_c$ ) defined as  
 367  $d\ln(\text{Albedo})/d\ln(N_c)$ . We estimate the susceptibility terms at each point with the  
 368 temporal (monthly mean) co-variance of these properties for each ensemble mem-  
 369 ber, and then similar to Figure 4, correlate that with the total ACI (difference in  
 370 LW+SW CRE between PD and PI) in Figure 8A. Because albedo has a strong sea-  
 371 sonal dependence at high latitudes, we limit this analysis to latitudes equatorward of  
 372  $60^\circ$ .

373 There is a consistent negative correlation between susceptibility and forcing  
 374 over the oceans, whereby increasing susceptibility of clouds to drop number is as-  
 375 sociated with stronger negative net ACI over the tropical and sub-tropical oceans.  
 376 A detailed analysis of the parameter sensitivity of susceptibility (not shown) sim-

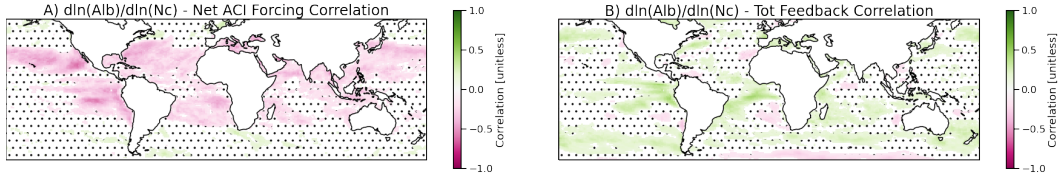


**Figure 8.** Correlation of susceptibility of cloud albedo to cloud drop number against A) Net ACI forcing and B) Total Cloud feedback.

377 ilar to that conducted for Figure 7 for forcing indicates that the susceptibility is  
 378 linked to the auto-conversion (*micro\_mg\_autocon\_lwp\_exp*) where more susceptible  
 379 clouds have a higher auto-conversion exponent for LWP (interestingly it is not re-  
 380 lated as much to the Nc exponent in the auto-conversion). In addition, susceptibility  
 381 varies with accretion (*micro\_mg\_accr\_enhan\_fact*), where more accretion reduces  
 382 susceptibility (perhaps because of thinner clouds). Finally, susceptibility is also asso-  
 383 ciated with *clubb\_C8*, where higher *clubb\_C8* is associated with higher susceptibility.  
 384 H. Guo et al. (2015) noted that increasing *clubb\_C8* increases cloud cover in the sub-  
 385 tropics. These results are consistent with the PI mean state correlations (Figure 4)  
 386 that thicker sub-tropical PI clouds in marginal regions are associated with higher  
 387 (negative) net ACI forcing.

### 388 3.3 Feedback

389 A similar analysis is conducted for cloud feedbacks. Cloud feedbacks are as-  
 390 sessed with the difference in cloud radiative effects between the SST+4K and PD  
 391 simulations (modified with radiative kernels to remove non-cloud effects). Because  
 392 global correlations can be misleading with positive and negative signs and cloud  
 393 feedbacks have multiple signs in different regimes (Figure 2), we move straight to  
 394 correlations with the mean present day state and total (LW+SW) cloud feedbacks at  
 395 each point in Figure 9. These figures are with respect to present day values, but the  
 396 correlations are the same whether present day or pre-industrial mean state is used.  
 397 Figure 9 includes all simulations, but is qualitatively consistent with less significance  
 398 if the 88 simulations constrained by CERES cloud radiative effect are used.

399 Regional correlations between cloud feedbacks and mean state cloud coverage  
 400 (Figure 9A) are negative at high latitudes (Arctic and Southern Ocean) and positive  
 401 at low latitudes. The correlations over the Sahara are spurious since there is nearly  
 402 zero cloud and feedbacks are small (Figure 2C). Similar relationships are found with  
 403 LWP (Figure 9B), cloud drop number (Figure 9J) and cloud top number (Figure 9I).  
 404 Base state SW Cloud Radiative Effect (Figure 9G) has an opposite sign correlation  
 405 (because it is negative) with similar pattern. However, over the Southern Ocean,  
 406 more cloud and LWP (more liquid cloud) has a negative correlation with cloud feed-  
 407 backs. IWP (Figure 9C) however has positive correlations over polar oceans. Base  
 408 state ice fraction (Figure 9H) is positively correlated with total cloud feedbacks as  
 409 well at high latitudes, and negatively correlated at low latitudes. All these corre-  
 410 lations indicate that at high latitudes stronger cloud feedbacks are associated with  
 411 less base state cloud, liquid and liquid drop number, as well as more ice. Note that  
 412 as with forcing, the net feedback sign changes at high latitudes, which affects these  
 413 correlations (the same change in mean state has a different sign with different signed  
 414 feedbacks). In low latitudes, the effects are opposite, with stronger feedbacks for  
 415 more and thicker cloud over land and ocean. There are weaker relationships between  
 416 feedbacks and column sulfate (Figure 9D) and CCN (Figure 9E), but in general



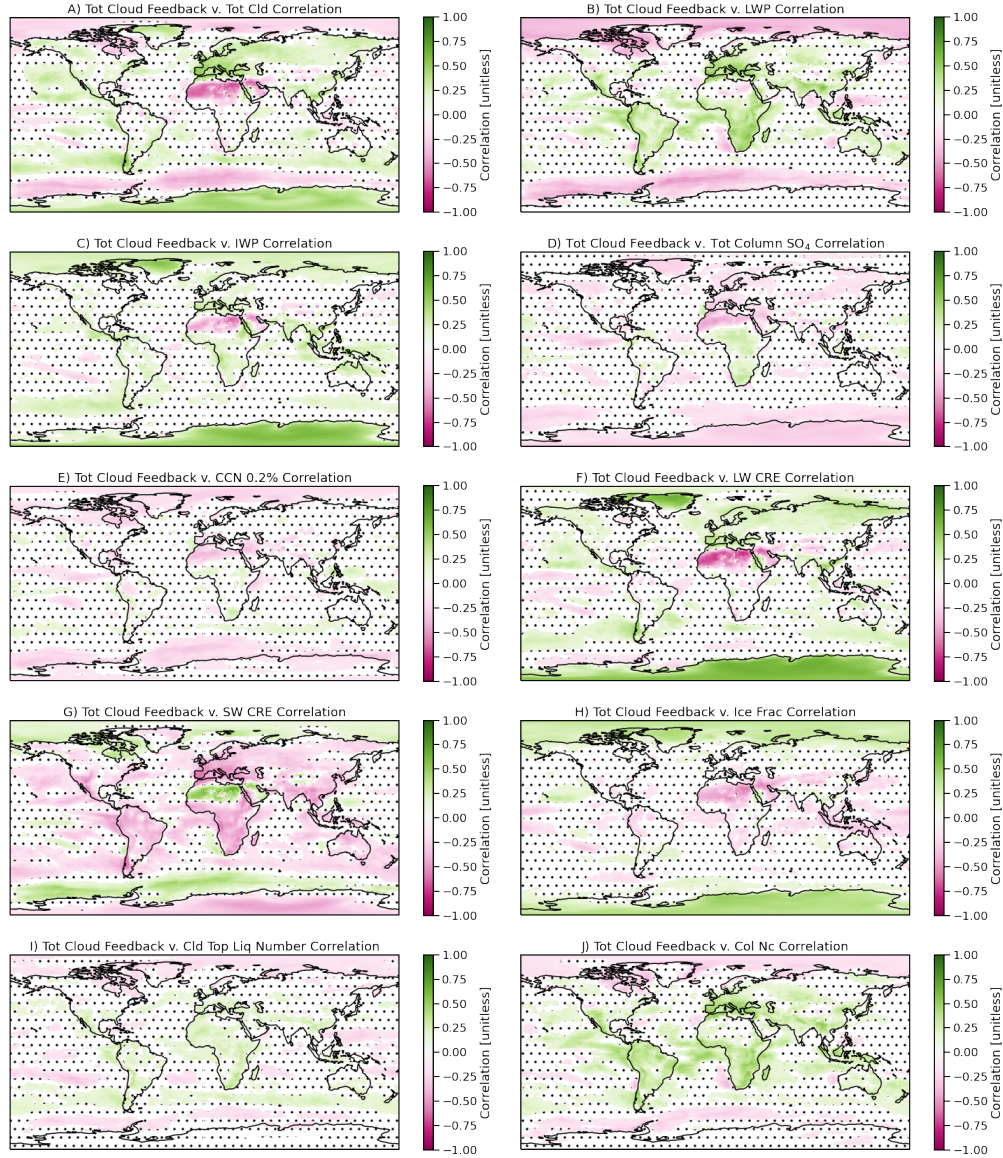


**Figure 9.** Map of linear correlation coefficient at each point between mean state in present day and the total (LW+SW) cloud feedbacks (estimated with SST4K v. PD) for different variables. Non-significant points are stippled. Significance is determined by a bootstrap fit.

417 more sulfate and CCN in the base (non-warmed) state is associated with lower feed-  
418 backs.

419 We investigate these relationships further by diving into processes by looking  
420 at key parameters. Figure 10 is similar to Figure 5 showing the normalized and  
421 standardized regressions between parameters and changes in the state SST4K - PD  
422 across regions. Some of the same parameters are important for cloud feedbacks (the  
423 last two variables on the right of each column): accretion, auto-conversion and the  
424 loss process of ice (fall speed and conversion from ice to snow). Note that the S.  
425 Ocean is not important for forcing since there is little change in aerosols PD-PI, but  
426 is more important for feedbacks (accretion, ice processes and some deep convection  
427 parameters are important here). As with the maps in Figure 9, the correlations vary  
428 by region, muting the global sensitivity (correlation) for many parameters.

429 There are several parameters in the deep convective parameterization that are  
430 important for cloud feedbacks, particularly in the Tropics and to a lesser extent the  
431 S. Ocean. These parameters govern the triggering of convection (*zmconv\_capelmt*  
432 is the threshold CAPE for firing convection and *zmconv\_tideke\_add* is a buoyancy  
433 perturbation that will increase the convective potential). Convective rain formation  
434 over land (*zmconv\_c0\_lnd*) is also important in the tropics, which is not surprising  
435 given the larger positive cloud feedbacks there (Figure 2). Convective entrainment  
436 (*zmconv\_dmpdz*) is important in the mid-latitudes and tropics. Deep convection  
437 acts by changing both the SW and the LW feedback, likely because it changes ice  
438 cloud radiative effects, while many of the other parameters primarily change the LW  
439 (for ice microphysical and aerosol processes) or SW (for liquid cloud microphysical  
440 and aerosol processes).

441 Finally for we look at maps of key parameter correlations with feedbacks in  
442 Figure 11. As with Forcing, we estimate the mean absolute correlation of significant  
443 points for each parameter, and rank them (Figure 6). The parameters with the 10  
444 highest correlations with total feedbacks (brown squares in Figure 6) are displayed  
445 in Figure 11.

446 The parameters identified are similar to those for forcing. There are several  
447 parameters linked to ice processes, including ice fall speed (*micro\_mg\_vtrmi\_scale*,  
448 Figure 11A), the sub-grid velocity for ice activation (*micro\_aero\_wsubi\_scale*: Fig-  
449 ure 11D) and the ice auto-conversion threshold (*micro\_mg\_dcs*, Figure 11F). Slower  
450 fall speed and more ice number (higher *micro\_aero\_wsubi\_scale*) at high latitudes  
451 are associated with more ice and higher total cloud feedbacks at high latitudes  
452 (Figure 9C). Ice auto-conversion (*micro\_mg\_dcs*) acts mostly in the tropics and S.  
453 Hemisphere, again with more base state ice (higher *micro\_mg\_dcs*) associated with  
454 higher cloud feedback, likely through the LW CRE (Figure 9F).

455 As with forcing, parameters linked to rain formation are important for cloud  
456 feedbacks, the auto-conversion LWP exponent (*micro\_mg\_autocon\_lwp\_exp*, Fig-  
457 ure 11B) and accretion enhancement (*micro\_mg\_accr\_enhan\_fact*, Figure 11E)  
458 have opposite signs. Higher auto conversion (leading to less liquid) is associated  
459 with smaller cloud feedbacks at high latitudes and larger cloud feedbacks at lower  
460 latitudes. Accretion has the opposite effect, with more accretion (reducing cloud wa-  
461 ter) associated with more high latitude cloud feedbacks, and reduced tropical cloud  
462 feedbacks over land. Both effects are consistent with the overall cloud and LWP  
463 correlations with feedbacks in Figure 9A and B.

464 In addition, there are three deep convective parameters that have regionally  
465 significant correlations with cloud feedback. In the tropics, deep convection supplies  
466 ice to the upper troposphere, *zmconv\_tiedke\_add* (Figure 11C) as well as *zmconv\_ke*  
467 (Figure 11I) increase convection over land with similar patterns. *zmconv\_capelmt*

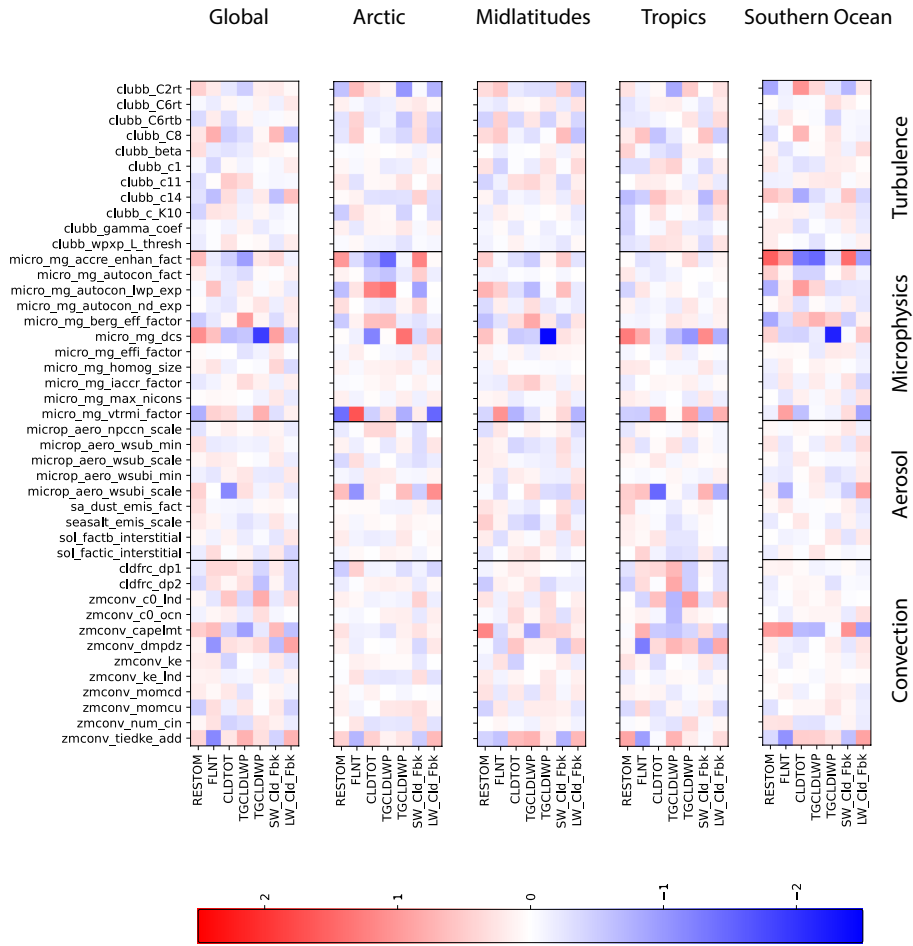


**Figure 10.** Normalized linear regression slope for the difference between SST4K and PD in 8 outputs (x axis) against all parameter values (y axis). The global mean results as well as four different regions are shown; Arctic, Midlatitudes, Tropics and the Southern Ocean. The parameters are grouped into deep convection, aerosol, microphysics and turbulence parameters.

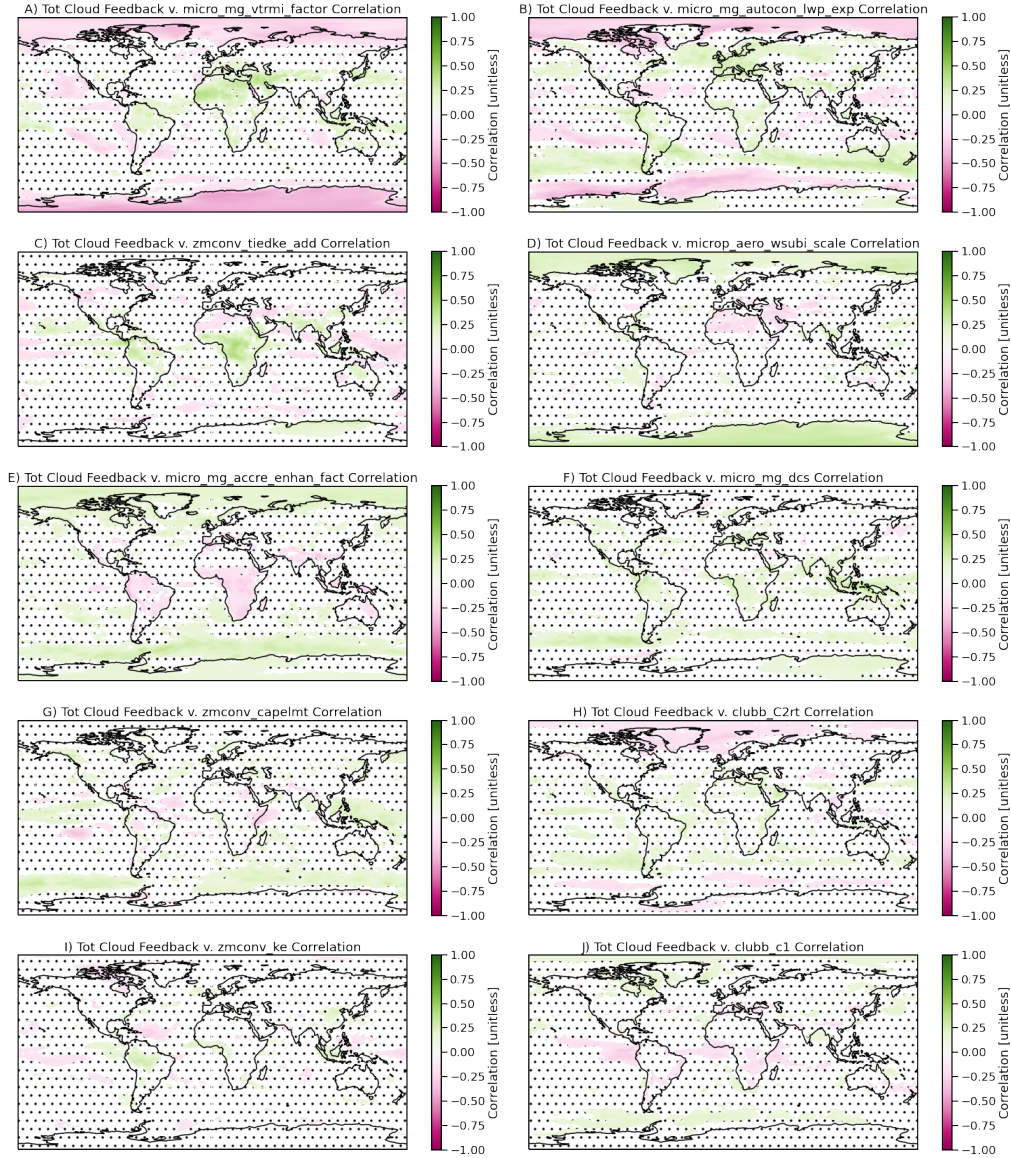


**Figure 11.** Map of linear correlation coefficient at each point between the total cloud feedbacks (SW + LW) estimated from SST4K v. PD and selected model parameters varied in the PPE. Non-significant points are stippled. Significance is determined by a bootstrap fit.

(Figure 11G) increases it over ocean. Increasing ice seems to increase cloud feed-backs in the tropics (Figure 9C). *zmconv\_capelmt* (Figure 11G) also seems to act over the Southern Ocean, with offsetting signs in the LW and SW (Figure 10).

Finally, two turbulence parameters, *clubb\_C2rt* (Figure 11H), *clubb\_c1* (Figure 11J) have small regional correlations, mostly over the oceans with opposite sign. *clubb\_C2rt* is related to the dissipation of temperature variance and increasing it increases cloud cover and SW CRE (Z. Guo et al., 2015) while *clubb\_c1* is related to the dissipation of vertical velocity variance and has the opposite effect (increasing it decreases cloud cover and SW CRE). The patterns indicate that these parameters may be driving some of the correlation with mean state total cloud cover and LWP (Figure 9A and B), in both the tropics and high latitudes.

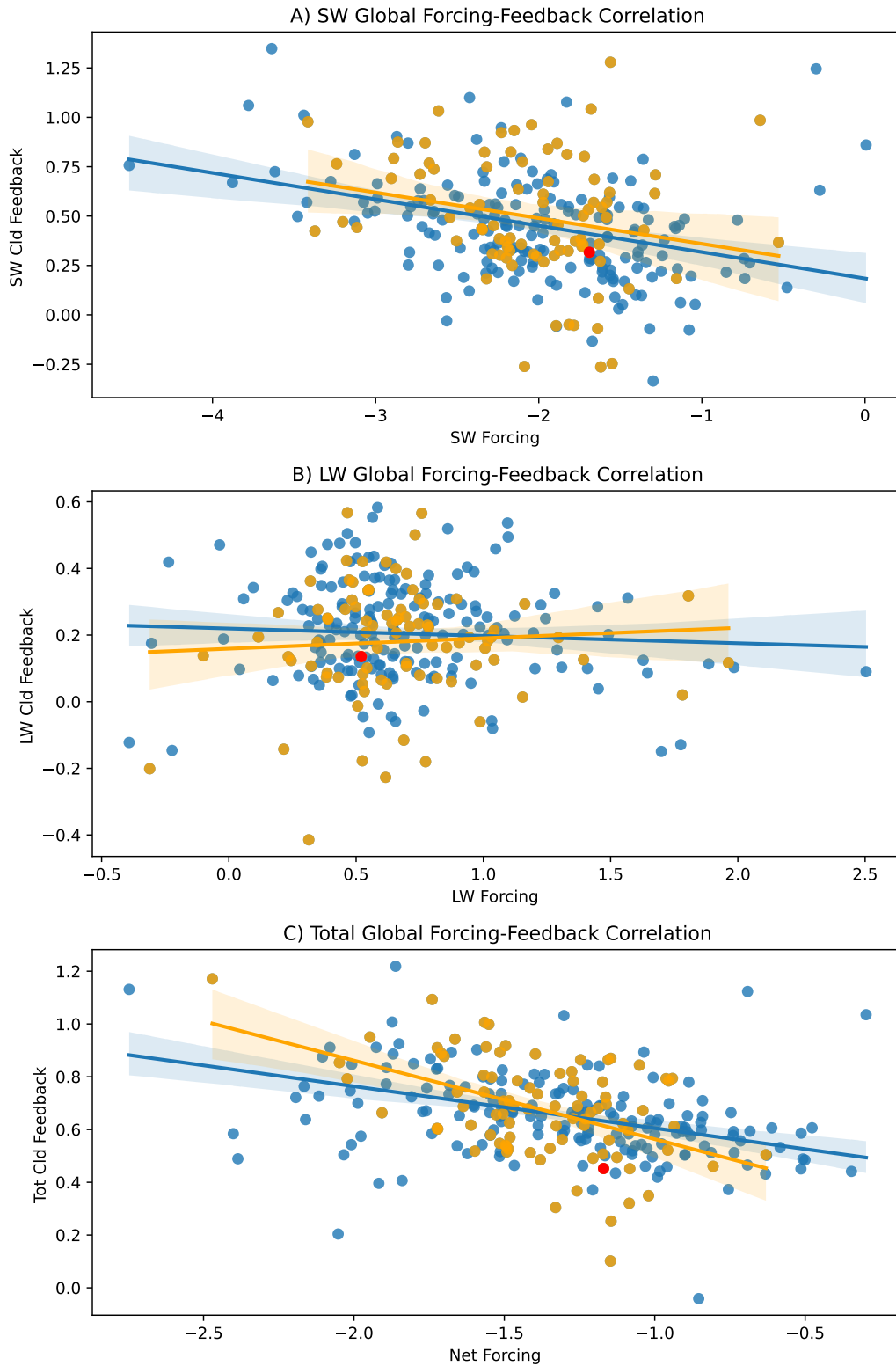
### 3.4 Forcing and Feedback Relationships

Figure 12 illustrates a global scatter plot of the cloud forcing (defined as above: the change in CRE between present day and pre-industrial) against the kernel adjusted cloud feedbacks both in the SW (Figure 12A), LW (Figure 12B) and total (LW+SW, Figure 12C). The blue colors and regression line are for all simulations. As in Figure 12, the orange points and regression lines are just those simulations whose mean annual value of SW CRE is within  $\pm 5 \text{ Wm}^{-2}$  of the observed CERES EBAF annual global mean ( $-45.3 \text{ Wm}^{-2}$ ). The red dot is the ‘default’ parameter set for CAM6.

In the SW, there is a clear relationship between the cloud feedbacks and cloud forcing. The relationship is similar whether just a constrained subset of simulations is used, or if the full data set is used, and the slope is significantly different than zero. In general the SW aerosol cloud forcing is negatively correlated with SW cloud feedback: larger positive feedbacks yield larger negative cloud forcing. There is no such correlation in the LW, and the slopes are not significantly different than zero, and the constrained simulations have a different (but still not significant) sign. The correlation of total (LW+SW), cloud forcing and feedback reflects mostly the SW correlation, and is actually stronger with constrained simulations.

As with forcing and feedback, we can decompose the global correlation of Figure 12 into each location on the planet, generate a correlation value at each point, and determine the significance of the correlation with a bootstrap fit yielding a confidence interval for the correlation between forcing and feedbacks being significantly different than zero (Figure 13) at each point. For the SW (Figure 13A), correlations are uniformly negative: stronger negative ACI is correlated with stronger positive cloud feedback. This maximizes over N. Hemisphere land and adjacent ocean basins. In large parts of the S. Hemisphere, there is very little forcing response, so there are small signals. Most of the negative correlation comes from the N. Hemisphere. Going back to the regional correlations between mean state SW CRE and ACI (Figure 4G) and total cloud feedbacks (Figure 9G), there is an anti-correlation, consistent with stronger forcing and feedbacks going together (since forcing is negative), with opposite signs over the Arctic and the rest of the N. Hemisphere. It is apparent over both ocean and land.

For the LW (Figure 13B), the sign is not monotonic, but there is a negative correlation in N. Hemisphere mid-latitudes, and a positive correlation between LW feedbacks and LW forcing (which are generally both of the same positive sign) in parts of the tropics and the Arctic, but with less significance. The patterns of LW forcing and feedbacks (shown in Figure 2) are less correlated than the SW, likely since the SW ACI magnitude and processes acting through liquid are stronger than for ice. Indeed, if we look at changes in the different climate states between forcing (PD - PI) and feedback (SST4K - PD), the strongest negative correlations are



**Figure 12.** Scatterplot of A) SW B) LW and C) Total (LW+SW) Aerosol forcing (horizontal axis) and kernel adjusted cloud feedbacks (vertical axis) from each simulation. Orange indicates those 88 simulations whose global mean PD Shortwave Cloud Radiative Effect is within  $\pm 5$   $\text{Wm}^{-2}$  of the CERES EBAF global annual mean. Default CAM6 parameters shown as the red dot.

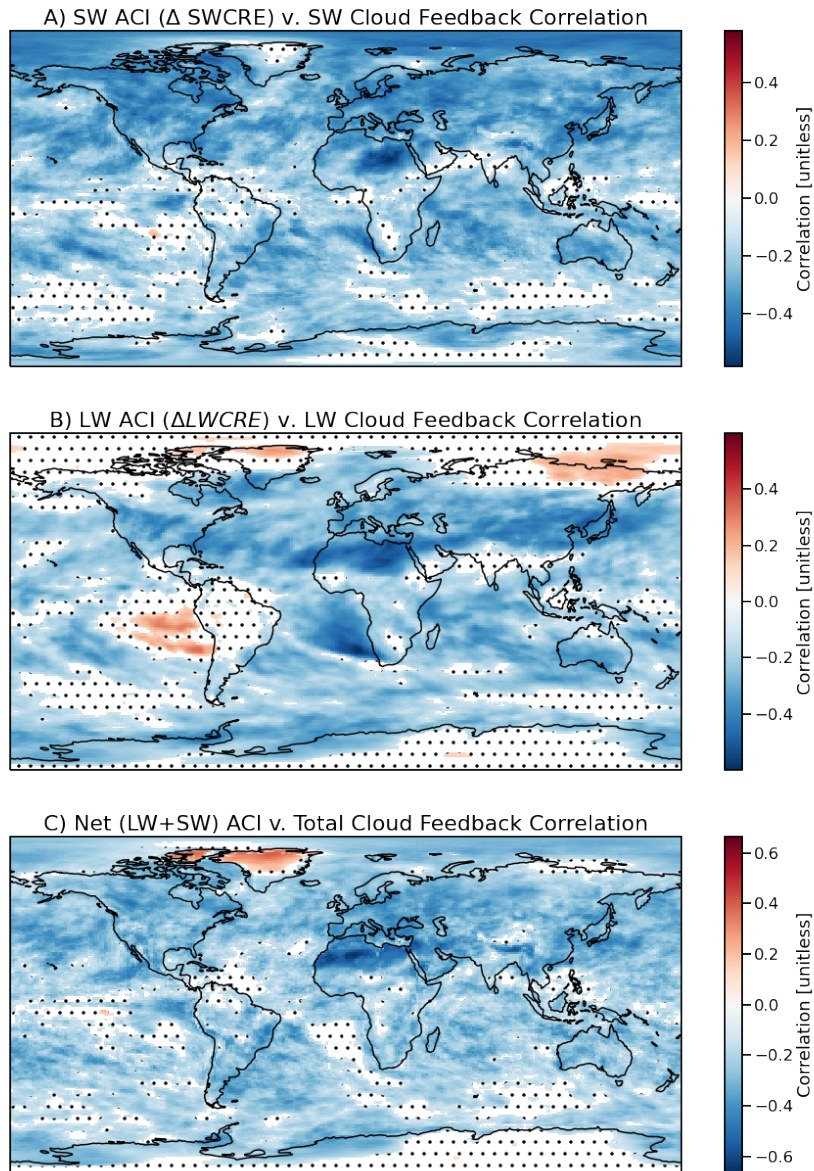


**Figure 13.** Correlation maps at each point between A) SW, B) LW and C) Total (SW+LW) Cloud Forcing and Feedback. Regions of less than 95% significance are stippled.

519 with N. Hemisphere mid-latitude LWP and column drop number (Figure B1), which  
 520 affect mostly SW radiation. The correlations between net forcing and feedbacks  
 521 (Figure 13C) are lower than the SW, but also negative.

522 There is also a positive relationship between cloud albedo susceptibility to  
 523 drop number and cloud feedbacks (Figure 8B). The correlation is the opposite as for  
 524 ACI forcing, which may be another reason for the anti-correlation between forcing  
 525 and feedback. Increased susceptibility (through the processes described above under  
 526 forcing), tends to create larger magnitude negative ACI forcing and positive cloud  
 527 feedbacks.

528 Finally, we note that some of the dominant parameters governing Forcing and  
 529 Feedbacks are similar. Using the mean absolute correlations by parameter (Fig-  
 530 ure 6), we determined the most relevant parameters for ACI forcing in Figure 7 and  
 531 cloud feedbacks in Figure 11. Figure 6 illustrates that of the top 10 correlations  
 532 between parameters and forcing and feedback, 6 of them are common (horizontal  
 533 lines). These include 3 parameters for ice: ice fall speed (*micro\_mg\_vtrmi\_scale*),  
 534 ice nucleation sub-grid velocity (*microp\_aero\_wsubi\_scale*) and ice to snow conver-  
 535 sion size threshold (*micro\_mg\_dcs*). There are two parameters related to warm rain  
 536 formation, one each for auto-conversion (*micro\_mg\_autocon\_lwp\_exp*) and accretion  
 537 (*micro\_mg\_accr\_enhan\_fact*). One parameter is related to the triggering of deep  
 538 convection (*zmconv\_tiedke\_add*).

539 To illustrate how the co-variation of these parameters affect forcing and feed-  
 540 back, we build a Gaussian process emulator using the global average forcing and  
 541 feedback. Inputs are the normalized parameter values and global net forcing and to-  
 542 tal feedbacks (LW+SW). Figure 14 illustrates how global mean total cloud feedbacks  
 543 and net ACI forcing vary around the default values as these parameters change in-  
 544 dividually based on the emulator. The emulator is not a perfect representation of  
 545 the total 45 dimensional parameter space, and it is built on global values (with at-  
 546 tendant problems of different responses by regime), but it is illustrative of another  
 547 method to understand the interaction of forcing and feedback.

548 In this emulator, some parameters affect only either feedbacks (ice conver-  
 549 sion threshold: *micro\_mg\_dcs*) or forcing (ice fall speed: *micro\_mg\_vtrmi\_factor*),  
 550 and some affect virtually neither in the emulator (deep convective triggering:  
 551 *zmconv\_tiedke\_add*). This might be because the global positive and negative  
 552 correlations cancel. Ice nucleation sub-grid velocity (*microp\_aero\_wsubi\_scale*),  
 553 which changes ice crystal number is weakly non-linear, while auto-conversion  
 554 (*micro\_mg\_autocon\_lwp\_exp*) and accretion (*micro\_mg\_accr\_enhan\_fact*) param-  
 555 eters have complex relationships and act differently for feedback, but similarly for  
 556 forcing. Such emulators can be used as a further guide for understanding the slices  
 557 through the parameter space. The opposite effects on feedbacks of auto-conversion  
 558 and accretion are consistent with correlations in Figure 11 for example. For forcing,  
 559 the different magnitudes of negative and positive responses (Figure 7) may make  
 560 emulating the global mean difficult.

## 561 4 Discussion

562 We can summarize this analysis with several comments about key processes for  
 563 forcing, feedbacks and their interaction in the CAM6 PPE.

### 564 4.1 Forcing

565 Stronger negative ACI forcing is associated with PI climates that have thicker,  
 566 more extensive clouds with higher drop numbers and water path in the subtropics.



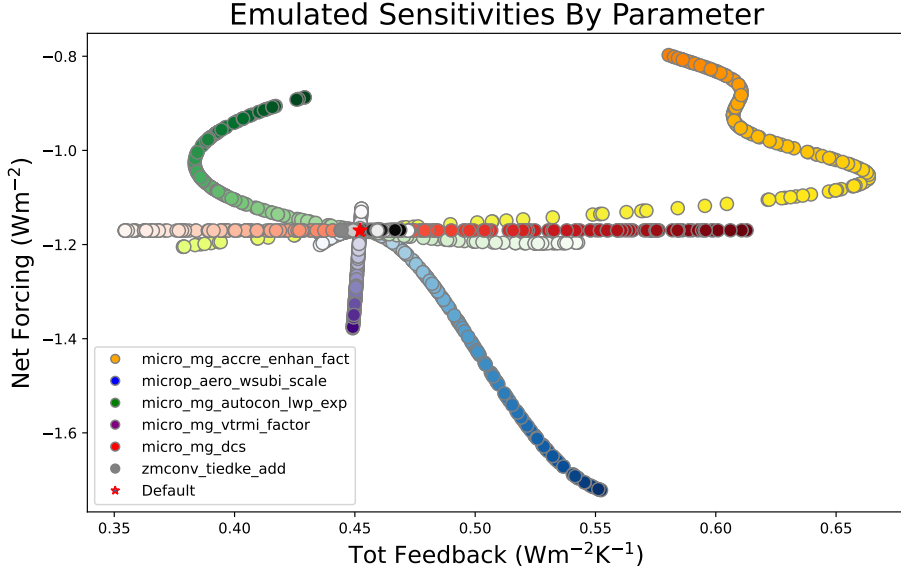


**Figure 14.** Sensitivities by parameter using the Gaussian Process emulator. Top common parameters are shown, varied around the default location (marked with a red star). Color hue varies from light (0) to dark (1) of the normalized range.

567 The regions in the sub-tropics that are most sensitive to parameter changes are re-  
 568 gions where there is very little cloud, so simulations with more extensive cloud in  
 569 these marginal regions, along with less PI CCN and sulfur, seem to yield larger net  
 570 ACI. This highlights that the pre-industrial state of clouds is important for ACI, as  
 571 noted by Carslaw et al. (2013) and others.

572 Auto-conversion and accretion are critical processes. Auto-conversion and ac-  
 573 cretion parameters that lead to increased cloud thickness in the subtropics increase  
 574 negative ACI (consistent with mean state effects). Increasing activation with in-  
 575 creased sub-grid vertical velocity leads to stronger negative ACI nearly everywhere  
 576 (more response to aerosols, more change in CCN, since lower CCN in PI are as-  
 577 sociated with stronger ACI). Increasing sea salt emission (which increases PI and  
 578 PD CCN similarly) reduces net ACI, because it means more CCN in PI (consistent  
 579 with the interactions with the mean state). Correlations with changes to the auto-  
 580 conversion LWP exponent seem larger than for accretion, but accretion is scaled  
 581 linearly, and the variations on the auto-conversion are larger (there is also a linear  
 582 auto-conversion scaling parameter which does NOT show up as being significant).  
 583 Accretion affects ACI through PI mean state (thicker clouds yield larger magnitude  
 584 ACI), while auto-conversion affects ACI through the sensitivity of PD-PI differences  
 585 in LWP.

586 Increasing susceptibility of cloud albedo to drop number increases negative  
 587 ACI forcing, over much broader regions than a single parameter or mean state prop-  
 588 erty. Susceptibility is driven by a slightly different set of parameters, including  
 589 auto-conversion and accretion, but also shallow turbulence parameters that increase  
 590 cloud cover in the sub-tropics, again, in regions where it is generally low.

## 591 4.2 Feedbacks

592 In low latitudes, stronger positive cloud feedbacks are associated with more  
 593 base state cloud, liquid and liquid drop number, as well as more ice over land and  
 594 ocean. More ice (and higher ice fraction) at high latitudes increases cloud feedback,  
 595 while correlations for liquid are the opposite (more liquid is associated with more  
 596 negative cloud feedback). There is a dipole in these effects over the S. Ocean where  
 597 the mean ice fraction crosses about 50%. This is related to the loss processes for  
 598 water (auto-conversion and accretion) as well as for ice (ice fall speed and ice acti-  
 599 vation), and the deep convective source for ice. It is near the region where feedbacks  
 600 turn from positive to negative. In ice dominated regions feedbacks are negative likely  
 601 due to the ice-albedo feedback, whereby warming melts ice and increases negative  
 602 SW CRE. This has been shown to be important in CAM6 (Gettelman et al., 2019).

603 Going strictly by the correlations, it appears that that auto conversion is more  
 604 important (or at least more related to) the base state cloud feedback sensitivity than  
 605 accretion (correlations for accretion are weaker). Raining and non-raining clouds  
 606 may have different effects, with perhaps the non-raining clouds more important  
 607 for feedback. Turbulence parameters also seem to play a role over the sub-tropical  
 608 oceans: they control the base state of clouds and thicker and more extensive clouds  
 609 have more positive cloud feedbacks. More ice yields stronger positive cloud feed-  
 610 backs (mostly through the LW) in both the tropics and high latitudes. Ice micro-  
 611 physics and deep convection parameters are important for regulating ice mass and  
 612 seem to influence feedbacks accordingly.

## 613 4.3 Interactions

614 Forcing and feedbacks are anti-correlated throughout the Northern Hemi-  
 615 sphere. Both forcing and feedback relationships to the mean state change sign from  
 616 high latitudes to lower latitudes, and they seem to do so in concert. Part of this is  
 617 simply the reduction in SW effects over high latitude ice covered surfaces. Stronger  
 618 negative forcing and positive feedbacks are associated with thinner clouds (less liq-  
 619 uid, more ice) at high latitudes and thicker clouds at low latitudes. This change  
 620 may occur because of the role of ice process, or the thickness of the clouds in the  
 621 stormtracks.

622 Even the important processes seem to be common between aerosol forcing and  
 623 cloud feedbacks. Microphysical controls on ice and ice nucleation, rain formation  
 624 (auto-conversion and accretion) as well as deep convection are important for both  
 625 forcing and feedback, with some shallow turbulence parameters (but different ones)  
 626 important over the oceans. Most of these parameters seem to be consistent with  
 627 sensitivity in the mean state.

628 One question arises: given that changing the method for auto-conversion and  
 629 accretion drastically (e.g., Gettelman et al., 2021) did not change ACI or cloud  
 630 feedbacks, how does that mesh with these results? We have not tested changing  
 631 auto-conversion and accretion fundamentally and altering other parameters, but it  
 632 may be that the balance required to maintain the mean state clouds constrains the  
 633 range of ACI and cloud feedbacks. This is consistent with the correlations with the  
 634 mean state of clouds, and would imply an emergent constraint dependent on the  
 635 present day state, but perhaps not a strong constraint.

## 636 5 Conclusions

637 This analysis of a large ensemble set of perturbed parameter experiments from  
 638 CAM6 (CAM6-PPE) yields several conclusions. Forcing and feedback are both cor-

639 related with the mean state. Higher magnitude cloud radiative effects generally  
640 mean larger forcing (negative for the SW, positive for the LW) and larger feedbacks  
641 (positive SW and LW). Aerosol forcing is broadly related to the susceptibility of  
642 clouds to drop number, which is impacted by a similar set of parameters, but with a  
643 different magnitude.

644 For aerosol forcing in particular, lower PI CCN and sulfate mass yield higher  
645 magnitude forcing. Accretion affects the mean state (and the total water mass in  
646 clouds), while auto-conversion seems to affect the sensitivity of LWP more strongly.

647 Thicker low latitude clouds with higher susceptibility are also associated with  
648 more positive cloud feedbacks. At high latitudes stronger positive cloud feedbacks  
649 are associated with less base state cloud, liquid and liquid drop number, as well as  
650 more ice at high latitudes. The shift happens about where ice starts to dominate  
651 the cloud (50% ice fraction). The fact that many important parameters reflect ice  
652 processes confirm the importance of ice in CAM6 feedbacks.

653 Aerosol forcing and cloud feedbacks are not independent in the CAM6 PPE,  
654 they are anti-correlated, such that stronger negative forcing is associated with  
655 stronger positive feedbacks. The fact that both forcing and feedbacks change sign  
656 in high latitudes of the N. Hemisphere at the same latitude is likely due to the LW  
657 and SW balance changing over an ice covered surface.

658 Even the processes governing forcing and feedback sensitivity in the PPE seem  
659 to be similar. The warm rain formation process (auto-conversion and accretion), ice  
660 loss processes (activation, fall speed, auto-conversion to snow) and deep convective  
661 intensity (which affects ice) are important for both forcing and feedbacks. Using  
662 these processes, it is possible to build emulators for forcing and feedbacks to try to  
663 understand the sensitivities.

664 This process-based view shows that in a consistent model system there are  
665 relationships between aerosol forcing and cloud feedbacks. Such relationships may  
666 be representative across multi-model ensembles as has been seen in the past (Kiehl,  
667 2007; Forster et al., 2013), but not necessarily given the small sample size (Smith et  
668 al., 2020).

669 This detailed analysis of cloud processes and their interactions with parameters  
670 to yield forcing and feedback sensitivities has yielded new insights into CAM6. But  
671 this is only one model of many different climate models, with a unique and complex  
672 representation of cloud processes. How applicable is this result across a range of  
673 models? Similar PPE methods should be and are being performed with other mod-  
674 els. Some aspects of this analysis should have broad applicability. For example, the  
675 parameterizations used in CAM6 for deep convection (G. J. Zhang & McFarlane,  
676 1995), cloud microphysics (Gettelman et al., 2015), aerosol activation (Abdul-Razzak  
677 & Ghan, 2002) and shallow turbulence Golaz et al. (2002) are used in other mod-  
678 els, so they feature similar or identical parameters. Beyond this, critical process  
679 treatments like auto-conversion and accretion (Khairoutdinov & Kogan, 2000), are  
680 described with similar parameters or using identical formulations in many models  
681 even with different parameterizations (Jing et al., 2019). It would be interesting to  
682 compare these results to those with other similar climate and weather models to as-  
683 certain if the behavior of individual processes is consistent, or if the process coupling  
684 within and between parameterizations induces different sensitivities. Some of the  
685 results are robust, like the importance of pre-industrial mean state sulfate and CCN  
686 by Carslaw et al. (2013). This work could be repeated on mean state relationships  
687 using data that is part of the traditional Coupled Model Intercomparison (CMIP)  
688 archives, but the parameter-level analysis would require dedicated simulations.

**Table A1.** A description of the parameters that are perturbed and their ranges. Note for  $zmoconv\_ke$  units  $KE = (\text{kg m}^{-2} \text{s}^{-1})^{0.5} \text{s}^{-1}$ 

Physics Scheme	Parameter Name	Description	Default	Min	Max	Units	
<i>CLUBB</i>	clubb_C2rt	Damping on scalar variances	1.0	0.2	2	-	
	clubb_C6rt	Low skewness in C6rt skewness function	4.0	2.0	6	-	
	clubb_C6rtb	High skewness in C6rt skewness function	6.0	2.0	8	-	
	clubb_C6thl	Low skewness in C6thl skewness function	4.0	2.0	6	-	
	clubb_C6thlb	High skewness in C6thl skewness function	6.0	2.0	8	-	
	clubb_C8	Coef. #1 in C8 skewness Equation	4.2	1.0	5	-	
	clubb_beta	Set plume widths for theta.l and rt	2.4	1.6	2.5	-	
	clubb.c1	Low Skewness in C1 Skw.	1.0	0.4	3	-	
	clubb.c11	Low Skewness in C11 Skw	0.7	0.2	0.8	-	
	clubb.c14	Constant for $u'^2$ and $v'^2$ terms	2.2	0.4	3	-	
	clubb.c.K10	Momentum coefficient of $Kh\_zm$	0.5	0.2	1.2	-	
	clubb_gamma_coef	Low Skw.: gamma coef. Skw	0.308	0.25	0.35	-	
	clubb_wpxp.L_thresh	Lscale threshold, damp C6 and C7	60	20	200	m	
	<i>MG2</i>	micro_mg_accr_enhan_fact	Accretion enhancing factor	1.0	0.1	10.0	-
		micro_mg_autocon_fact	auto-conversion factor	0.01	0.005	0.2	-
micro_mg_autocon_lwp_exp		KK2000 LWP exponent	2.47	2.10	3.30	-	
micro_mg_autocon_nd_exp		KK2000 auto-conversion exponent	-1.1	-0.8	-2	-	
micro_mg_berg_eff_factor		Bergeron efficiency factor	1.0	0.1	1.0	-	
micro_mg_dcs		auto-conversion size threshold ice-snow	500e-06	50e-06	1000e-06	m	
micro_mg_effi_factor		Scale effective radius for optics calculation	1.0	0.1	2.0	-	
micro_mg_homog_size		Homogeneous freezing ice particle size	25e-6	10e-6	200e-6	m	
micro_mg_iaccr_factor		Scaling ice/snow accretion	1.0	0.2	1.0	-	
micro_mg_max_nicons		Maximum allowed ice number concentration	100e6	1e5	10,000e6	# $\text{kg}^{-1}$	
micro_mg_vtrmi_factor		Ice fall speed scaling	1.0	0.2	5.0	$\text{m s}^{-1}$	
<i>Aerosol</i>	microp_aero_npccn_scale	Scale activated liquid number	1	0.33	3	-	
	microp_aero_wsub_min	Min subgrid velocity for liq activation	0.2	0	0.5	$\text{m s}^{-1}$	
	microp_aero_wsub_scale	Subgrid velocity for liquid activation scaling	1	0.1	5	-	
	microp_aero_wsubi_min	Min subgrid velocity for ice activation	0.001	0	0.2	$\text{m s}^{-1}$	
	microp_aero_wsubi_scale	Subgrid velocity for ice activation scaling	1	0.1	5	-	
	dust_emis_fact	Dust emission scaling factor	0.7	0.1	1.0	-	
	seasalt_emis_scale	Seasalt emission scaling factor	1.0	0.5	2.5	-	
	sol_factb_interstitial	Below cloud scavenging of interstitial modal aerosols	0.1	0.1	1	-	
sol_factic_interstitial	In-cloud scavenging of interstitial modal aerosols	0.4	0.1	1	-		
<i>ZM</i>	cldfrc_dp1	Parameter for deep convection cloud fraction	0.1	0.05	0.25	-	
	cldfrc_dp2	Parameter for deep convection cloud fraction	500	100	1,000	-	
	zmconv_c0_lnd	Convective auto-conversion over land	0.0075	0.002	0.1	$\text{m}^{-1}$	
	zmconv_c0_ocn	Convective auto-conversion over ocean	0.03	0.02	0.1	$\text{m}^{-1}$	
	zmconv_capelmt	Triggering threshold for ZM convection	70	35	350	$\text{J kg}^{-1}$	
	zmconv_dmpdz	Entrainment parameter	-1.0e-3	-2.0e-3	-2.0e-4	$\text{m}^{-1}$	
	zmconv_ke	Convective evaporation efficiency	5.0e-6	1.0e-6	1.0e-5	KE	
	zmconv_ke_lnd	Convective evaporation efficiency over land	1.0e-5	1.0e-6	1.0e-5	KE	
	zmconv_momcd	Efficiency of pressure term in ZM downdraft CMT	0.7	0	1	-	
	mconv_momcu	Efficiency of pressure term in ZM updraft CMT	0.7	0	1	-	
	zmconv_num_cin	Allowed number of negative buoyancy crossings	1	1	5	-	
	zmconv_tiedke_add	Convective parcel temperature perturbation	0.5	0	2	K	

689 It is also clear that better constraining the warm rain process and ice processes  
690 in the atmosphere are critical for narrowing the uncertainty in climate forcing and  
691 feedbacks.

## 692 Appendix A Parameters

693 Table A1, based on Eidhammer et al. (2024), describes the parameters used in  
694 the PPE by physical parameterization, with formal name, description, default value,  
695 minimum, maximum and units.

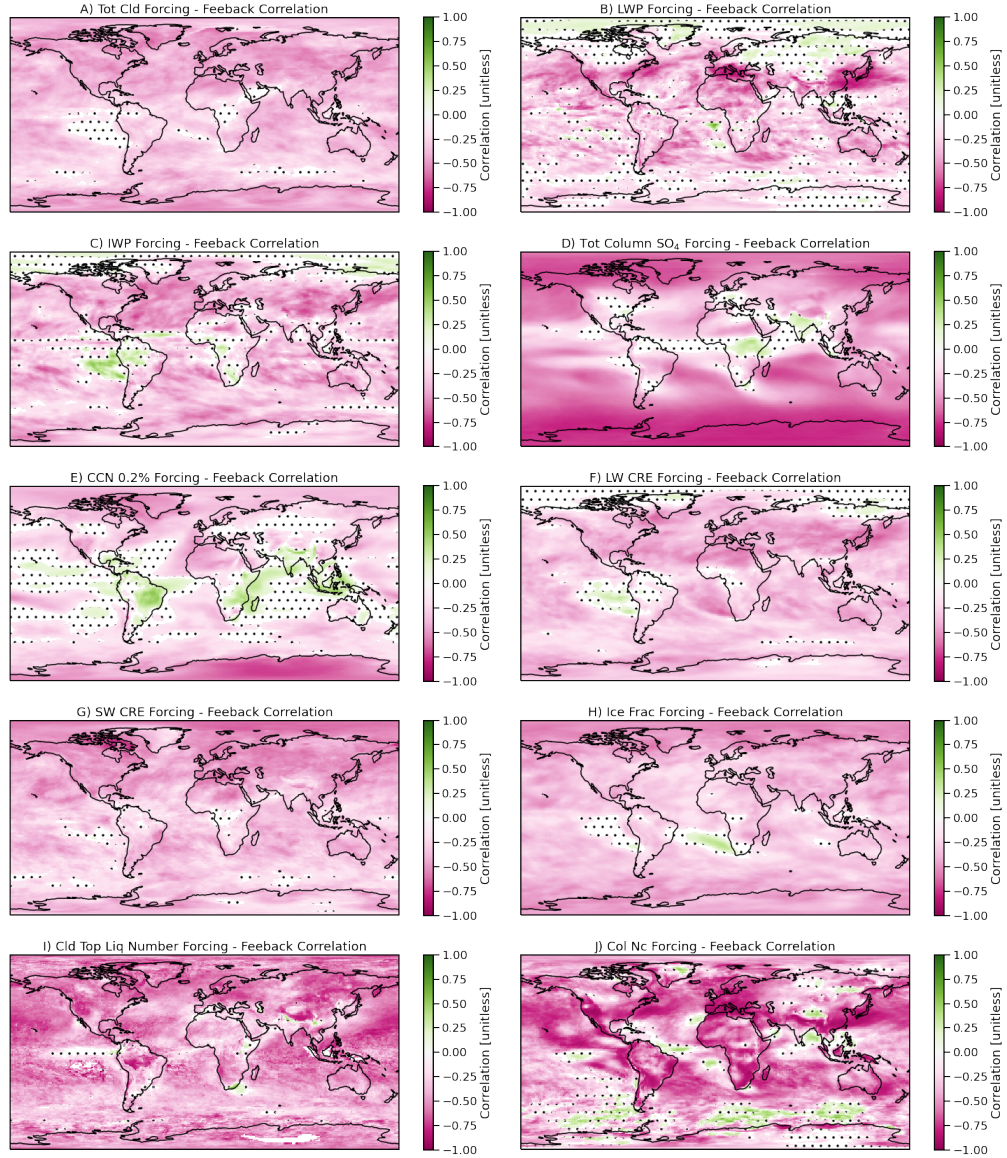


**Figure B1.** Map of linear correlation coefficient at each point between differences in variables due to forcing (PD-PI) and feedbacks (SST+4K - PD) for different variables. Non-significant points are stippled. Significance is determined by a bootstrap fit.

696 **Appendix B Supplementary Figures**

697 **Appendix C Open Research**

698 Model output used is described by Eidhammer et al. (2024), and is available  
699 the Climate Data Gateway at NCAR (<https://doi.org/10.26024/bzne-yf09>)

700 Analysis code used in this work is available on zenodo at  
701 <https://zenodo.org/doi/10.5281/zenodo.10553073>

702 **Acknowledgments**

703 NCAR is supported by the U. S. National Science Foundation. The Pacific North-  
704 west National Laboratory is operated for the U.S. Department of Energy by the  
705 Battelle Memorial Institute under contract DE-AC05-76RL01830.

706 **References**

- 707 Abdul-Razzak, H., & Ghan, S. J. (2002). A parameterization of aerosol activation 3.  
708 Sectional Representation. *J. Geophys. Res.*, *107*(D3), AAC 1-1 – AAC 1-6. doi: 10  
709 .1029/2001JD000483
- 710 Ackerman, A. S., Kirkpatrick, M. P., Stevens, D. E., & Toon, O. B. (2004). The im-  
711 pact of humidity above stratiform clouds on indirect aerosol climate forcing. *Na-  
712 ture*, *432*, 1014–1017.
- 713 Albrecht, B. A. (1989). Aerosols, Cloud Microphysics and Fractional Cloudiness.  
714 *Science*, *245*, 1227–1230. doi: 10.1126/science.245.4923.1227
- 715 Bellouin, N., Quaas, J., Gryspeerdt, E., Kinne, S., Stier, P., Watson-Parris,  
716 D., . . . Stevens, B. (2020). Bounding Global Aerosol Radiative Forcing  
717 of Climate Change. *Reviews of Geophysics*, *58*(1), e2019RG000660. doi:  
718 10.1029/2019RG000660
- 719 Carslaw, KS., Lee, LA., Reddington, CL., Pringle, KJ., Rap, A., Forster, PM., . . .  
720 others (2013). Large contribution of natural aerosols to uncertainty in indirect  
721 forcing. *Nature*, *503*(7474), 67–71. doi: 10.1038/nature12674
- 722 Cess, R. D., et al. (1989). Interpretation of Cloud-Climate Feedback as Produced by  
723 14 Atmospheric General Circulation Models. *Science*, *245*, 513–516.
- 724 Eidhammer, T., Gettelman, A., Thayer-Calder, K., Watson-Parris, D., Elsaesser, G.,  
725 Morrison, H., . . . McCoy, D. (2024, January). An Extensible Perturbed Parameter  
726 Ensemble (PPE) for the Community Atmosphere Model Version 6. *EGUsphere*,  
727 1–27. doi: 10.5194/egusphere-2023-2165
- 728 Forster, P. M., Andrews, T., Good, P., Gregory, J. M., Jackson, L. S., & Zelinka,  
729 M. (2013, February). Evaluating adjusted forcing and model spread for historical  
730 and future scenarios in the CMIP5 generation of climate models: FORCING IN  
731 CMIP5 CLIMATE MODELS. *Journal of Geophysical Research: Atmospheres*,  
732 *118*(3), 1139–1150. doi: 10.1002/jgrd.50174
- 733 Gettelman, A., Gagne, D. J., Chen, C.-C., Christensen, M. W., Lebo, Z. J., Mor-  
734 rison, H., & Gantos, G. (2021). Machine Learning the Warm Rain Process.  
735 *Journal of Advances in Modeling Earth Systems*, *13*(2), e2020MS002268. doi:  
736 10.1029/2020MS002268
- 737 Gettelman, A., Hannay, C., Bacmeister, J. T., Neale, R. B., Pendergrass, A. G.,  
738 Danabasoglu, G., . . . Mills, M. J. (2019). High Climate Sensitivity in the Com-  
739 munity Earth System Model Version 2 (CESM2). *Geophysical Research Letters*,  
740 *46*(14), 8329–8337. doi: 10.1029/2019GL083978
- 741 Gettelman, A., Lin, L., Medeiros, B., & Olson, J. (2016, June). Climate Feed-  
742 back Variance and the Interaction of Aerosol Forcing and Feedbacks. *J. Climate*,  
743 *29*(18), 6659–6675. doi: 10.1175/JCLI-D-16-0151.1

- 744 Gettelman, A., Morrison, H., Santos, S., Bogenschutz, P., & Caldwell, P. M. (2015).  
 745 Advanced Two-Moment Bulk Microphysics for Global Models. Part II: Global  
 746 Model Solutions and Aerosol–Cloud Interactions. *J. Climate*, *28*(3), 1288–1307.  
 747 doi: 10.1175/JCLI-D-14-00103.1
- 748 Gettelman, A., & Sherwood, S. C. (2016, October). Processes Responsible for Cloud  
 749 Feedback. *Curr Clim Change Rep*, 1–11. doi: 10.1007/s40641-016-0052-8
- 750 Golaz, J.-C., Larson, V. E., & Cotton, W. R. (2002). A PDF-Based Model for  
 751 Boundary Layer Clouds. Part II: Model Results. *J. Atmos. Sci.*, *59*, 3552–3571.
- 752 Guo, H., Golaz, J.-C., Donner, L. J., Wyman, B., Zhao, M., & Ginoux, P. (2015,  
 753 May). CLUBB as a unified cloud parameterization: Opportunities and challenges.  
 754 *Geophys. Res. Lett.*, 2015GL063672. doi: 10.1002/2015GL063672
- 755 Guo, Z., Wang, M., Qian, Y., Larson, V. E., Ghan, S., Ovchinnikov, M., . . . Zhou,  
 756 T. (2015, July). Parametric behaviors of CLUBB in simulations of low clouds in  
 757 the Community Atmosphere Model (CAM). *J. Adv. Model. Earth Syst.*, n/a-n/a.  
 758 doi: 10.1002/2014MS000405
- 759 Jing, X., Suzuki, K., & Michibata, T. (2019, July). The Key Role of Warm Rain  
 760 Parameterization in Determining the Aerosol Indirect Effect in a Global Climate  
 761 Model. *Journal of Climate*, *32*(14), 4409–4430. doi: 10.1175/JCLI-D-18-0789.1
- 762 Khairoutdinov, M. F., & Kogan, Y. (2000). A new cloud physics parameterization in  
 763 a large-eddy simulation model of marine stratocumulus. *Monthly Weather Review*,  
 764 *128*, 229–243.
- 765 Kiehl, J. T. (2007, November). Twentieth century climate model response  
 766 and climate sensitivity. *Geophys. Res. Lett.*, *34*(22), L22710. doi: 10.1029/  
 767 2007GL031383
- 768 Lee, L. A., Reddington, C. L., & Carslaw, K. S. (2016, May). On the relation-  
 769 ship between aerosol model uncertainty and radiative forcing uncertainty. *PNAS*,  
 770 *113*(21), 5820–5827. doi: 10.1073/pnas.1507050113
- 771 Loeb, N. G., Doelling, D. R., Wang, H., Su, W., Nguyen, C., Corbett, J. G., . . .  
 772 Kato, S. (2018). Clouds and the Earth’s Radiant Energy System (CERES) En-  
 773 ergy Balanced and Filled (EBAF) Top-of-Atmosphere (TOA) Edition-4.0 Data  
 774 Product. *J. Climate*, *31*(2), 895–918. doi: 10.1175/JCLI-D-17-0208.1
- 775 Qian, Y., Wan, H., Yang, B., Golaz, J.-C., Harrop, B., Hou, Z., . . . Zhang, K.  
 776 (2018). Parametric Sensitivity and Uncertainty Quantification in the Version 1  
 777 of E3SM Atmosphere Model Based on Short Perturbed Parameter Ensemble Sim-  
 778 ulations. *Journal of Geophysical Research: Atmospheres*, *123*(23), 13,046–13,073.  
 779 doi: 10.1029/2018JD028927
- 780 Regayre, L. A., Deaconu, L., Grosvenor, D. P., Sexton, D. M. H., Symonds,  
 781 C., Langton, T., . . . Carslaw, K. S. (2023, August). Identifying climate  
 782 model structural inconsistencies allows for tight constraint of aerosol radia-  
 783 tive forcing. *Atmospheric Chemistry and Physics*, *23*(15), 8749–8768. doi:  
 784 10.5194/acp-23-8749-2023
- 785 Sherwood, S., Webb, M. J., Annan, J. D., Armour, K. C., Forster, P. M., Har-  
 786 greaves, J. C., . . . Zelinka, M. D. (2020). An assessment of Earth’s climate  
 787 sensitivity using multiple lines of evidence. *Reviews of Geophysics*, *58*(n/a),  
 788 e2019RG000678. doi: 10.1029/2019RG000678
- 789 Sherwood, S. C., Bony, S., & Dufresne, J.-L. (2014, January). Spread in model cli-  
 790 mate sensitivity traced to atmospheric convective mixing. *Nature*, *505*(7481), 37–  
 791 42. doi: 10.1038/nature12829
- 792 Smith, C. J., Kramer, R. J., Myhre, G., Alterskjær, K., Collins, W., Sima, A., . . .  
 793 Forster, P. M. (2020, January). Effective radiative forcing and adjustments in  
 794 CMIP6 models. *Atmospheric Chemistry and Physics Discussions*, 1–37. doi:  
 795 10.5194/acp-2019-1212
- 796 Soden, B. J., Held, I. M., Colman, R., Shell, K. M., Kiehl, J. T., & Shields, C. A.  
 797 (2008). Quantifying Climate Feedbacks Using Radiative Kernels. *J. Climate*,

- 798 21(14), 3504–3520. doi: 10.1175/2007JCLI2110.1
- 799 Summary for Policymakers. (2021). In Intergovernmental Panel on Climate Change  
800 (IPCC) (Ed.), *Climate Change 2021 – The Physical Science Basis: Working*  
801 *Group I Contribution to the Sixth Assessment Report of the Intergovernmental*  
802 *Panel on Climate Change* (pp. 3–32). Cambridge: Cambridge University Press.  
803 doi: 10.1017/9781009157896.001
- 804 Twomey, S. (1974). Pollution and the planetary albedo. *Atmospheric Environment*  
805 (1967), 8(12), 1251–1256.
- 806 Watson-Parris, D., & Smith, C. J. (2022, December). Large uncertainty in future  
807 warming due to aerosol forcing. *Nat. Clim. Chang.*, 12(12), 1111–1113. doi: 10  
808 .1038/s41558-022-01516-0
- 809 Watson-Parris, D., Williams, A., Deaconu, L., & Stier, P. (2021, December). Model  
810 calibration using ESEm v1.1.0 – an open, scalable Earth system emulator. *Geosci-*  
811 *entific Model Development*, 14(12), 7659–7672. doi: 10.5194/gmd-14-7659-2021
- 812 Zelinka, M., Klein, S., & Hartmann, D. (2012). Computing and partitioning cloud  
813 feedbacks using cloud property histograms. Part I: Cloud radiative kernels. *J. Cli-*  
814 *mate*, 25(11), 3715–3735.
- 815 Zhang, G. J., & McFarlane, N. A. (1995). Sensitivity of climate simulations to the  
816 parameterization of cumulus convection in the Canadian Climate Center general  
817 circulation model. *Atmos. Ocean*, 33, 407–446.
- 818 Zhang, H., Wang, M., Guo, Z., Zhou, C., Zhou, T., Qian, Y., . . . Gettelman, A.  
819 (2018). Low-Cloud Feedback in CAM5-CLUBB: Physical Mechanisms and Param-  
820 eter Sensitivity Analysis. *Journal of Advances in Modeling Earth Systems*, 10(11),  
821 2844–2864. doi: 10.1029/2018MS001423



# The Interaction Between Climate Forcing and Feedbacks

A. Gettelman<sup>1\*</sup>, T. Eidhammer<sup>2</sup>, M. L. Duffy<sup>2</sup>, D. T. McCoy<sup>3</sup>, C. Song<sup>3</sup>, D.  
Watson-Parris<sup>4</sup>

<sup>1</sup>Pacific Northwest National Laboratory, Richland, WA, USA

<sup>2</sup>NSF National Center for Atmospheric Research, Boulder, CO, USA

<sup>3</sup>Department of Atmospheric Sciences, University of Wyoming, Laramie, WY, USA

<sup>4</sup>University of California San Diego, La Jolla, CA, USA

## Key Points:

- Parametric uncertainty of Aerosol Forcing and Cloud Feedbacks are large
- Aerosol Forcing and Cloud Feedbacks are related through cloud processes and depend on the mean state of clouds
- Warm rain formation and ice processes are critical sensitivities that couple forcing and feedback

---

\*Formerly at NCAR

Corresponding author: Andrew Gettelman, [andrew.gettelman@pnnl.gov](mailto:andrew.gettelman@pnnl.gov)

**Abstract**

A Perturbed Parameter Ensemble (PPE) with the Community Atmosphere Model version 6 (CAM6) is used to better understand the sensitivity of simulated clouds to both aerosol forcing and cloud feedbacks and the interactions between them. Aerosol forcing through aerosol-cloud interactions is mostly negative (a cooling) due to shortwave radiation, while feedbacks are positive or negative in different regions due to contrasting longwave and shortwave effects. Both forcing and feedbacks are related to the mean climate state. Higher magnitude cloud radiative effects generally mean larger net forcing and larger net feedback. Aerosol forcing is broadly related to the susceptibility of clouds to drop number. Feedbacks are less related to susceptibility, and in different regions. Aerosol forcing and cloud feedbacks are anti-correlated in the CAM6 PPE such that stronger negative forcing is associated with stronger positive feedbacks. Even the processes governing forcing and feedback sensitivity in the PPE are similar. These include the warm rain formation process, ice loss processes and deep convective intensity.

**Plain Language Summary**

A climate model is run many times with modified parameters to see how the parameters affect key aspects of climate change. The paper focuses on two aspects of climate change. First, the cloud response to aerosol particles tends to create a cooling, which partially offsets greenhouse gas warming, but the magnitude of the cooling is not well known. It varies a lot in the model when parameters are changed. Second, the paper examines the cloud response to surface temperature increases, called cloud feedbacks, which are the largest uncertainty in estimating the level of future climate change. Cloud feedbacks are also sensitive to parameters. The results show that the cloud feedbacks and aerosol forcing changes are similar but opposite in the model: the cooling and warming generally increase together. This occurs because they are linked to similar parameters, which indicate sensitivity to critical processes, including how rain forms, and how much ice is in the atmosphere.

**1 Introduction**

Uncertainties in predicting the evolution of the Earth’s climate arise from complexity in the response of the system to anthropogenic radiative forcing, and in the actual level of radiative forcing. The largest uncertainty in the fast response of the climate system is due to the response of clouds to changes in the environment: cloud feedbacks (Gettelman & Sherwood, 2016; S. Sherwood et al., 2020). In addition, the largest uncertainty in anthropogenic radiative forcing is the response of clouds to aerosol perturbations (“Summary for Policymakers”, 2021), often termed Aerosol-Cloud Interactions (ACI). These perturbations are significant but complex (Bellouin et al., 2020). More aerosol particles increase cloud drop numbers and lead to brighter clouds (Twomey, 1974) and potentially longer-lived or thicker clouds (Albrecht, 1989). To assess these processes globally, comprehensive Earth System Models (ESMs) with atmospheric components that include a detailed representation of cloud physics, aerosol physics as well as the interactions between them must be used. The scale of these models, typically 100km horizontal, several hundred meter vertical and 10-30 minute time-steps is too coarse to explicitly resolve key cloud and aerosol processes and therefore introduces very large uncertainties in cloud physics representations.

Much has been written about analyzing model and observational analogs for ACI (Bellouin et al., 2020) and cloud feedbacks (S. Sherwood et al., 2020). Many of the processes which control both ACI and cloud feedback responses are the same. For example, extensive decks of bright liquid cloud at the top of the Planetary Boundary Layer (PBL) over the darker ocean significantly cool the planet by reflecting solar radiation

64 back to space. These clouds exist due to an inversion that traps moist ocean air near the  
 65 surface. The strength of that inversion has been shown to be important in cloud forma-  
 66 tion and maintenance, and how that inversion changes over time is important for how  
 67 clouds will respond to climate change: how thick they are and their propensity to rain  
 68 (S. C. Sherwood et al., 2014). Similarly, aerosols impact clouds by changing the drop pop-  
 69 ulation (more aerosols implies more cloud drops), and how these clouds evolve may also  
 70 be determined by the inversion at the top of the boundary layer (Ackerman et al., 2004),  
 71 and their propensity to rain.

72 Given the importance of cloud processes at the nexus of forcing and feedback, there  
 73 has yet been little work on the interaction between these two effects beyond global means.  
 74 Kiehl (2007) noted that in ESMs there was a relationship across models between the total  
 75 response to climate change and aerosol forcing. This was updated by Forster et al.  
 76 (2013) to show less of an overall relationship. The latest generation of ESMs show no  
 77 relationship (Smith et al., 2020), though Watson-Parris & Smith (2022) find a relation-  
 78 ship between forcing and feedback when constrained on historical surface temperature.  
 79 Gettelman et al. (2016) noted other process level interactions such as an ‘Aerosol Me-  
 80 diated Cloud Feedback’ whereby the mechanism for cloud feedbacks occurs by climate  
 81 change altering aerosol populations. An example noted by Gettelman et al. (2016) is that  
 82 increasing wind speeds over the S. Ocean increase sea spray and cloud drop number, bright-  
 83 ening clouds. This negative cloud feedback is mediated by aerosols. This work will seek  
 84 to examine the relationship between cloud feedbacks and aerosol forcing of clouds in more  
 85 detail by taking advantage of a unique dataset with a modern ESM.

86 Here we will look at the interaction between aerosol forcing and cloud feedbacks  
 87 with a large Perturbed Parameter Ensemble (PPE) from the Community Atmosphere  
 88 Model version 6 (CAM6). The CAM6-PPE uses parameter perturbations to sample model  
 89 structural uncertainty, and produce a wide range of climates resulting from very differ-  
 90 ent adjustments to cloud and aerosol processes. Similar PPEs have been used to under-  
 91 stand model parametric uncertainty (Qian et al., 2018), constrain aerosol forcing (Re-  
 92 gayre et al., 2023; Lee et al., 2016) and low cloud feedbacks (H. Zhang et al., 2018). In  
 93 this work, we will use the CAM6-PPE to better understand the interaction between forc-  
 94 ing and feedback with the goal of understanding critical process and how they interact.

95 Section 2 describes the data and methods to be used. Section 3 presents detailed  
 96 results of forcing sensitivity, feedback sensitivity and their interactions. Discussion is in  
 97 Section 4 and conclusions are in Section 5.

## 98 2 Methods

99 The simulations used for this analysis are from the Community Atmosphere Model  
 100 version 6 (CAM6) PPE. The CAM6-PPE is described in detail by Eidhammer et al. (2024).  
 101 It consists of 263 ensemble members in which latin hypercube sampling is used to mod-  
 102 ify 45 parameters in the microphysics, convection, turbulence and aerosol schemes. Note  
 103 that one of the simulations did not complete, and that two pairs of parameters are var-  
 104 ied together, so effectively 43 parameters are varied. These atmospheric parameters are  
 105 typically the most uncertain in many climate models and contain many variables which  
 106 alter cloud and aerosol processes. Parameter ranges are chosen to be physically plausi-  
 107 ble for each parameter. We also will subset the parameter space based on physically real-  
 108 istic climates as described below. Simulations are run with an atmosphere-land con-  
 109 figuration for 3 years, for Present Day (PD) climatological boundary conditions, repeat-  
 110 ing climatological averaged Sea Surface Temperatures (SSTs) each year. In addition, two  
 111 other additional sets of 263 simulations are run with the same parameters. In one set,  
 112 SSTs are uniformly increased by 4K to assess the cloud response to warming, following  
 113 Cess et al. (1989), termed SST4K. In the other set of 263 simulations, PD SSTs and the

114 same boundary conditions are used, except aerosol emissions are set to 1850 ‘Pre-Industrial’  
 115 levels (hereafter PI simulations).

116 The principle we will exploit is that different parameters modify different specific  
 117 processes in the cloud physics (e.g., frequency or intensity of deep convection, rain for-  
 118 mation processes, freezing and ice nucleation processes, etc). The changing balance of  
 119 processes alters the climate. First, we will use the PPE to understand if forcing and feed-  
 120 backs depend on the base climate state of those simulations. Then we will use the PPE  
 121 to understand which parameters give rise to variations and sensitivity in forcing and feed-  
 122 backs. Finally we will explore the relationship between aerosol forcing and cloud feed-  
 123 backs. The parameters map to the underlying physical mechanisms. While the param-  
 124 eters in the PPE are model specific, the process representations are very similar to (or  
 125 even the same as) other modern ESMs. Thus the results may have more general applica-  
 126 tion since the relationships we elucidate are well founded in processes, not just in pa-  
 127 rameters.

128 As described by Gettelman et al. (2019), the aerosol induced cloud forcing (ACI,  
 129 or just ‘forcing’) is defined as the change in Cloud Radiative Effect (CRE) between sim-  
 130 ulations with Present Day (PD) and Pre-Industrial (PI) aerosol emissions. Typically we  
 131 are concerned with the Shortwave (SW) cloud forcing (SW ACI =  $\Delta\text{SWCRE}$ ), but there  
 132 is also Longwave (LW) forcing (LW ACI =  $\Delta\text{LWCRE}$ ). Cloud feedbacks are defined as  
 133 the kernel adjusted cloud feedbacks (Soden et al., 2008) using the kernels from Zelinka  
 134 et al. (2012) as applied by Duffy et al (2023). The kernels adjust LW and SW CRE to  
 135 remove effects of changes to the atmospheric temperature and water vapor, and the ef-  
 136 fect of a changing surface albedo.

137 To constrain the simulations for fidelity against observations we also compare them  
 138 to observations of radiative fluxes and clouds from the CERES (Clouds and the Earth’s  
 139 Radiant Energy System) satellite Energy Balanced and Filled (EBAF) products (Loeb  
 140 et al., 2018).

141 Finally, for analysis of the simulations and sensitivity to parameters (and hence pro-  
 142 cesses), we use Gaussian process emulators (Watson-Parris et al., 2021) trained on the  
 143 PPE ensemble to determine the sensitivity of forcing and feedbacks to each parameter.

### 144 **3 Results**

145 First we illustrate the parametric uncertainty (i.e. the PPE spread) of feedbacks  
 146 and forcing (Section 3.1). Then we examine how aerosol forcing is related to the mean  
 147 state and to different parameters, which are both indicative of specific processes (Sec-  
 148 tion 3.2). Next we will do the same analysis for cloud feedbacks (Section 3.3) and then  
 149 we will explore the interaction between aerosol forcing and cloud feedbacks (Section 3.4)

#### 150 **3.1 PPE Mean and Spread**

151 Figure 1 illustrates the global mean change in SW (Figure 1A), LW (Figure 1B)  
 152 net TOA radiation (Figure 1C) and change in total cloud fraction (Figure 1D) for the  
 153 263 PPE members. The forcing in Figure 1A and B is the change in CRE, while the feed-  
 154 backs are the kernel-adjusted feedbacks. The spread estimates the parametric uncertainty  
 155 in forcing and feedback.

156 The spread in net ACI forcing is only  $\sim 2\text{Wm}^{-2}$ , because the global mean SW and  
 157 LW are of opposite sign and are strongly anti-correlated, resulting in a fairly narrow range  
 158 in total net TOA change (Figure 1C). The anti-correlation is not as strong for cloud feed-  
 159 backs where the SW and LW components are both positive in most ensemble members.  
 160 Note that the TOA change for feedbacks includes a significant change NOT associated  
 161 with clouds, but rather for the clear sky (due to a warmer surface). There is also far less

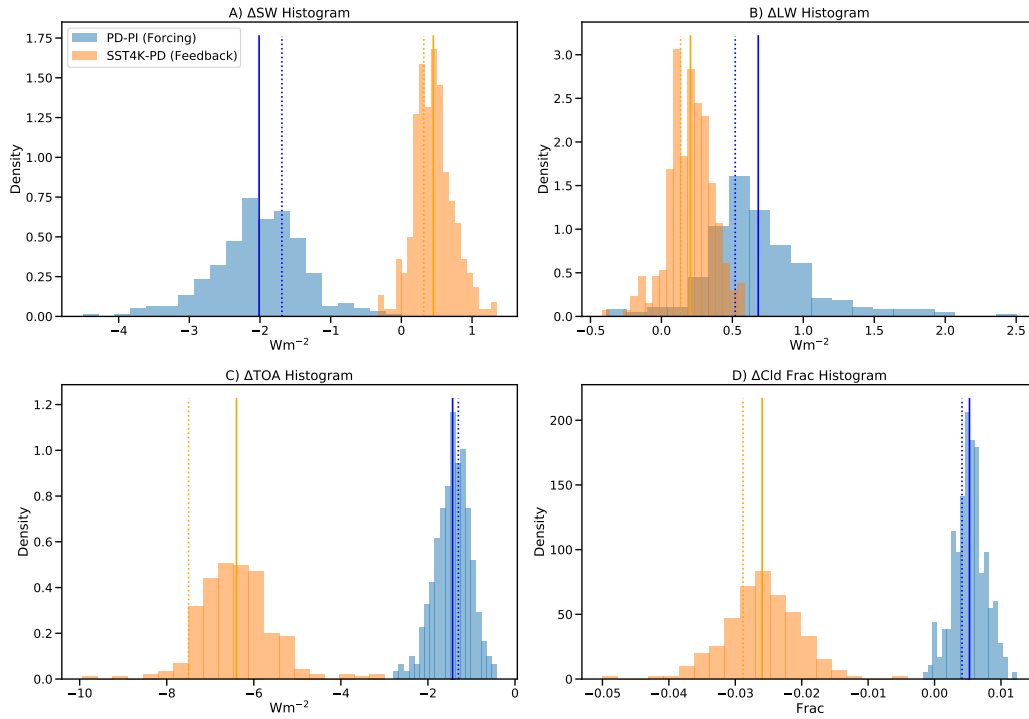


**Figure 1.** Histograms of global A) TOA SW change, B) TOA LW change, C) Net TOA change and D) Cloud Fraction change for Present Day - Pre-Industrial (Aerosol Forcing, Blue) and SST+4K - Present Day (Feedback response, orange). Forcing is change in TOA Cloud Radiative Effect (CRE) and feedbacks are the kernel adjusted cloud feedbacks as described in the text. Solid lines are the mean of the distribution, dotted lines are results with the default CAM6 parameter settings.

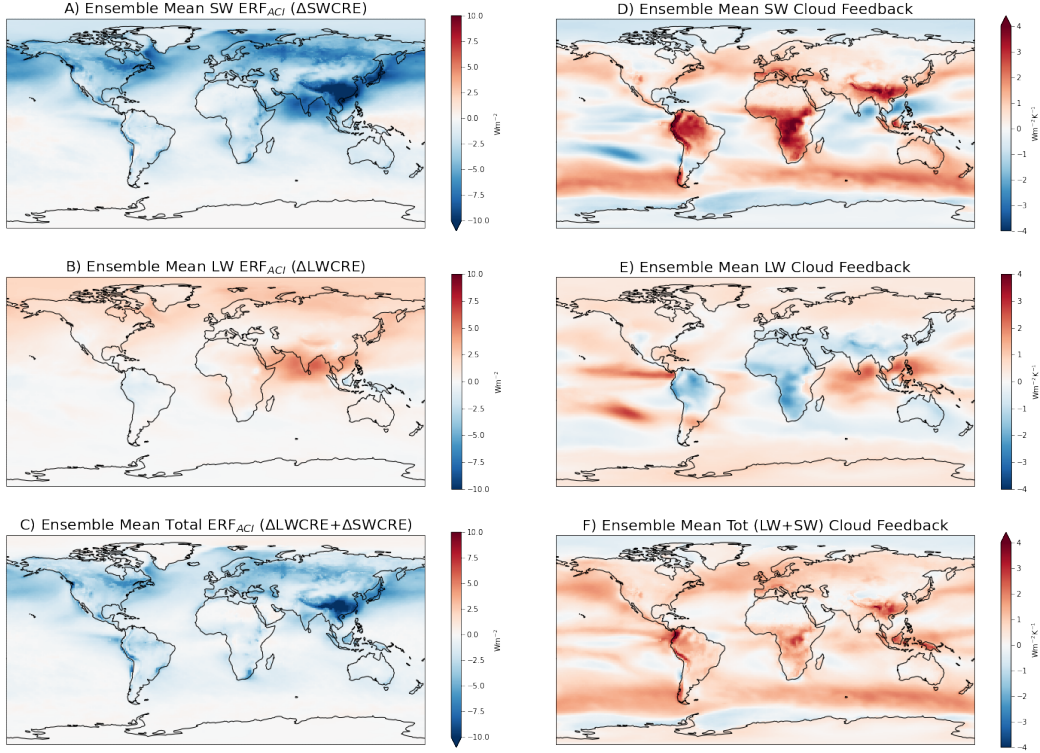


**Figure 2.** PPE ensemble means of Aerosol Cloud Interactions (Forcing) for the A) SW, B) LW and C) Total (LW+SW) as well as Cloud Feedbacks for the D) SW, E) LW and F) Total (LW+SW).

162 cloud fraction change (Figure 1D), both the mean and PPE spread, for aerosol forcing  
 163 than for cloud feedbacks.

164 Figure 2 illustrates the ensemble mean cloud forcing (ACI) as the change in CRE  
 165 between present (PD) and pre-industrial (PI) simulations for the SW (Figure 2A), LW  
 166 (Figure 2B) and Net (Figure 2C). Figure 1A and B indicate that for both forcing and  
 167 feedback, the ensemble mean (solid vertical lines in Figure 1) is similar to the default  
 168 (dotted vertical lines in Figure 1). We have verified that this is qualitatively the case for  
 169 maps as well by mapping the default case individually: the ensemble mean just provides  
 170 better statistics to smooth out noise in the short 3 year simulations. ACI is strongest  
 171 in the SW, concentrated in the N. Hemisphere, with the largest values over oceans down-  
 172 wind of source regions (N. Pacific, N. Atlantic and N. Indian Ocean), and a strong SW  
 173 signal over China. SW is larger than LW, with the largest LW effect near India, due per-  
 174 haps to aerosol effects on tropical ice clouds, which mostly cancel the SW effects. There  
 175 is virtually no aerosol forcing in the S. Hemisphere. SW and LW are of opposite sign in  
 176 most regions, but there is not a 1:1 correlation in the magnitude. Net ACI becomes weakly  
 177 positive over the Arctic ocean due to lack of SW cooling from clouds over a bright ice-  
 178 covered surface.

179 Figure 2 also illustrates the ensemble mean cloud feedbacks for the SW (Figure 2D),  
 180 LW (Figure 2E) and total (Figure 2F). As with forcing, the ensemble mean is qualita-  
 181 tively similar to the default case. There are significant positive (and net) SW Cloud Feed-  
 182 backs over tropical continents in convective regions, as well as in the mid-latitude storm

183 tracks in both hemispheres. In the tropical convecting regions, the two mechanisms con-  
 184 trolling cloud feedbacks are the increase in altitude of high clouds and a reduction in anvil  
 185 cloud area (S. Sherwood et al., 2020). The increase in the altitude of high clouds is a pos-  
 186 itive LW cloud feedback (the red area over the tropical west Pacific/Indian ocean). The  
 187 reduction in anvil cloud area should have competing LW positive and SW negative ef-  
 188 fects as illustrated in Figure 2D and Figure 2E. The net cloud feedbacks are positive,  
 189 except over polar regions with frequent sea-ice coverage.

### 190 3.2 Forcing

191 We start by focusing on the aerosol forcing, again defining ACI as the change in  
 192 CRE between PD and PI simulations (either LW, SW or Net=SW+LW). First we at-  
 193 tempt to understand whether ACI is related to properties of the mean state climate. Aerosol  
 194 forcing is a series of processes that might be reflected in correlations between the forc-  
 195 ing and the mean state. Increases in emissions increase aerosols (largely sulfate) which  
 196 increase the Cloud Condensation Nuclei (CCN) and Ice Nuclei (IN), and hence cloud drop  
 197 and ice crystal number. This might affect cloud fraction and/or cloud mass (Ice Water  
 198 Path [IWP] and Liquid Water Path [LWP]). The mean state might make the clouds more  
 199 or less ‘susceptible’ to these changes. For example: higher base state sulfur and higher  
 200 CCN and/or drop number for PI conditions might make a perturbation to sulfur less im-  
 201 portant. Or having more clouds (either larger negative SW CRE or higher cloud frac-  
 202 tion) might result in more ‘marginal’ clouds that could be affected by ACI.

203 We focus on the mean state climate of the PI simulations. In the present day, some  
 204 of the correlation between mean state and aerosols is due to anthropogenic aerosol forc-  
 205 ing, and we are interested in the ‘unaffected’ state. We start with correlations of global  
 206 mean state properties with global mean ACI. Figure 3 illustrates that the magnitude of  
 207 globally averaged Net ACI is correlated with several properties of the mean state: To-  
 208 tal Cloud Fraction (Figure 3A), Sulfate ( $\text{SO}_4$ ) Burden (Figure 3B), CCN at 0.2% super-  
 209 saturation (Figure 3C) and Cloud Top Drop Number ( $N_c$ , Figure 3D). We looked at sev-  
 210 eral PI mean state properties not strongly correlated with global mean forcing: LWP and  
 211 IWP. Column drop number is similar to cloud top drop number (Figure 3D).

212 The orange points are the sub-set of simulations whose mean annual value of SW  
 213 CRE is within  $\pm 5 \text{ Wm}^{-2}$  of the observed CERES EBAF annual global mean ( $-45.3 \text{ Wm}^{-2}$ ).  
 214 This constraint is a gross measure of whether the ‘climate’ in any simulation (specifically  
 215 the cloud climatology) is similar to present day observations. The slopes (orange lines)  
 216 are qualitatively similar (with lower correlation) if we consider only the constrained data  
 217 rather than all the data for most of the variables except cloud coverage. The red dot is  
 218 the ‘default’ parameter set for CAM6.

219 Figure 3A indicates that as total mean state cloud fraction increases, net ACI in-  
 220 creases in magnitude (negative). This implies more cloudiness may mean more marginal  
 221 or thin clouds that are more susceptible to changes. As mean PI sulfate burden increases,  
 222 net ACI forcing is reduced (lower magnitude) (Figure 3B) with a similar relationship for  
 223 CCN (Figure 3C). These both indicate that PI environments with higher sulfur and more  
 224 CCN are less sensitive to additional sulfur, a result noted in other models (Carslaw et  
 225 al., 2013). There is also a relationship between cloud top drop number and Net ACI forc-  
 226 ing (Figure 3D) whereby higher PI drop numbers give rise to larger forcing, which seems  
 227 to work in the opposite way to more PI CCN. In general, these correlations using global  
 228 means are quite low. SW ACI only correlations are a little stronger (not shown). The  
 229 CERES constrained simulations have similar correlations to all simulations, with lower  
 230 magnitude (except for total cloud coverage, where constrained simulations have a smaller  
 231 correlation of the opposite sign).

232 To understand these relationships better, we can map the correlations at each point  
 233 to determine what regimes are important. Figure 4 illustrates the same relationships as

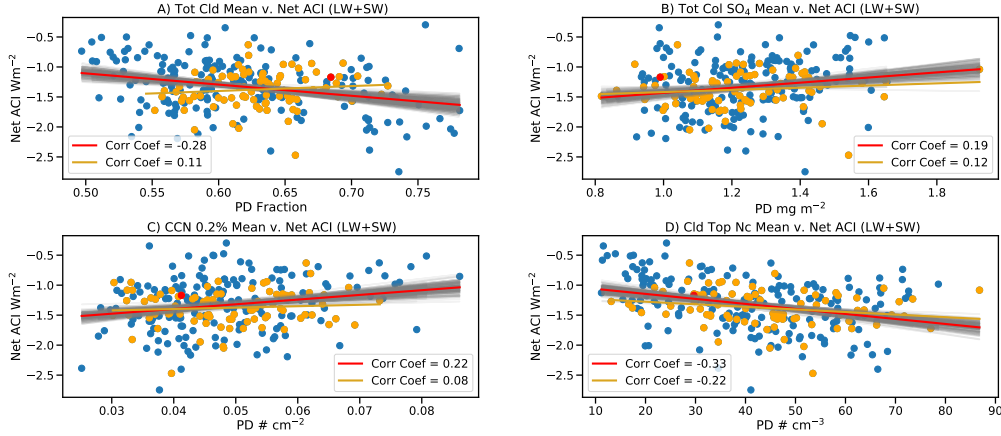


**Figure 3.** Global correlations between mean state for A) Total Cloud Fraction, B) Total Column Sulfate, C) CCN at 0.2% supersaturation and D) Cloud top drop number with Pre-Industrial aerosols (horizontal axis and the Net ACI forcing (PD-PI, vertical axis). Blue points: all simulations, red line, linear regression. Orange indicates those 87 simulations whose global mean PD Shortwave Cloud Radiative Effect is within  $\pm 5 \text{ Wm}^{-2}$  of the CERES EBAF global annual mean. Orange line is the linear regression of these points. Default CAM6 parameters shown as the red dot.

234 Figure 3 using PI mean climate and aerosol net forcing (PD - PI change in SW+LW CRE)  
 235 but now as a map at each point. An expanded set of mean state indicators are illustrated.  
 236 The linear correlation coefficient at each point is plotted, with the stippling indicating  
 237 regions which are NOT significant based on a bootstrap fit. Maps are similar if only the  
 238 simulations constrained by the observed satellite SW CRE climatology are used, but with  
 239 less significance (similar to Figure 3). We have examined the LW and SW components  
 240 separately, and in general net ACI forcing is dominated by the SW as seen in Figure 2.

241 The weak global correlations in Figure 3 belie stronger regional correlations, which  
 242 can be of different sign between regions and hence cloud types. In many cases there are  
 243 opposite sign correlations over the Arctic ocean where the SW ACI goes to zero (Fig-  
 244 ure 2A) and the positive LW ACI component dominates (Figure 2C). The opposite sign  
 245 correlation is due to the local ACI being dominated by the LW and changing sign. There  
 246 is a strong positive correlation between the net ACI forcing (net ACI =  $\Delta \text{SWCRE} +$   
 247  $\Delta \text{LWCRE}$ ) and the PI SW Cloud Radiative Effect (SW CRE, Figure 4G) at low lati-  
 248 tudes over the ocean. Stronger negative PI mean state SW CRE in the subtropics is as-  
 249 sociated with stronger negative ACI. Similar patterns of opposite sign (since SW CRE  
 250 is negative) are seen for total cloud coverage (Figure 4A), LWP (Figure 4B), LW CRE  
 251 (Figure 4F), cloud top liquid number (Figure 4I) and column drop number (Figure 4J).  
 252 Column drop number is integrated to the top of the atmosphere. CCN effects (fewer CCN  
 253 in PI result in stronger magnitude ACI) are mostly positive throughout the N. Hemi-  
 254 sphere. (Figure 4E). Stronger positive ACI at high latitudes (dominated by the LW) is  
 255 associated with more ice fraction at high latitudes (Figure 4H).

256 Figure 3 indicates that stronger magnitude net ACI is associated with PI climates  
 257 that have radiatively thicker sub-tropical liquid clouds. These ‘radiatively thicker’ clouds  
 258 have larger magnitude cloud radiative effect due to being more extensive, with higher  
 259 drop number and LWP. Stronger net ACI can also be associated with less PI CCN at  
 260 middle and high latitudes and less sulfate over the land regions in mid-latitudes. To some  
 261 extent these effects will offset (higher PI CCN should lead to higher Nc), but the effects



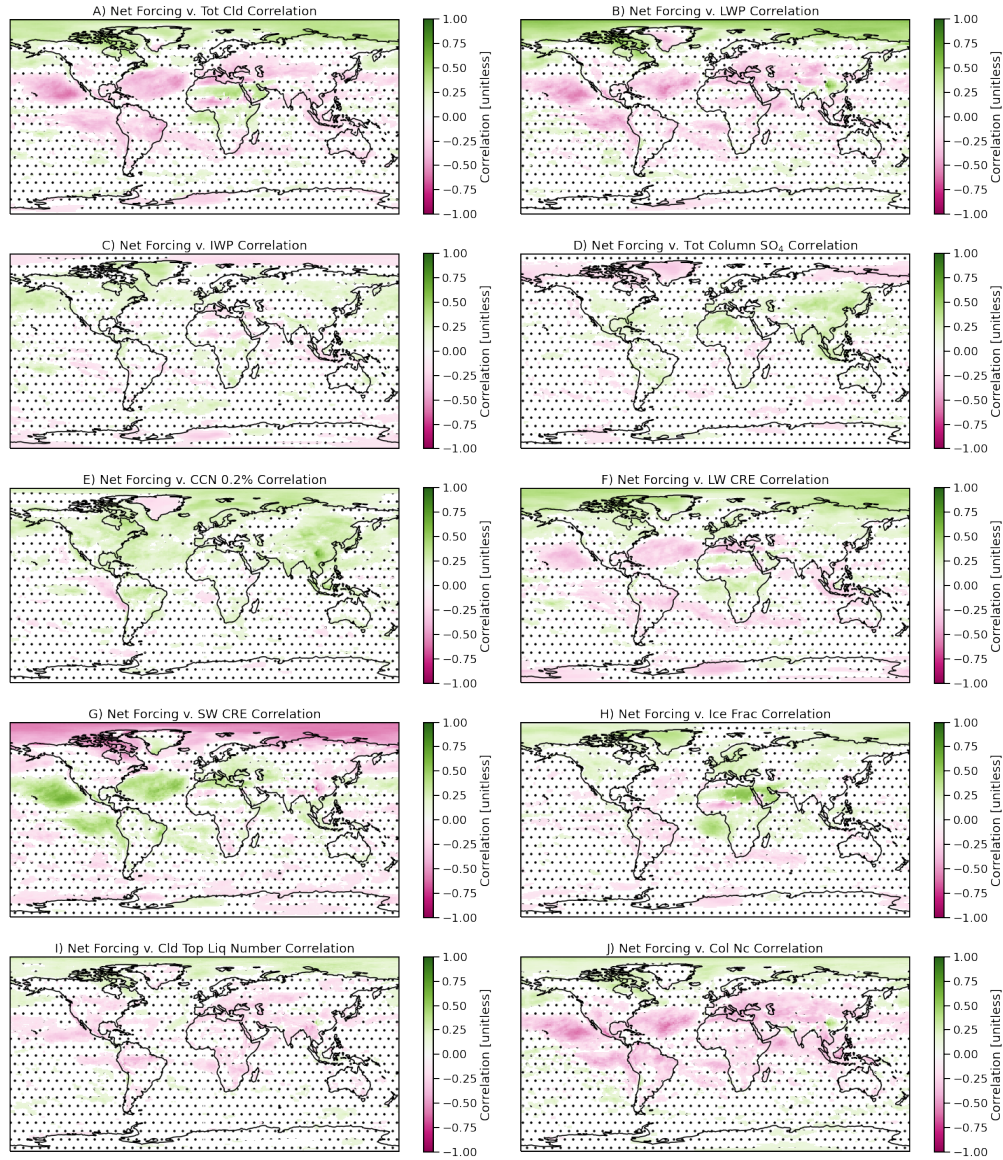


**Figure 4.** Map of linear correlation coefficient at each point between mean state in PI and the ACI forcing (PD-PI) for different variables. Non-significant points are stippled. Significance is determined by a bootstrap fit.

262 occur in different regions (subtropical clouds, and more mid-latitude for CCN). The sub-  
 263 tropical regions noted are regions where there is very little cloud, so simulations with more  
 264 extensive cloud in these marginal regions, along with less PI CCN (and sulfur) to main-  
 265 tain clouds in mid-latitudes, yield larger net ACI response. The strong opposite sign of  
 266 the high latitude correlations as noted are likely due more to the change in ACI com-  
 267 ponents over the Arctic than changes in the mean state.

268 We can also look for which parameters give rise to the largest sensitivity in changes  
 269 between pre-industrial and present day. Parameters affect particular processes, so we can  
 270 use parameter sensitivity as a means to focus on particular processes or sets of processes.  
 271 Since the PPE spans parametric uncertainty, this analysis identifies the sensitivity of pro-  
 272 cesses to parametric uncertainty, and the impact of those processes on forcing and feed-  
 273 back. For example, parameters for auto-conversion and accretion alter the rain forma-  
 274 tion process which is the main sink for cloud water (regulating LWP).

275 Following Eidhammer et al. (2024), we examine changes in model state (PD - PI)  
 276 as a function of parameter in Figure 5. The parameter values (y-axis) are normalized  
 277 (scaled by the minimum and maximum parameter values) while the differences in the  
 278 outputs (x-axis) are standardized (scaled by the mean and standard deviation of the out-  
 279 put values) and then regression slopes are calculated for global and regionally averaged  
 280 values. Figure 5 illustrates the slopes for the normalized regression. The normalization  
 281 and standardization helps show which parameters drive PD-PI changes in each output.  
 282 Parameters are listed by parameterization and the regressions are calculated for differ-  
 283 ent latitude bands as well as global. There are many commonalities across regions, with  
 284 the exception being that cold cloud parameters are more important in the tropics and  
 285 mixed phase cloud parameters are important in the Arctic. Given that ACI forcing is  
 286 mostly in the N. Hemisphere, we do not expect any strong relationships over the South-  
 287 ern Ocean.

288 Important parameters for ACI changes (PD - PI mean quantities) are concen-  
 289 trated, not surprisingly, in the cloud microphysics and aerosol activation parame-  
 290 terizations since ACI processes trace aerosol changes, effects on cloud drop number  
 291 and cloud microphysical adjustments to drop number perturbations. Total aerosol  
 292 forcing (ACI and direct radiative effects of aerosols) is expressed in the residual  
 293 TOA flux (RESTOM) difference, and the cloud forcing (SW CRE and LW CRE are  
 294 the PD - PI change in these quantities). Important parameters alter both accretion  
 295 (*micro\_mg\_accr\_enhan\_fact*) and auto-conversion (*micro\_mg\_autocon\_lwp\_exp* and  
 296 *micro\_mg\_autocon\_nd\_exp*): the main loss process for cloud liquid water. In the Ar-  
 297 ctic, the threshold size of ice crystals for conversion of ice to snow (*micro\_mg\_dcs*) is  
 298 important for ice cloud effects, including changes in ice cloud mass and the changes  
 299 in both LW and SW CRE (LWCF, SWCF). Ice fall speed (*micro\_mg\_vtrmi\_factor*)  
 300 is also important globally. The scaling of the sub-grid vertical velocity for ice nu-  
 301 cleation (*microp\_aero\_wsubi\_scale*) is important in the tropics and globally for gov-  
 302 erning the ice number and hence the LW and SW radiation. Note that it does not  
 303 impact the net TOA balance change because of the offsetting SW and LW effects.  
 304 The sub-grid vertical velocity for liquid drop activation (*microp\_aero\_wsub\_scale*) is  
 305 also important. Liquid drop activation affect CCN formation. In the mid-latitudes,  
 306 including the regions over the ocean where thicker PI clouds increase ACI magni-  
 307 tude, several of the turbulence parameters from CLUBB are important.

308 To take this a bit further, we can break down some of the key correlations  
 309 in Figure 5 by correlating parameter values and net ACI forcing at each point.  
 310 As in Figure 4, we estimate significant correlations with a bootstrap fit. We then  
 311 determine the global average mean absolute correlation from only the location of  
 312 significant correlations. Figure 6 illustrates the mean absolute correlation for each  
 313 parameter for 6 different forcing and feedback components (different colors): To-  
 314 tal, LW and SW for ACI and Cloud Feedback. The squares in Figure 6 show the

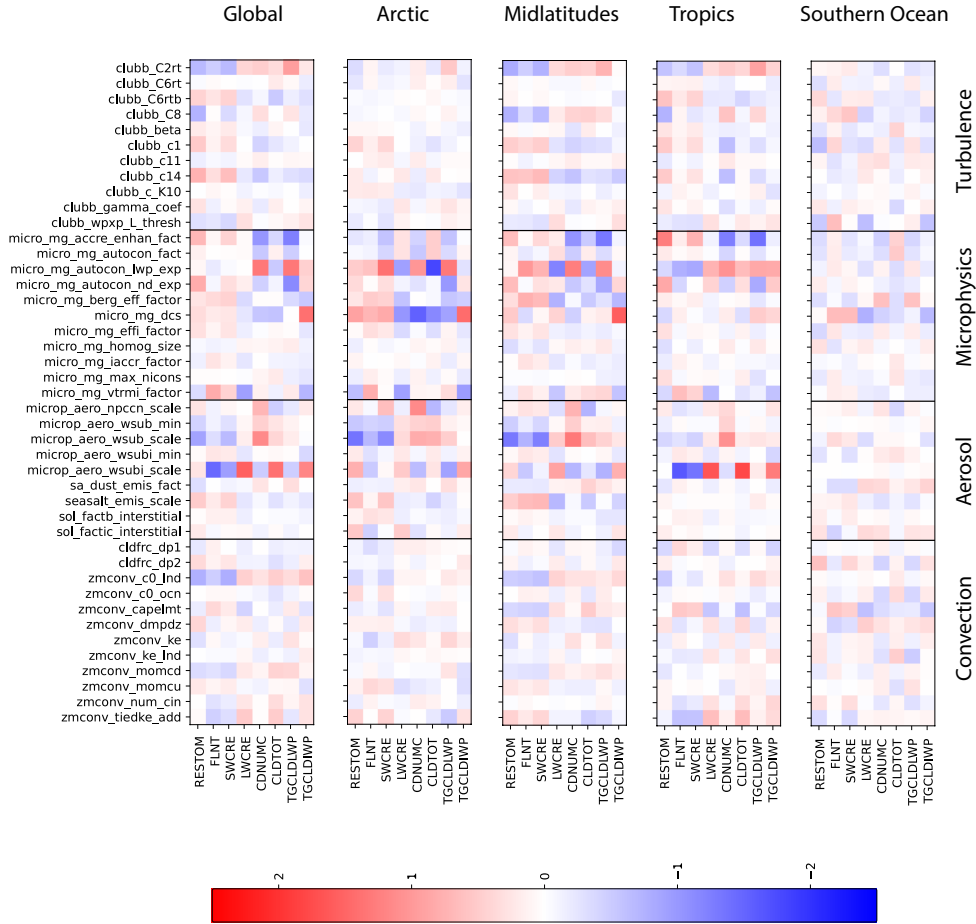


**Figure 5.** Normalized linear regression slope for the difference between PD and PI in 8 different model outputs (x axis) against all parameter values (y axis). The global mean results as well as four different regions are shown; Arctic ( $|lat| > 60^\circ$ ), Midlatitudes ( $30^\circ < |lat| < 60^\circ$ ), Tropics ( $|lat| < 30^\circ$ ) and the Southern Ocean ( $60^\circ S > lat > 30^\circ S$ ). The parameters are grouped into deep convection, aerosol, microphysics and turbulence parameters.

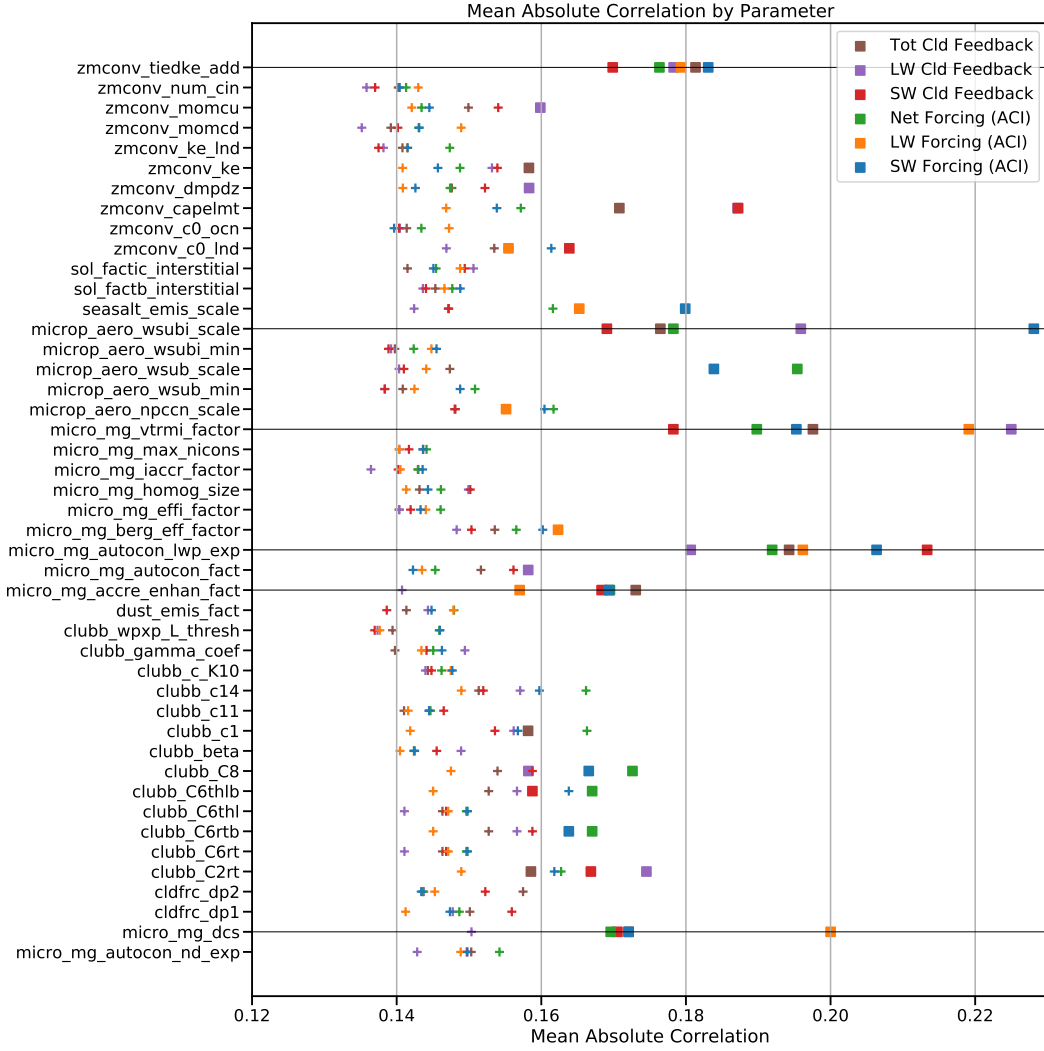


**Figure 6.** Global mean absolute correlation by parameter for ACI Forcing and Cloud Feedbacks. LW, SW and Net are different colors as noted in the legend (e.g. net ACI forcing is green). Parameters with the 10 highest absolute correlations for each component are shown as colored solid squares. The rest of the parameters are plus signs (+). The horizontal lines show the 6 parameters which are in the top 10 correlations for both total cloud feedback (brown) and net forcing (green).

315 parameters with the 10 highest correlations for each component. We will focus on  
 316 the common important parameters across forcing and feedback (horizontal lines) in  
 317 Section 3.4.

318 Focusing on the net ACI Forcing (green in Figure 6), we highlight the param-  
 319 eters with the 10 highest mean absolute correlations (green squares). In general  
 320 the LW (orange) and SW (blue) forcing components also have strong correlations  
 321 with these parameters. Figure 7 illustrates maps of these correlations, ranked as in  
 322 Figure 6 in order of correlation from highest (A) to 10th highest (J).

323 Figure 7 reinforces the global and regional correlations in Figure 5, with a  
 324 bit more insight into processes. Several parameters are related to ice, including the

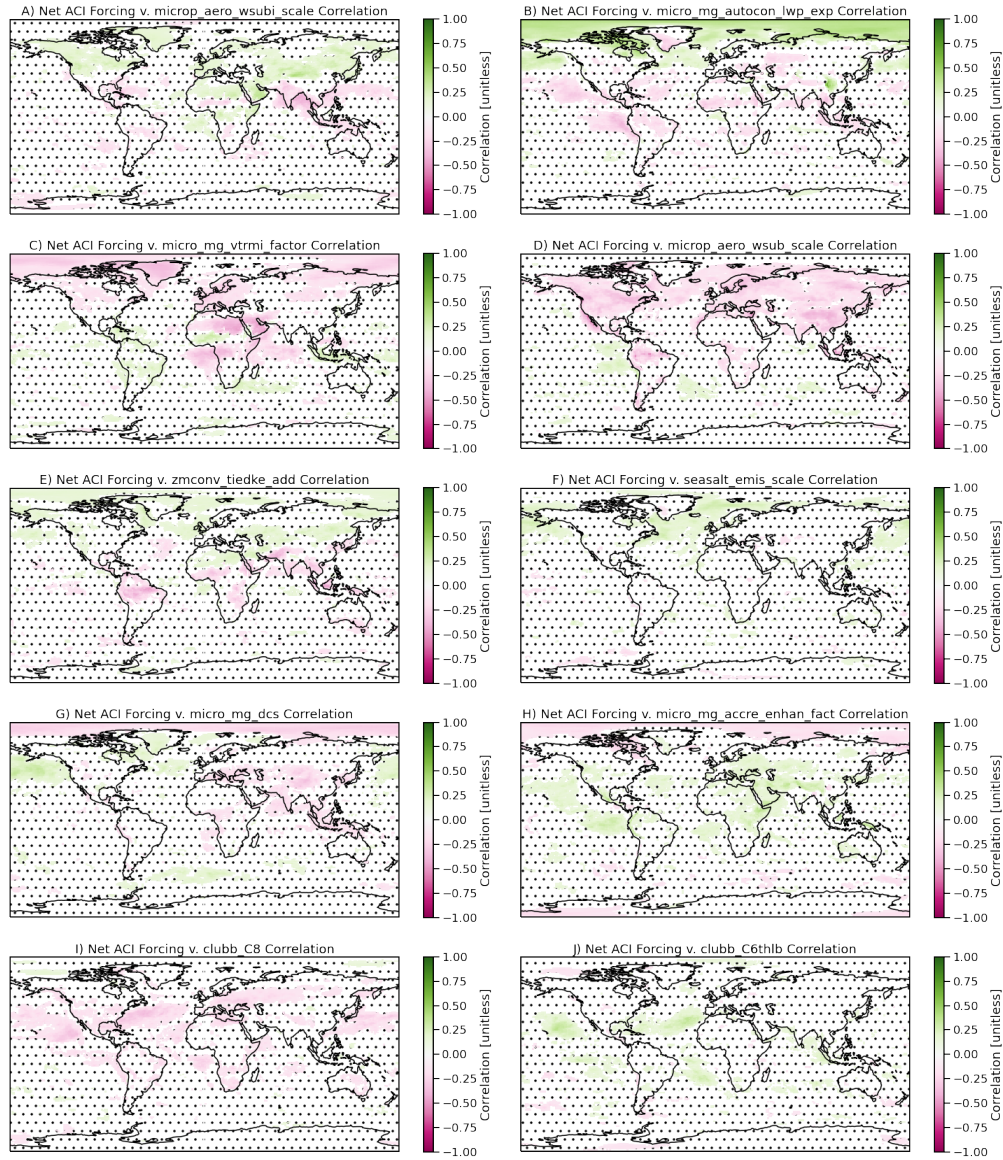


**Figure 7.** Map of linear correlation coefficient at each point between the SW ACI forcing (PD-PI) and selected model parameters varied in the PPE. Non-significant points are stippled. Significance is determined by a bootstrap fit.

325 sub-grid velocity for ice activation (*micro\_aero\_wsubi\_scale*: Figure 7A), the ice  
 326 fall speed scaling (*micro\_mg\_vtrmi\_scale*: Figure 7C) and the ice auto-conversion  
 327 size threshold (*micro\_mg\_dcs*: Figure 7G). The temperature perturbation for deep  
 328 convective triggering (*zmconv\_tiedke\_add*, Figure 7E) likely also plays a role in  
 329 supplying ice to the upper troposphere. Increasing the sub-grid velocity for ice nu-  
 330 cleation will increase ice number (which seems to weaken ACI over land). The ice  
 331 fall speed scaling results in less ice and snow in the atmosphere (associated with  
 332 stronger ACI), while increasing the ice auto-conversion size threshold will increase  
 333 the ice mass, which seems to weaken ACI in mid-latitudes but increase it at high  
 334 latitudes (so more ice will result in stronger ACI at high latitudes, consistent with  
 335 the PI mean state IWP relationship in Figure 4C).

336 Liquid cloud processes are also important. The auto-conversion LWP expo-  
 337 nent (*micro\_mg\_autocon\_lwp\_exp*: Figure 7B) and accretion enhancement factor  
 338 (*micro\_mg\_accr\_enhan\_fact*: Figure 7H) control rain formation and depletion of  
 339 liquid. They have similar patterns and opposite sign. Increasing the LWP exponent  
 340 for auto-conversion results in more sensitivity of cloud water loss to LWP: higher  
 341 auto-conversion sensitivity in the subtropics in results in stronger (more negative)  
 342 ACI, while higher auto-conversion sensitivity in the Arctic results in weaker (less  
 343 negative) ACI. Accretion is also a sink for cloud water, and the enhancement is a  
 344 linear scaling for the loss. In the sub-tropics, more accretion leads to reduced (neg-  
 345 ative) ACI, and would be associated with thinner clouds. The accretion scaling is  
 346 consistent with the sensitivity of ACI to PI mean state sensitivity of clouds in Fig-  
 347 ure 4, while the auto-conversion exponent is more related to the changes in the state  
 348 between PI and PD.

349 Two parameters are related to liquid aerosol activation: increasing  
 350 *microp\_aero\_wsub\_scale* (Figure 7D) is associated with larger negative ACI. Higher  
 351 scaling would increase CCN in PI, but also the sensitivity to changes between PI  
 352 and PD ( $\Delta\text{CCN}$ ). Given that the correlation with ACI in Figure 7D is opposite to  
 353 the mean state effect of PI CCN in Figure 4E, it would appear that it affects ACI  
 354 more through  $\Delta\text{CCN}$ . Increasing sea salt emission (*seasalt\_emis\_scale*), will in-  
 355 crease CCN in the base state, and has a similar correlation with ACI as PI CCN  
 356 (Figure 4E) over the oceans.

357 The last two parameters are related to the unified shallow turbulence  
 358 (CLUBB) and act over the sub-tropical oceans. *clubb\_C8* (Figure 7I) is the coeffi-  
 359 cient of the skewness in the vertical velocity while *clubb\_C6thlb* (Figure 7J) affects  
 360 the high skewness of the liquid water potential temperature. They tend to act in op-  
 361 posite ways. Increasing *clubb\_C8* tends to increase cloud fraction, so the correlation  
 362 matches the total cloud response in Figure 4A.

363 Looking beyond the mean state, we can also try to understand how ACI is  
 364 related to the sensitivity or susceptibility of cloud radiative effects to changes  
 365 in cloud properties. To look at this we examine the susceptibility of cloud ra-  
 366 diative effect (or cloud albedo) to changes in cloud drop number ( $N_c$ ) defined as  
 367  $d\ln(\text{Albedo})/d\ln(N_c)$ . We estimate the susceptibility terms at each point with the  
 368 temporal (monthly mean) co-variance of these properties for each ensemble mem-  
 369 ber, and then similar to Figure 4, correlate that with the total ACI (difference in  
 370 LW+SW CRE between PD and PI) in Figure 8A. Because albedo has a strong sea-  
 371 sonal dependence at high latitudes, we limit this analysis to latitudes equatorward of  
 372  $60^\circ$ .

373 There is a consistent negative correlation between susceptibility and forcing  
 374 over the oceans, whereby increasing susceptibility of clouds to drop number is as-  
 375 sociated with stronger negative net ACI over the tropical and sub-tropical oceans.  
 376 A detailed analysis of the parameter sensitivity of susceptibility (not shown) sim-

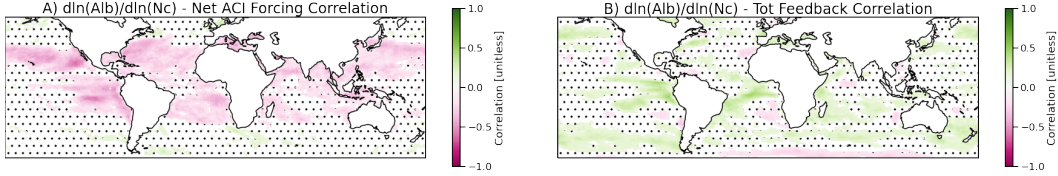


**Figure 8.** Correlation of susceptibility of cloud albedo to cloud drop number against A) Net ACI forcing and B) Total Cloud feedback.

377 ilar to that conducted for Figure 7 for forcing indicates that the susceptibility is  
 378 linked to the auto-conversion (*micro\_mg\_autocon\_lwp\_exp*) where more susceptible  
 379 clouds have a higher auto-conversion exponent for LWP (interestingly it is not re-  
 380 lated as much to the Nc exponent in the auto-conversion). In addition, susceptibility  
 381 varies with accretion (*micro\_mg\_accr\_enhan\_fact*), where more accretion reduces  
 382 susceptibility (perhaps because of thinner clouds). Finally, susceptibility is also asso-  
 383 ciated with *clubb\_C8*, where higher *clubb\_C8* is associated with higher susceptibility.  
 384 H. Guo et al. (2015) noted that increasing *clubb\_C8* increases cloud cover in the sub-  
 385 tropics. These results are consistent with the PI mean state correlations (Figure 4)  
 386 that thicker sub-tropical PI clouds in marginal regions are associated with higher  
 387 (negative) net ACI forcing.

388 **3.3 Feedback**

389 A similar analysis is conducted for cloud feedbacks. Cloud feedbacks are as-  
 390 sessed with the difference in cloud radiative effects between the SST+4K and PD  
 391 simulations (modified with radiative kernels to remove non-cloud effects). Because  
 392 global correlations can be misleading with positive and negative signs and cloud  
 393 feedbacks have multiple signs in different regimes (Figure 2), we move straight to  
 394 correlations with the mean present day state and total (LW+SW) cloud feedbacks at  
 395 each point in Figure 9. These figures are with respect to present day values, but the  
 396 correlations are the same whether present day or pre-industrial mean state is used.  
 397 Figure 9 includes all simulations, but is qualitatively consistent with less significance  
 398 if the 88 simulations constrained by CERES cloud radiative effect are used.

399 Regional correlations between cloud feedbacks and mean state cloud coverage  
 400 (Figure 9A) are negative at high latitudes (Arctic and Southern Ocean) and positive  
 401 at low latitudes. The correlations over the Sahara are spurious since there is nearly  
 402 zero cloud and feedbacks are small (Figure 2C). Similar relationships are found with  
 403 LWP (Figure 9B), cloud drop number (Figure 9J) and cloud top number (Figure 9I).  
 404 Base state SW Cloud Radiative Effect (Figure 9G) has an opposite sign correlation  
 405 (because it is negative) with similar pattern. However, over the Southern Ocean,  
 406 more cloud and LWP (more liquid cloud) has a negative correlation with cloud feed-  
 407 backs. IWP (Figure 9C) however has positive correlations over polar oceans. Base  
 408 state ice fraction (Figure 9H) is positively correlated with total cloud feedbacks as  
 409 well at high latitudes, and negatively correlated at low latitudes. All these corre-  
 410 lations indicate that at high latitudes stronger cloud feedbacks are associated with  
 411 less base state cloud, liquid and liquid drop number, as well as more ice. Note that  
 412 as with forcing, the net feedback sign changes at high latitudes, which affects these  
 413 correlations (the same change in mean state has a different sign with different signed  
 414 feedbacks). In low latitudes, the effects are opposite, with stronger feedbacks for  
 415 more and thicker cloud over land and ocean. There are weaker relationships between  
 416 feedbacks and column sulfate (Figure 9D) and CCN (Figure 9E), but in general

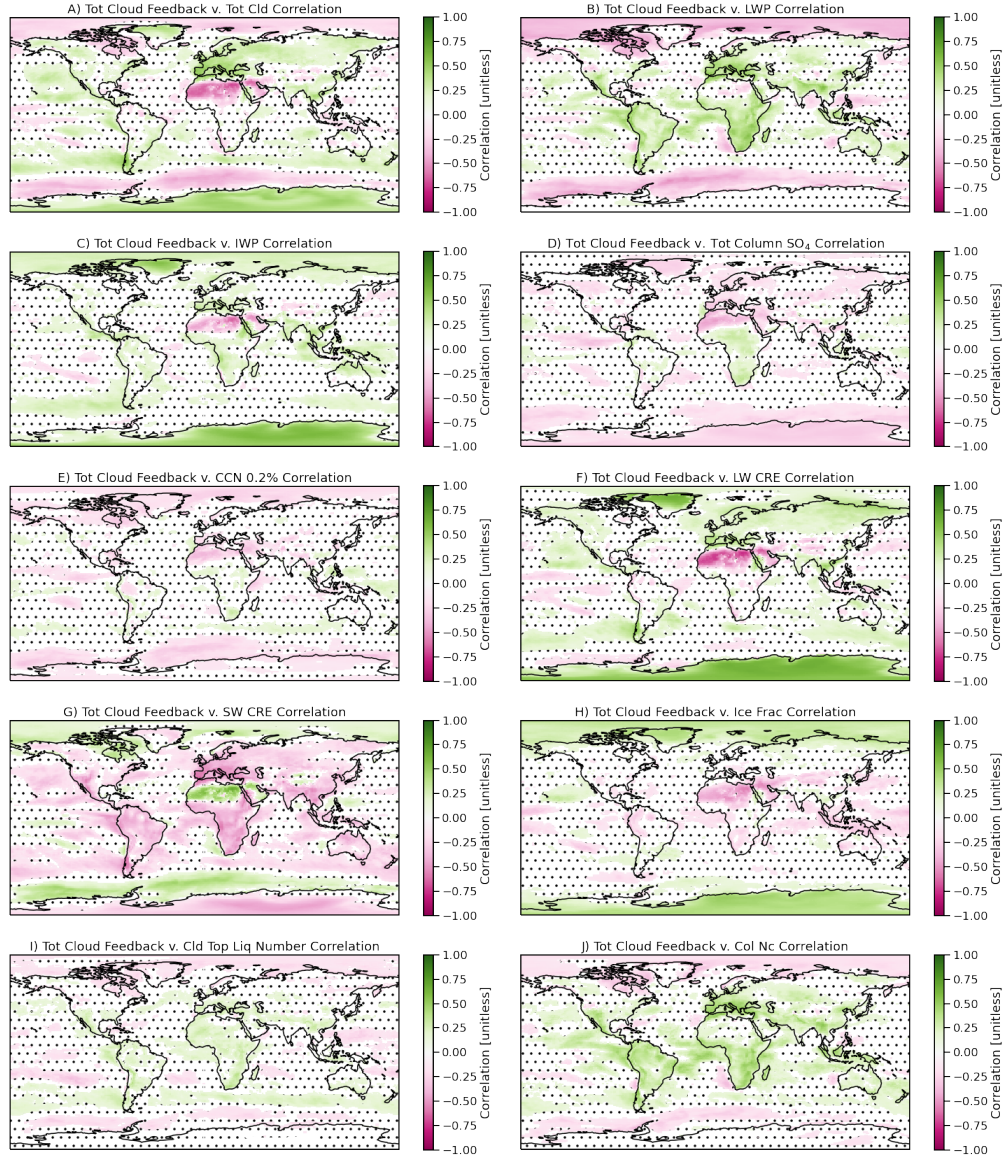


**Figure 9.** Map of linear correlation coefficient at each point between mean state in present day and the total (LW+SW) cloud feedbacks (estimated with SST4K v. PD) for different variables. Non-significant points are stippled. Significance is determined by a bootstrap fit.



417 more sulfate and CCN in the base (non-warmed) state is associated with lower feed-  
418 backs.

419 We investigate these relationships further by diving into processes by looking  
420 at key parameters. Figure 10 is similar to Figure 5 showing the normalized and  
421 standardized regressions between parameters and changes in the state SST4K - PD  
422 across regions. Some of the same parameters are important for cloud feedbacks (the  
423 last two variables on the right of each column): accretion, auto-conversion and the  
424 loss process of ice (fall speed and conversion from ice to snow). Note that the S.  
425 Ocean is not important for forcing since there is little change in aerosols PD-PI, but  
426 is more important for feedbacks (accretion, ice processes and some deep convection  
427 parameters are important here). As with the maps in Figure 9, the correlations vary  
428 by region, muting the global sensitivity (correlation) for many parameters.

429 There are several parameters in the deep convective parameterization that are  
430 important for cloud feedbacks, particularly in the Tropics and to a lesser extent the  
431 S. Ocean. These parameters govern the triggering of convection (*zmconv\_capelmt*  
432 is the threshold CAPE for firing convection and *zmconv\_tideke\_add* is a buoyancy  
433 perturbation that will increase the convective potential). Convective rain formation  
434 over land (*zmconv\_c0\_lnd*) is also important in the tropics, which is not surprising  
435 given the larger positive cloud feedbacks there (Figure 2). Convective entrainment  
436 (*zmconv\_dmpdz*) is important in the mid-latitudes and tropics. Deep convection  
437 acts by changing both the SW and the LW feedback, likely because it changes ice  
438 cloud radiative effects, while many of the other parameters primarily change the LW  
439 (for ice microphysical and aerosol processes) or SW (for liquid cloud microphysical  
440 and aerosol processes).

441 Finally for we look at maps of key parameter correlations with feedbacks in  
442 Figure 11. As with Forcing, we estimate the mean absolute correlation of significant  
443 points for each parameter, and rank them (Figure 6). The parameters with the 10  
444 highest correlations with total feedbacks (brown squares in Figure 6) are displayed  
445 in Figure 11.

446 The parameters identified are similar to those for forcing. There are several  
447 parameters linked to ice processes, including ice fall speed (*micro\_mg\_vtrmi\_scale*,  
448 Figure 11A), the sub-grid velocity for ice activation (*micro\_aero\_wsubi\_scale*: Fig-  
449 ure 11D) and the ice auto-conversion threshold (*micro\_mg\_dcs*, Figure 11F). Slower  
450 fall speed and more ice number (higher *micro\_aero\_wsubi\_scale*) at high latitudes  
451 are associated with more ice and higher total cloud feedbacks at high latitudes  
452 (Figure 9C). Ice auto-conversion (*micro\_mg\_dcs*) acts mostly in the tropics and S.  
453 Hemisphere, again with more base state ice (higher *micro\_mg\_dcs*) associated with  
454 higher cloud feedback, likely through the LW CRE (Figure 9F).

455 As with forcing, parameters linked to rain formation are important for cloud  
456 feedbacks, the auto-conversion LWP exponent (*micro\_mg\_autocon\_lwp\_exp*, Fig-  
457 ure 11B) and accretion enhancement (*micro\_mg\_accr\_enhan\_fact*, Figure 11E)  
458 have opposite signs. Higher auto conversion (leading to less liquid) is associated  
459 with smaller cloud feedbacks at high latitudes and larger cloud feedbacks at lower  
460 latitudes. Accretion has the opposite effect, with more accretion (reducing cloud wa-  
461 ter) associated with more high latitude cloud feedbacks, and reduced tropical cloud  
462 feedbacks over land. Both effects are consistent with the overall cloud and LWP  
463 correlations with feedbacks in Figure 9A and B.

464 In addition, there are three deep convective parameters that have regionally  
465 significant correlations with cloud feedback. In the tropics, deep convection supplies  
466 ice to the upper troposphere, *zmconv\_tiedke\_add* (Figure 11C) as well as *zmconv\_ke*  
467 (Figure 11I) increase convection over land with similar patterns. *zmconv\_capelmt*

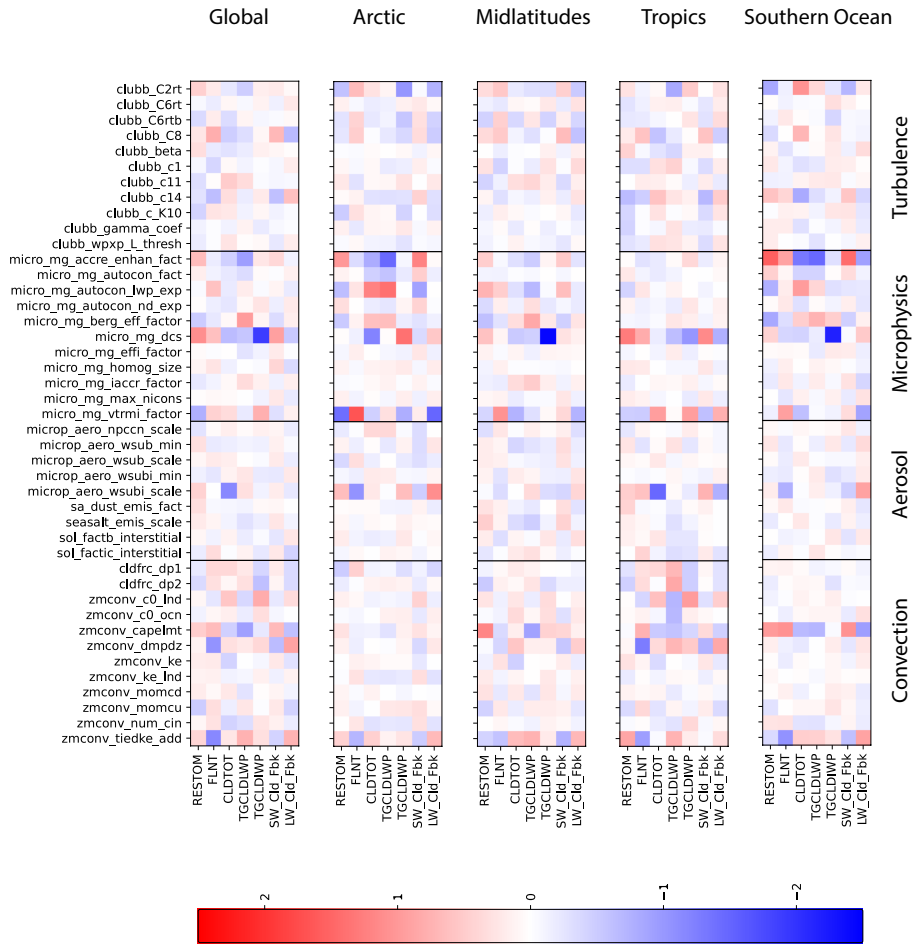


**Figure 10.** Normalized linear regression slope for the difference between SST4K and PD in 8 outputs (x axis) against all parameter values (y axis). The global mean results as well as four different regions are shown; Arctic, Midlatitudes, Tropics and the Southern Ocean. The parameters are grouped into deep convection, aerosol, microphysics and turbulence parameters.

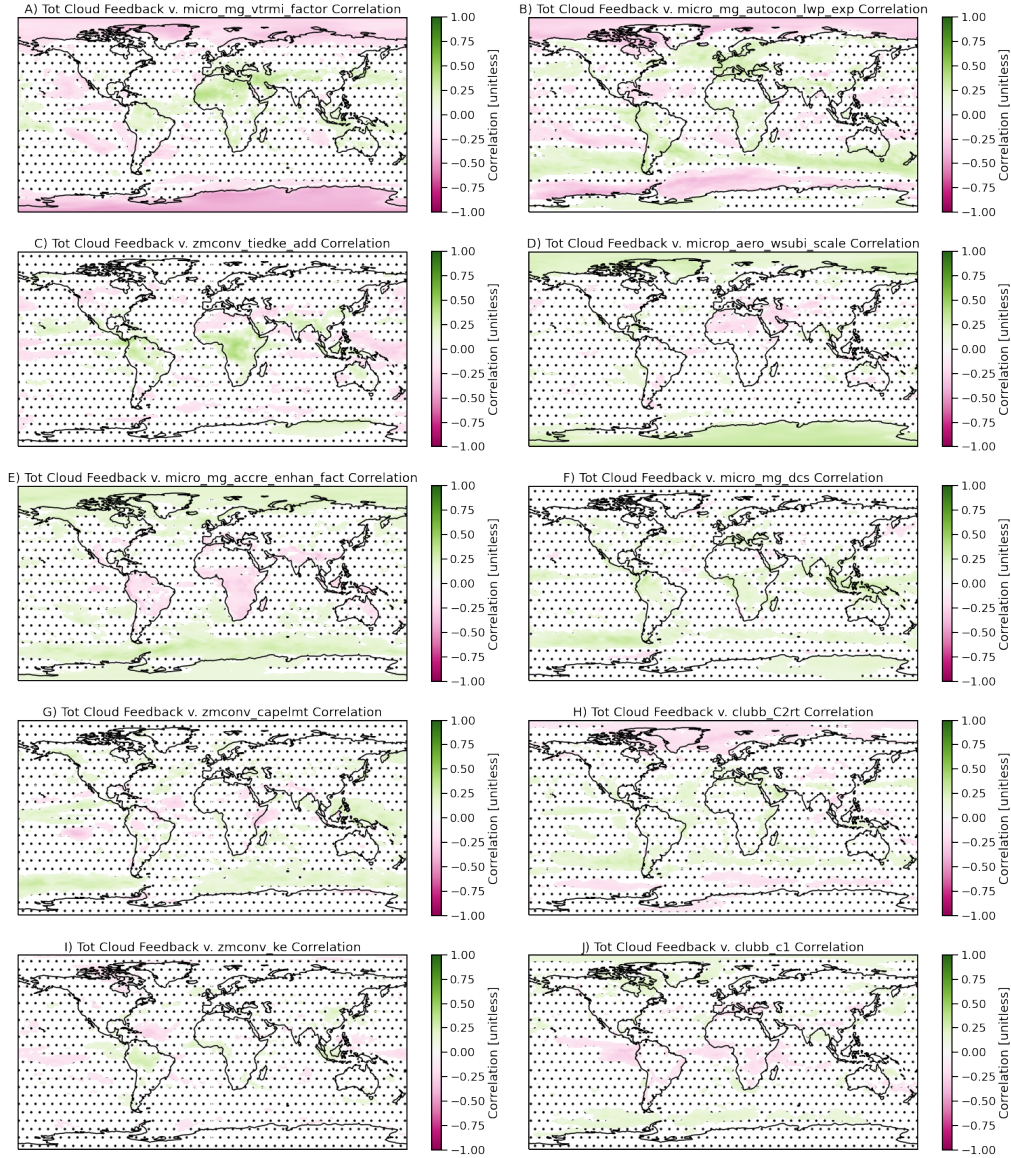


**Figure 11.** Map of linear correlation coefficient at each point between the total cloud feedbacks (SW + LW) estimated from SST4K v. PD and selected model parameters varied in the PPE. Non-significant points are stippled. Significance is determined by a bootstrap fit.

(Figure 11G) increases it over ocean. Increasing ice seems to increase cloud feed-backs in the tropics (Figure 9C). *zmconv\_capelmt* (Figure 11G) also seems to act over the Southern Ocean, with offsetting signs in the LW and SW (Figure 10).

Finally, two turbulence parameters, *clubb\_C2rt* (Figure 11H), *clubb\_c1* (Figure 11J) have small regional correlations, mostly over the oceans with opposite sign. *clubb\_C2rt* is related to the dissipation of temperature variance and increasing it increases cloud cover and SW CRE (Z. Guo et al., 2015) while *clubb\_c1* is related to the dissipation of vertical velocity variance and has the opposite effect (increasing it decreases cloud cover and SW CRE). The patterns indicate that these parameters may be driving some of the correlation with mean state total cloud cover and LWP (Figure 9A and B), in both the tropics and high latitudes.

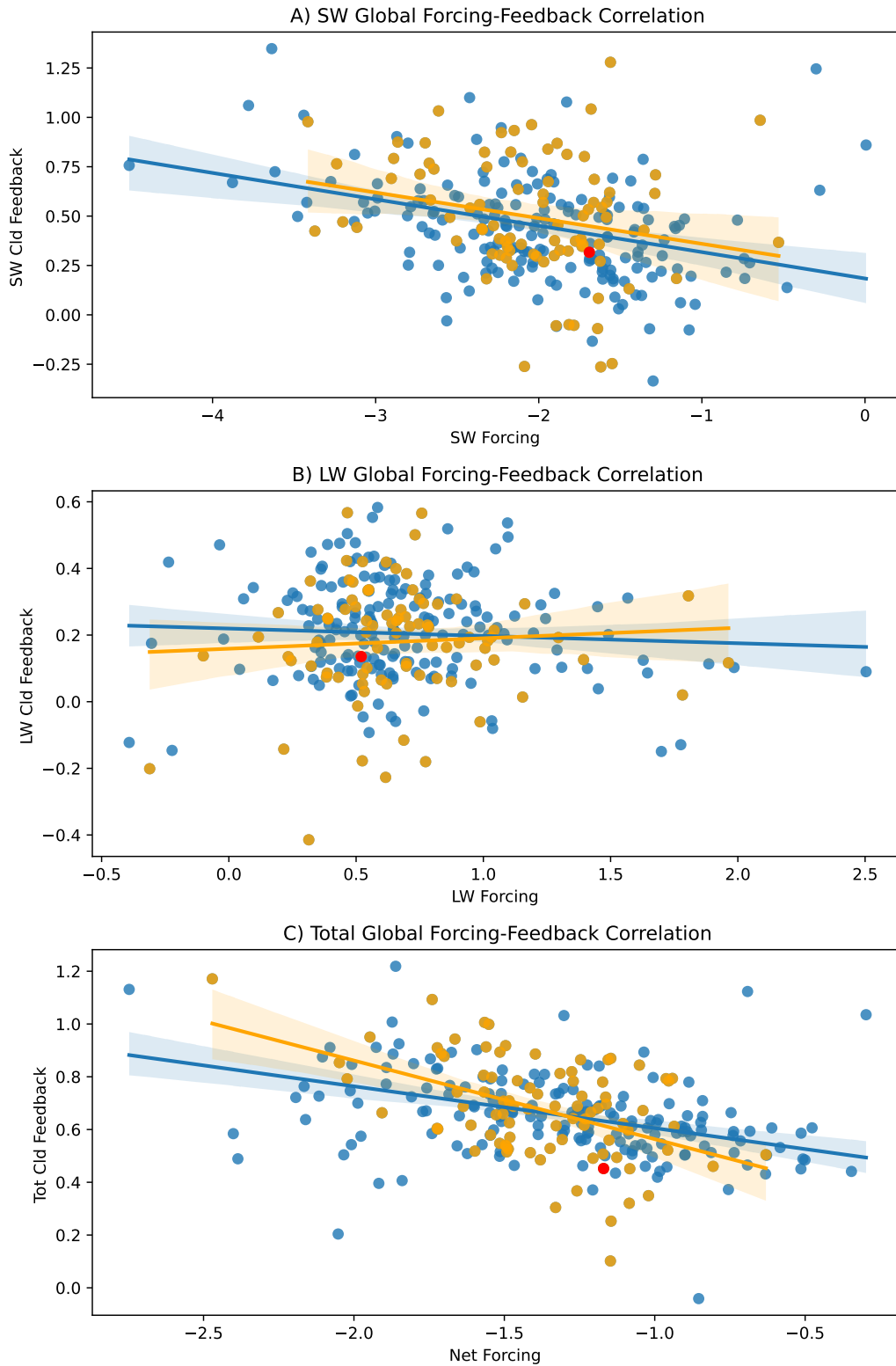
### 3.4 Forcing and Feedback Relationships

Figure 12 illustrates a global scatter plot of the cloud forcing (defined as above: the change in CRE between present day and pre-industrial) against the kernel adjusted cloud feedbacks both in the SW (Figure 12A), LW (Figure 12B) and total (LW+SW, Figure 12C). The blue colors and regression line are for all simulations. As in Figure 12, the orange points and regression lines are just those simulations whose mean annual value of SW CRE is within  $\pm 5 \text{ Wm}^{-2}$  of the observed CERES EBAF annual global mean ( $-45.3 \text{ Wm}^{-2}$ ). The red dot is the ‘default’ parameter set for CAM6.

In the SW, there is a clear relationship between the cloud feedbacks and cloud forcing. The relationship is similar whether just a constrained subset of simulations is used, or if the full data set is used, and the slope is significantly different than zero. In general the SW aerosol cloud forcing is negatively correlated with SW cloud feedback: larger positive feedbacks yield larger negative cloud forcing. There is no such correlation in the LW, and the slopes are not significantly different than zero, and the constrained simulations have a different (but still not significant) sign. The correlation of total (LW+SW), cloud forcing and feedback reflects mostly the SW correlation, and is actually stronger with constrained simulations.

As with forcing and feedback, we can decompose the global correlation of Figure 12 into each location on the planet, generate a correlation value at each point, and determine the significance of the correlation with a bootstrap fit yielding a confidence interval for the correlation between forcing and feedbacks being significantly different than zero (Figure 13) at each point. For the SW (Figure 13A), correlations are uniformly negative: stronger negative ACI is correlated with stronger positive cloud feedback. This maximizes over N. Hemisphere land and adjacent ocean basins. In large parts of the S. Hemisphere, there is very little forcing response, so there are small signals. Most of the negative correlation comes from the N. Hemisphere. Going back to the regional correlations between mean state SW CRE and ACI (Figure 4G) and total cloud feedbacks (Figure 9G), there is an anti-correlation, consistent with stronger forcing and feedbacks going together (since forcing is negative), with opposite signs over the Arctic and the rest of the N. Hemisphere. It is apparent over both ocean and land.

For the LW (Figure 13B), the sign is not monotonic, but there is a negative correlation in N. Hemisphere mid-latitudes, and a positive correlation between LW feedbacks and LW forcing (which are generally both of the same positive sign) in parts of the tropics and the Arctic, but with less significance. The patterns of LW forcing and feedbacks (shown in Figure 2) are less correlated than the SW, likely since the SW ACI magnitude and processes acting through liquid are stronger than for ice. Indeed, if we look at changes in the different climate states between forcing (PD - PI) and feedback (SST4K - PD), the strongest negative correlations are



**Figure 12.** Scatterplot of A) SW B) LW and C) Total (LW+SW) Aerosol forcing (horizontal axis) and kernel adjusted cloud feedbacks (vertical axis) from each simulation. Orange indicates those 88 simulations whose global mean PD Shortwave Cloud Radiative Effect is within  $\pm 5$   $\text{Wm}^{-2}$  of the CERES EBAF global annual mean. Default CAM6 parameters shown as the red dot.

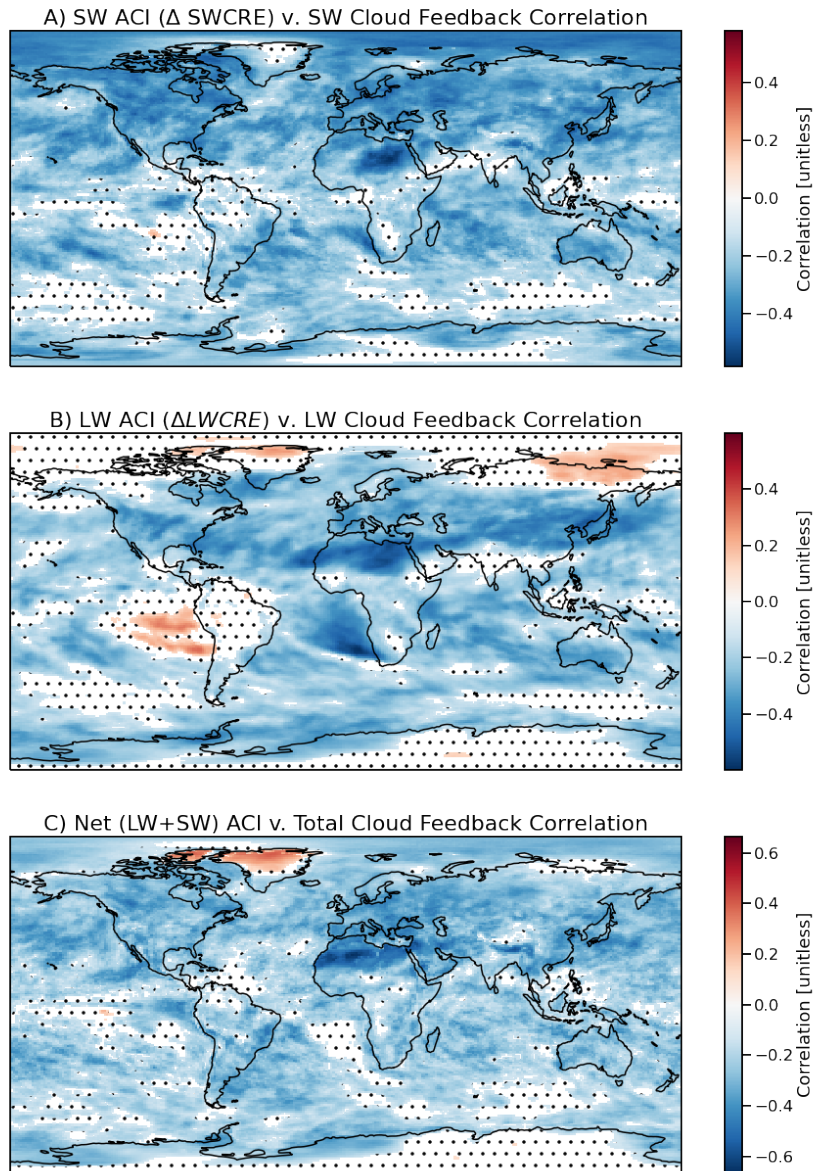


**Figure 13.** Correlation maps at each point between A) SW, B) LW and C) Total (SW+LW) Cloud Forcing and Feedback. Regions of less than 95% significance are stippled.

519 with N. Hemisphere mid-latitude LWP and column drop number (Figure B1), which  
 520 affect mostly SW radiation. The correlations between net forcing and feedbacks  
 521 (Figure 13C) are lower than the SW, but also negative.

522 There is also a positive relationship between cloud albedo susceptibility to  
 523 drop number and cloud feedbacks (Figure 8B). The correlation is the opposite as for  
 524 ACI forcing, which may be another reason for the anti-correlation between forcing  
 525 and feedback. Increased susceptibility (through the processes described above under  
 526 forcing), tends to create larger magnitude negative ACI forcing and positive cloud  
 527 feedbacks.

528 Finally, we note that some of the dominant parameters governing Forcing and  
 529 Feedbacks are similar. Using the mean absolute correlations by parameter (Fig-  
 530 ure 6), we determined the most relevant parameters for ACI forcing in Figure 7 and  
 531 cloud feedbacks in Figure 11. Figure 6 illustrates that of the top 10 correlations  
 532 between parameters and forcing and feedback, 6 of them are common (horizontal  
 533 lines). These include 3 parameters for ice: ice fall speed (*micro\_mg\_vtrmi\_scale*),  
 534 ice nucleation sub-grid velocity (*microp\_aero\_wsubi\_scale*) and ice to snow conver-  
 535 sion size threshold (*micro\_mg\_dcs*). There are two parameters related to warm rain  
 536 formation, one each for auto-conversion (*micro\_mg\_autocon\_lwp\_exp*) and accretion  
 537 (*micro\_mg\_accr\_enhan\_fact*). One parameter is related to the triggering of deep  
 538 convection (*zmconv\_tiedke\_add*).

539 To illustrate how the co-variation of these parameters affect forcing and feed-  
 540 back, we build a Gaussian process emulator using the global average forcing and  
 541 feedback. Inputs are the normalized parameter values and global net forcing and to-  
 542 tal feedbacks (LW+SW). Figure 14 illustrates how global mean total cloud feedbacks  
 543 and net ACI forcing vary around the default values as these parameters change in-  
 544 dividually based on the emulator. The emulator is not a perfect representation of  
 545 the total 45 dimensional parameter space, and it is built on global values (with at-  
 546 tendant problems of different responses by regime), but it is illustrative of another  
 547 method to understand the interaction of forcing and feedback.

548 In this emulator, some parameters affect only either feedbacks (ice conver-  
 549 sion threshold: *micro\_mg\_dcs*) or forcing (ice fall speed: *micro\_mg\_vtrmi\_factor*),  
 550 and some affect virtually neither in the emulator (deep convective triggering:  
 551 *zmconv\_tiedke\_add*). This might be because the global positive and negative  
 552 correlations cancel. Ice nucleation sub-grid velocity (*microp\_aero\_wsubi\_scale*),  
 553 which changes ice crystal number is weakly non-linear, while auto-conversion  
 554 (*micro\_mg\_autocon\_lwp\_exp*) and accretion (*micro\_mg\_accr\_enhan\_fact*) param-  
 555 eters have complex relationships and act differently for feedback, but similarly for  
 556 forcing. Such emulators can be used as a further guide for understanding the slices  
 557 through the parameter space. The opposite effects on feedbacks of auto-conversion  
 558 and accretion are consistent with correlations in Figure 11 for example. For forcing,  
 559 the different magnitudes of negative and positive responses (Figure 7) may make  
 560 emulating the global mean difficult.

## 561 4 Discussion

562 We can summarize this analysis with several comments about key processes for  
 563 forcing, feedbacks and their interaction in the CAM6 PPE.

### 564 4.1 Forcing

565 Stronger negative ACI forcing is associated with PI climates that have thicker,  
 566 more extensive clouds with higher drop numbers and water path in the subtropics.

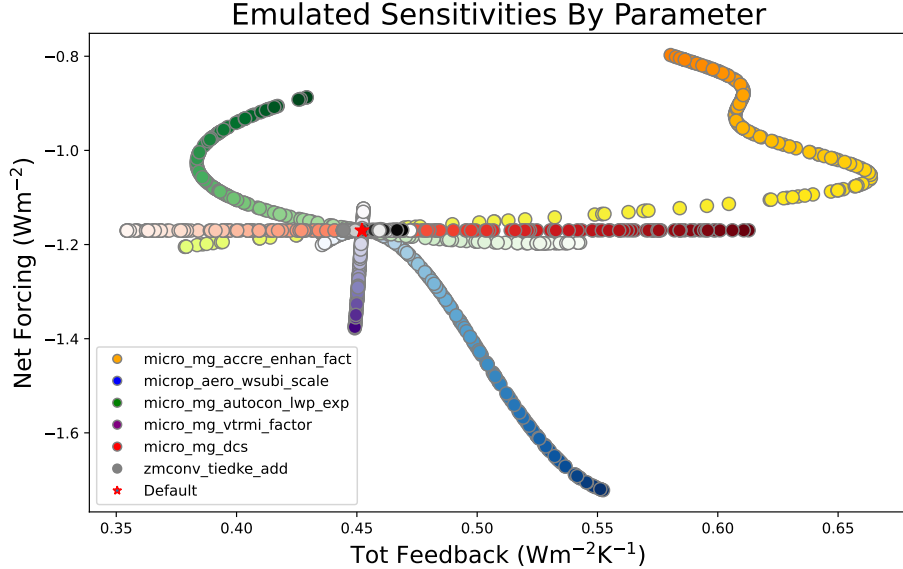


**Figure 14.** Sensitivities by parameter using the Gaussian Process emulator. Top common parameters are shown, varied around the default location (marked with a red star). Color hue varies from light (0) to dark (1) of the normalized range.

567 The regions in the sub-tropics that are most sensitive to parameter changes are re-  
 568 gions where there is very little cloud, so simulations with more extensive cloud in  
 569 these marginal regions, along with less PI CCN and sulfur, seem to yield larger net  
 570 ACI. This highlights that the pre-industrial state of clouds is important for ACI, as  
 571 noted by Carslaw et al. (2013) and others.

572 Auto-conversion and accretion are critical processes. Auto-conversion and ac-  
 573 cretion parameters that lead to increased cloud thickness in the subtropics increase  
 574 negative ACI (consistent with mean state effects). Increasing activation with in-  
 575 creased sub-grid vertical velocity leads to stronger negative ACI nearly everywhere  
 576 (more response to aerosols, more change in CCN, since lower CCN in PI are as-  
 577 sociated with stronger ACI). Increasing sea salt emission (which increases PI and  
 578 PD CCN similarly) reduces net ACI, because it means more CCN in PI (consistent  
 579 with the interactions with the mean state). Correlations with changes to the auto-  
 580 conversion LWP exponent seem larger than for accretion, but accretion is scaled  
 581 linearly, and the variations on the auto-conversion are larger (there is also a linear  
 582 auto-conversion scaling parameter which does NOT show up as being significant).  
 583 Accretion affects ACI through PI mean state (thicker clouds yield larger magnitude  
 584 ACI), while auto-conversion affects ACI through the sensitivity of PD-PI differences  
 585 in LWP.

586 Increasing susceptibility of cloud albedo to drop number increases negative  
 587 ACI forcing, over much broader regions than a single parameter or mean state prop-  
 588 erty. Susceptibility is driven by a slightly different set of parameters, including  
 589 auto-conversion and accretion, but also shallow turbulence parameters that increase  
 590 cloud cover in the sub-tropics, again, in regions where it is generally low.



## 591 4.2 Feedbacks

592 In low latitudes, stronger positive cloud feedbacks are associated with more  
 593 base state cloud, liquid and liquid drop number, as well as more ice over land and  
 594 ocean. More ice (and higher ice fraction) at high latitudes increases cloud feedback,  
 595 while correlations for liquid are the opposite (more liquid is associated with more  
 596 negative cloud feedback). There is a dipole in these effects over the S. Ocean where  
 597 the mean ice fraction crosses about 50%. This is related to the loss processes for  
 598 water (auto-conversion and accretion) as well as for ice (ice fall speed and ice acti-  
 599 vation), and the deep convective source for ice. It is near the region where feedbacks  
 600 turn from positive to negative. In ice dominated regions feedbacks are negative likely  
 601 due to the ice-albedo feedback, whereby warming melts ice and increases negative  
 602 SW CRE. This has been shown to be important in CAM6 (Gettelman et al., 2019).

603 Going strictly by the correlations, it appears that that auto conversion is more  
 604 important (or at least more related to) the base state cloud feedback sensitivity than  
 605 accretion (correlations for accretion are weaker). Raining and non-raining clouds  
 606 may have different effects, with perhaps the non-raining clouds more important  
 607 for feedback. Turbulence parameters also seem to play a role over the sub-tropical  
 608 oceans: they control the base state of clouds and thicker and more extensive clouds  
 609 have more positive cloud feedbacks. More ice yields stronger positive cloud feed-  
 610 backs (mostly through the LW) in both the tropics and high latitudes. Ice micro-  
 611 physics and deep convection parameters are important for regulating ice mass and  
 612 seem to influence feedbacks accordingly.

## 613 4.3 Interactions

614 Forcing and feedbacks are anti-correlated throughout the Northern Hemi-  
 615 sphere. Both forcing and feedback relationships to the mean state change sign from  
 616 high latitudes to lower latitudes, and they seem to do so in concert. Part of this is  
 617 simply the reduction in SW effects over high latitude ice covered surfaces. Stronger  
 618 negative forcing and positive feedbacks are associated with thinner clouds (less liq-  
 619 uid, more ice) at high latitudes and thicker clouds at low latitudes. This change  
 620 may occur because of the role of ice process, or the thickness of the clouds in the  
 621 stormtracks.

622 Even the important processes seem to be common between aerosol forcing and  
 623 cloud feedbacks. Microphysical controls on ice and ice nucleation, rain formation  
 624 (auto-conversion and accretion) as well as deep convection are important for both  
 625 forcing and feedback, with some shallow turbulence parameters (but different ones)  
 626 important over the oceans. Most of these parameters seem to be consistent with  
 627 sensitivity in the mean state.

628 One question arises: given that changing the method for auto-conversion and  
 629 accretion drastically (e.g., Gettelman et al., 2021) did not change ACI or cloud  
 630 feedbacks, how does that mesh with these results? We have not tested changing  
 631 auto-conversion and accretion fundamentally and altering other parameters, but it  
 632 may be that the balance required to maintain the mean state clouds constrains the  
 633 range of ACI and cloud feedbacks. This is consistent with the correlations with the  
 634 mean state of clouds, and would imply an emergent constraint dependent on the  
 635 present day state, but perhaps not a strong constraint.

## 636 5 Conclusions

637 This analysis of a large ensemble set of perturbed parameter experiments from  
 638 CAM6 (CAM6-PPE) yields several conclusions. Forcing and feedback are both cor-

639 related with the mean state. Higher magnitude cloud radiative effects generally  
640 mean larger forcing (negative for the SW, positive for the LW) and larger feedbacks  
641 (positive SW and LW). Aerosol forcing is broadly related to the susceptibility of  
642 clouds to drop number, which is impacted by a similar set of parameters, but with a  
643 different magnitude.

644 For aerosol forcing in particular, lower PI CCN and sulfate mass yield higher  
645 magnitude forcing. Accretion affects the mean state (and the total water mass in  
646 clouds), while auto-conversion seems to affect the sensitivity of LWP more strongly.

647 Thicker low latitude clouds with higher susceptibility are also associated with  
648 more positive cloud feedbacks. At high latitudes stronger positive cloud feedbacks  
649 are associated with less base state cloud, liquid and liquid drop number, as well as  
650 more ice at high latitudes. The shift happens about where ice starts to dominate  
651 the cloud (50% ice fraction). The fact that many important parameters reflect ice  
652 processes confirm the importance of ice in CAM6 feedbacks.

653 Aerosol forcing and cloud feedbacks are not independent in the CAM6 PPE,  
654 they are anti-correlated, such that stronger negative forcing is associated with  
655 stronger positive feedbacks. The fact that both forcing and feedbacks change sign  
656 in high latitudes of the N. Hemisphere at the same latitude is likely due to the LW  
657 and SW balance changing over an ice covered surface.

658 Even the processes governing forcing and feedback sensitivity in the PPE seem  
659 to be similar. The warm rain formation process (auto-conversion and accretion), ice  
660 loss processes (activation, fall speed, auto-conversion to snow) and deep convective  
661 intensity (which affects ice) are important for both forcing and feedbacks. Using  
662 these processes, it is possible to build emulators for forcing and feedbacks to try to  
663 understand the sensitivities.

664 This process-based view shows that in a consistent model system there are  
665 relationships between aerosol forcing and cloud feedbacks. Such relationships may  
666 be representative across multi-model ensembles as has been seen in the past (Kiehl,  
667 2007; Forster et al., 2013), but not necessarily given the small sample size (Smith et  
668 al., 2020).

669 This detailed analysis of cloud processes and their interactions with parameters  
670 to yield forcing and feedback sensitivities has yielded new insights into CAM6. But  
671 this is only one model of many different climate models, with a unique and complex  
672 representation of cloud processes. How applicable is this result across a range of  
673 models? Similar PPE methods should be and are being performed with other mod-  
674 els. Some aspects of this analysis should have broad applicability. For example, the  
675 parameterizations used in CAM6 for deep convection (G. J. Zhang & McFarlane,  
676 1995), cloud microphysics (Gettelman et al., 2015), aerosol activation (Abdul-Razzak  
677 & Ghan, 2002) and shallow turbulence Golaz et al. (2002) are used in other mod-  
678 els, so they feature similar or identical parameters. Beyond this, critical process  
679 treatments like auto-conversion and accretion (Khairoutdinov & Kogan, 2000), are  
680 described with similar parameters or using identical formulations in many models  
681 even with different parameterizations (Jing et al., 2019). It would be interesting to  
682 compare these results to those with other similar climate and weather models to as-  
683 certain if the behavior of individual processes is consistent, or if the process coupling  
684 within and between parameterizations induces different sensitivities. Some of the  
685 results are robust, like the importance of pre-industrial mean state sulfate and CCN  
686 by Carslaw et al. (2013). This work could be repeated on mean state relationships  
687 using data that is part of the traditional Coupled Model Intercomparison (CMIP)  
688 archives, but the parameter-level analysis would require dedicated simulations.

**Table A1.** A description of the parameters that are perturbed and their ranges. Note for  $zmoconv\_ke$  units  $KE = (\text{kg m}^{-2} \text{s}^{-1})^{0.5} \text{s}^{-1}$ 

Physics Scheme	Parameter Name	Description	Default	Min	Max	Units	
<i>CLUBB</i>	clubb_C2rt	Damping on scalar variances	1.0	0.2	2	-	
	clubb_C6rt	Low skewness in C6rt skewness function	4.0	2.0	6	-	
	clubb_C6rtb	High skewness in C6rt skewness function	6.0	2.0	8	-	
	clubb_C6thl	Low skewness in C6thl skewness function	4.0	2.0	6	-	
	clubb_C6thlb	High skewness in C6thl skewness function	6.0	2.0	8	-	
	clubb_C8	Coef. #1 in C8 skewness Equation	4.2	1.0	5	-	
	clubb_beta	Set plume widths for theta.l and rt	2.4	1.6	2.5	-	
	clubb.c1	Low Skewness in C1 Skw.	1.0	0.4	3	-	
	clubb.c11	Low Skewness in C11 Skw	0.7	0.2	0.8	-	
	clubb.c14	Constant for $u'^2$ and $v'^2$ terms	2.2	0.4	3	-	
	clubb.c.K10	Momentum coefficient of $Kh\_zm$	0.5	0.2	1.2	-	
	clubb_gamma_coef	Low Skw.: gamma coef. Skw	0.308	0.25	0.35	-	
	clubb_wpxp.L_thresh	Lscale threshold, damp C6 and C7	60	20	200	m	
	<i>MG2</i>	micro_mg_accre_enhan_fact	Accretion enhancing factor	1.0	0.1	10.0	-
		micro_mg_autocon_fact	auto-conversion factor	0.01	0.005	0.2	-
micro_mg_autocon_lwp_exp		KK2000 LWP exponent	2.47	2.10	3.30	-	
micro_mg_autocon_nd_exp		KK2000 auto-conversion exponent	-1.1	-0.8	-2	-	
micro_mg_berg_eff_factor		Bergeron efficiency factor	1.0	0.1	1.0	-	
micro_mg_dcs		auto-conversion size threshold ice-snow	500e-06	50e-06	1000e-06	m	
micro_mg_effi_factor		Scale effective radius for optics calculation	1.0	0.1	2.0	-	
micro_mg_homog_size		Homogeneous freezing ice particle size	25e-6	10e-6	200e-6	m	
micro_mg_iaccr_factor		Scaling ice/snow accretion	1.0	0.2	1.0	-	
micro_mg_max_nicons		Maximum allowed ice number concentration	100e6	1e5	10,000e6	# $\text{kg}^{-1}$	
micro_mg_vtrmi_factor		Ice fall speed scaling	1.0	0.2	5.0	$\text{m s}^{-1}$	
<i>Aerosol</i>	microp_aero_npccn_scale	Scale activated liquid number	1	0.33	3	-	
	microp_aero_wsub_min	Min subgrid velocity for liq activation	0.2	0	0.5	$\text{m s}^{-1}$	
	microp_aero_wsub_scale	Subgrid velocity for liquid activation scaling	1	0.1	5	-	
	microp_aero_wsubi_min	Min subgrid velocity for ice activation	0.001	0	0.2	$\text{m s}^{-1}$	
	microp_aero_wsubi_scale	Subgrid velocity for ice activation scaling	1	0.1	5	-	
	dust_emis_fact	Dust emission scaling factor	0.7	0.1	1.0	-	
	seasalt_emis_scale	Seasalt emission scaling factor	1.0	0.5	2.5	-	
	sol_factb_interstitial	Below cloud scavenging of interstitial modal aerosols	0.1	0.1	1	-	
sol_factic_interstitial	In-cloud scavenging of interstitial modal aerosols	0.4	0.1	1	-		
<i>ZM</i>	cldfrc_dp1	Parameter for deep convection cloud fraction	0.1	0.05	0.25	-	
	cldfrc_dp2	Parameter for deep convection cloud fraction	500	100	1,000	-	
	zmconv_c0_lnd	Convective auto-conversion over land	0.0075	0.002	0.1	$\text{m}^{-1}$	
	zmconv_c0_ocn	Convective auto-conversion over ocean	0.03	0.02	0.1	$\text{m}^{-1}$	
	zmconv_capelmt	Triggering threshold for ZM convection	70	35	350	$\text{J kg}^{-1}$	
	zmconv_dmpdz	Entrainment parameter	-1.0e-3	-2.0e-3	-2.0e-4	$\text{m}^{-1}$	
	zmconv_ke	Convective evaporation efficiency	5.0e-6	1.0e-6	1.0e-5	KE	
	zmconv_ke_lnd	Convective evaporation efficiency over land	1.0e-5	1.0e-6	1.0e-5	KE	
	zmconv_momcd	Efficiency of pressure term in ZM downdraft CMT	0.7	0	1	-	
	mconv_momcu	Efficiency of pressure term in ZM updraft CMT	0.7	0	1	-	
	zmconv_num_cin	Allowed number of negative buoyancy crossings	1	1	5	-	
	zmconv_tiedke_add	Convective parcel temperature perturbation	0.5	0	2	K	

689 It is also clear that better constraining the warm rain process and ice processes  
690 in the atmosphere are critical for narrowing the uncertainty in climate forcing and  
691 feedbacks.

## 692 Appendix A Parameters

693 Table A1, based on Eidhammer et al. (2024), describes the parameters used in  
694 the PPE by physical parameterization, with formal name, description, default value,  
695 minimum, maximum and units.

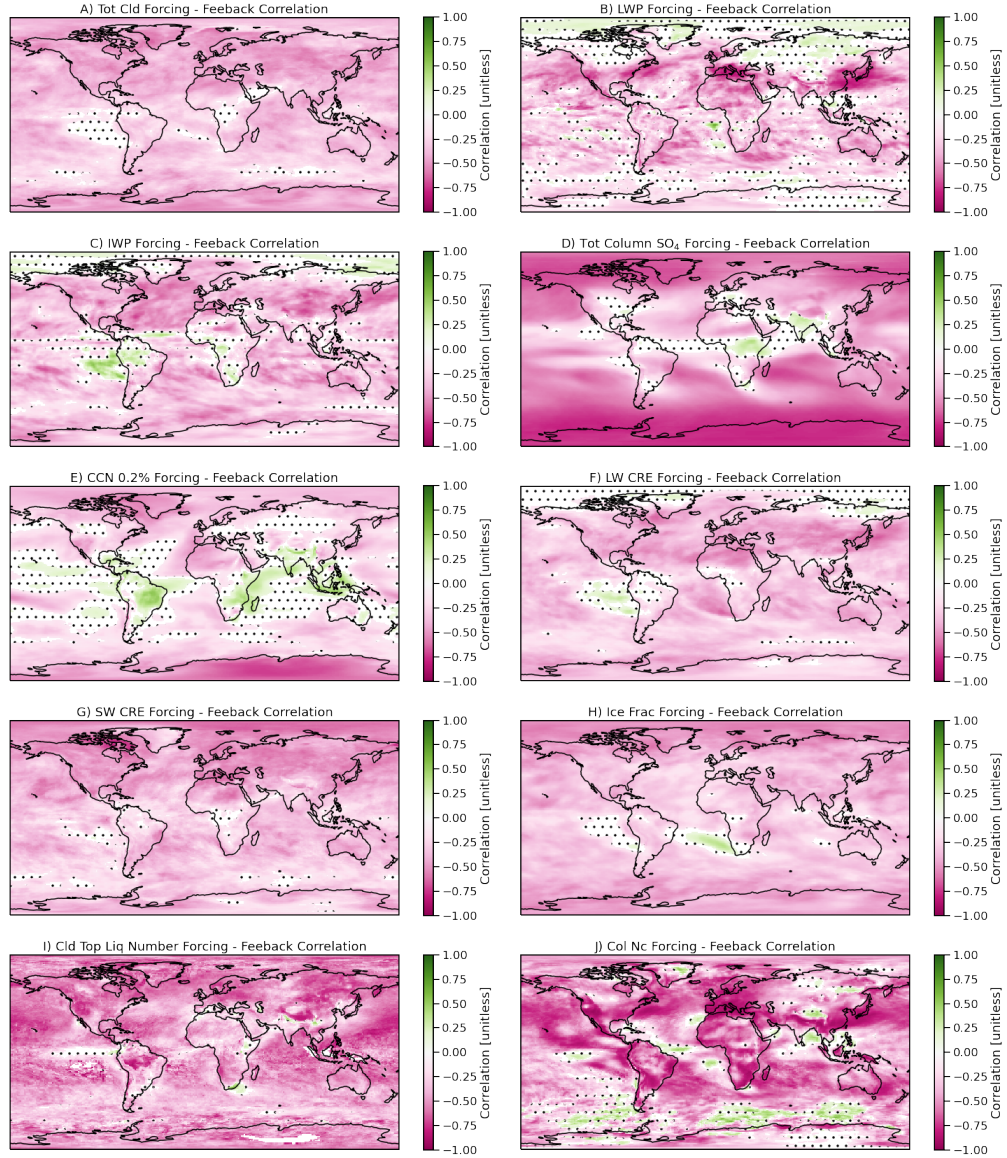


**Figure B1.** Map of linear correlation coefficient at each point between differences in variables due to forcing (PD-PI) and feedbacks (SST+4K - PD) for different variables. Non-significant points are stippled. Significance is determined by a bootstrap fit.

696 **Appendix B Supplementary Figures**

697 **Appendix C Open Research**

698 Model output used is described by Eidhammer et al. (2024), and is available  
699 the Climate Data Gateway at NCAR (<https://doi.org/10.26024/bzne-yf09>)

700 Analysis code used in this work is available on zenodo at  
701 <https://zenodo.org/doi/10.5281/zenodo.10553073>

702 **Acknowledgments**

703 NCAR is supported by the U. S. National Science Foundation. The Pacific North-  
704 west National Laboratory is operated for the U.S. Department of Energy by the  
705 Battelle Memorial Institute under contract DE-AC05-76RL01830.

706 **References**

- 707 Abdul-Razzak, H., & Ghan, S. J. (2002). A parameterization of aerosol activation 3.  
708 Sectional Representation. *J. Geophys. Res.*, *107*(D3), AAC 1-1 – AAC 1-6. doi: 10  
709 .1029/2001JD000483
- 710 Ackerman, A. S., Kirkpatrick, M. P., Stevens, D. E., & Toon, O. B. (2004). The im-  
711 pact of humidity above stratiform clouds on indirect aerosol climate forcing. *Na-  
712 ture*, *432*, 1014–1017.
- 713 Albrecht, B. A. (1989). Aerosols, Cloud Microphysics and Fractional Cloudiness.  
714 *Science*, *245*, 1227–1230. doi: 10.1126/science.245.4923.1227
- 715 Bellouin, N., Quaas, J., Gryspeerdt, E., Kinne, S., Stier, P., Watson-Parris,  
716 D., . . . Stevens, B. (2020). Bounding Global Aerosol Radiative Forcing  
717 of Climate Change. *Reviews of Geophysics*, *58*(1), e2019RG000660. doi:  
718 10.1029/2019RG000660
- 719 Carslaw, KS., Lee, LA., Reddington, CL., Pringle, KJ., Rap, A., Forster, PM., . . .  
720 others (2013). Large contribution of natural aerosols to uncertainty in indirect  
721 forcing. *Nature*, *503*(7474), 67–71. doi: 10.1038/nature12674
- 722 Cess, R. D., et al. (1989). Interpretation of Cloud-Climate Feedback as Produced by  
723 14 Atmospheric General Circulation Models. *Science*, *245*, 513–516.
- 724 Eidhammer, T., Gettelman, A., Thayer-Calder, K., Watson-Parris, D., Elsaesser, G.,  
725 Morrison, H., . . . McCoy, D. (2024, January). An Extensible Perturbed Parameter  
726 Ensemble (PPE) for the Community Atmosphere Model Version 6. *EGUsphere*,  
727 1–27. doi: 10.5194/egusphere-2023-2165
- 728 Forster, P. M., Andrews, T., Good, P., Gregory, J. M., Jackson, L. S., & Zelinka,  
729 M. (2013, February). Evaluating adjusted forcing and model spread for historical  
730 and future scenarios in the CMIP5 generation of climate models: FORCING IN  
731 CMIP5 CLIMATE MODELS. *Journal of Geophysical Research: Atmospheres*,  
732 *118*(3), 1139–1150. doi: 10.1002/jgrd.50174
- 733 Gettelman, A., Gagne, D. J., Chen, C.-C., Christensen, M. W., Lebo, Z. J., Mor-  
734 rison, H., & Gantos, G. (2021). Machine Learning the Warm Rain Process.  
735 *Journal of Advances in Modeling Earth Systems*, *13*(2), e2020MS002268. doi:  
736 10.1029/2020MS002268
- 737 Gettelman, A., Hannay, C., Bacmeister, J. T., Neale, R. B., Pendergrass, A. G.,  
738 Danabasoglu, G., . . . Mills, M. J. (2019). High Climate Sensitivity in the Com-  
739 munity Earth System Model Version 2 (CESM2). *Geophysical Research Letters*,  
740 *46*(14), 8329–8337. doi: 10.1029/2019GL083978
- 741 Gettelman, A., Lin, L., Medeiros, B., & Olson, J. (2016, June). Climate Feed-  
742 back Variance and the Interaction of Aerosol Forcing and Feedbacks. *J. Climate*,  
743 *29*(18), 6659–6675. doi: 10.1175/JCLI-D-16-0151.1

- 744 Gettelman, A., Morrison, H., Santos, S., Bogenschutz, P., & Caldwell, P. M. (2015).  
 745 Advanced Two-Moment Bulk Microphysics for Global Models. Part II: Global  
 746 Model Solutions and Aerosol–Cloud Interactions. *J. Climate*, *28*(3), 1288–1307.  
 747 doi: 10.1175/JCLI-D-14-00103.1
- 748 Gettelman, A., & Sherwood, S. C. (2016, October). Processes Responsible for Cloud  
 749 Feedback. *Curr Clim Change Rep*, 1–11. doi: 10.1007/s40641-016-0052-8
- 750 Golaz, J.-C., Larson, V. E., & Cotton, W. R. (2002). A PDF-Based Model for  
 751 Boundary Layer Clouds. Part II: Model Results. *J. Atmos. Sci.*, *59*, 3552–3571.
- 752 Guo, H., Golaz, J.-C., Donner, L. J., Wyman, B., Zhao, M., & Ginoux, P. (2015,  
 753 May). CLUBB as a unified cloud parameterization: Opportunities and challenges.  
 754 *Geophys. Res. Lett.*, 2015GL063672. doi: 10.1002/2015GL063672
- 755 Guo, Z., Wang, M., Qian, Y., Larson, V. E., Ghan, S., Ovchinnikov, M., . . . Zhou,  
 756 T. (2015, July). Parametric behaviors of CLUBB in simulations of low clouds in  
 757 the Community Atmosphere Model (CAM). *J. Adv. Model. Earth Syst.*, n/a-n/a.  
 758 doi: 10.1002/2014MS000405
- 759 Jing, X., Suzuki, K., & Michibata, T. (2019, July). The Key Role of Warm Rain  
 760 Parameterization in Determining the Aerosol Indirect Effect in a Global Climate  
 761 Model. *Journal of Climate*, *32*(14), 4409–4430. doi: 10.1175/JCLI-D-18-0789.1
- 762 Khairoutdinov, M. F., & Kogan, Y. (2000). A new cloud physics parameterization in  
 763 a large-eddy simulation model of marine stratocumulus. *Monthly Weather Review*,  
 764 *128*, 229–243.
- 765 Kiehl, J. T. (2007, November). Twentieth century climate model response  
 766 and climate sensitivity. *Geophys. Res. Lett.*, *34*(22), L22710. doi: 10.1029/  
 767 2007GL031383
- 768 Lee, L. A., Reddington, C. L., & Carslaw, K. S. (2016, May). On the relation-  
 769 ship between aerosol model uncertainty and radiative forcing uncertainty. *PNAS*,  
 770 *113*(21), 5820–5827. doi: 10.1073/pnas.1507050113
- 771 Loeb, N. G., Doelling, D. R., Wang, H., Su, W., Nguyen, C., Corbett, J. G., . . .  
 772 Kato, S. (2018). Clouds and the Earth’s Radiant Energy System (CERES) En-  
 773 ergy Balanced and Filled (EBAF) Top-of-Atmosphere (TOA) Edition-4.0 Data  
 774 Product. *J. Climate*, *31*(2), 895–918. doi: 10.1175/JCLI-D-17-0208.1
- 775 Qian, Y., Wan, H., Yang, B., Golaz, J.-C., Harrop, B., Hou, Z., . . . Zhang, K.  
 776 (2018). Parametric Sensitivity and Uncertainty Quantification in the Version 1  
 777 of E3SM Atmosphere Model Based on Short Perturbed Parameter Ensemble Sim-  
 778 ulations. *Journal of Geophysical Research: Atmospheres*, *123*(23), 13,046–13,073.  
 779 doi: 10.1029/2018JD028927
- 780 Regayre, L. A., Deaconu, L., Grosvenor, D. P., Sexton, D. M. H., Symonds,  
 781 C., Langton, T., . . . Carslaw, K. S. (2023, August). Identifying climate  
 782 model structural inconsistencies allows for tight constraint of aerosol radia-  
 783 tive forcing. *Atmospheric Chemistry and Physics*, *23*(15), 8749–8768. doi:  
 784 10.5194/acp-23-8749-2023
- 785 Sherwood, S., Webb, M. J., Annan, J. D., Armour, K. C., Forster, P. M., Har-  
 786 greaves, J. C., . . . Zelinka, M. D. (2020). An assessment of Earth’s climate  
 787 sensitivity using multiple lines of evidence. *Reviews of Geophysics*, *58*(n/a),  
 788 e2019RG000678. doi: 10.1029/2019RG000678
- 789 Sherwood, S. C., Bony, S., & Dufresne, J.-L. (2014, January). Spread in model cli-  
 790 mate sensitivity traced to atmospheric convective mixing. *Nature*, *505*(7481), 37–  
 791 42. doi: 10.1038/nature12829
- 792 Smith, C. J., Kramer, R. J., Myhre, G., Alterskjær, K., Collins, W., Sima, A., . . .  
 793 Forster, P. M. (2020, January). Effective radiative forcing and adjustments in  
 794 CMIP6 models. *Atmospheric Chemistry and Physics Discussions*, 1–37. doi:  
 795 10.5194/acp-2019-1212
- 796 Soden, B. J., Held, I. M., Colman, R., Shell, K. M., Kiehl, J. T., & Shields, C. A.  
 797 (2008). Quantifying Climate Feedbacks Using Radiative Kernels. *J. Climate*,

- 798 21(14), 3504–3520. doi: 10.1175/2007JCLI2110.1
- 799 Summary for Policymakers. (2021). In Intergovernmental Panel on Climate Change  
800 (IPCC) (Ed.), *Climate Change 2021 – The Physical Science Basis: Working*  
801 *Group I Contribution to the Sixth Assessment Report of the Intergovernmental*  
802 *Panel on Climate Change* (pp. 3–32). Cambridge: Cambridge University Press.  
803 doi: 10.1017/9781009157896.001
- 804 Twomey, S. (1974). Pollution and the planetary albedo. *Atmospheric Environment*  
805 (1967), 8(12), 1251–1256.
- 806 Watson-Parris, D., & Smith, C. J. (2022, December). Large uncertainty in future  
807 warming due to aerosol forcing. *Nat. Clim. Chang.*, 12(12), 1111–1113. doi: 10  
808 .1038/s41558-022-01516-0
- 809 Watson-Parris, D., Williams, A., Deaconu, L., & Stier, P. (2021, December). Model  
810 calibration using ESEm v1.1.0 – an open, scalable Earth system emulator. *Geosci-*  
811 *entific Model Development*, 14(12), 7659–7672. doi: 10.5194/gmd-14-7659-2021
- 812 Zelinka, M., Klein, S., & Hartmann, D. (2012). Computing and partitioning cloud  
813 feedbacks using cloud property histograms. Part I: Cloud radiative kernels. *J. Cli-*  
814 *mate*, 25(11), 3715–3735.
- 815 Zhang, G. J., & McFarlane, N. A. (1995). Sensitivity of climate simulations to the  
816 parameterization of cumulus convection in the Canadian Climate Center general  
817 circulation model. *Atmos. Ocean*, 33, 407–446.
- 818 Zhang, H., Wang, M., Guo, Z., Zhou, C., Zhou, T., Qian, Y., . . . Gettelman, A.  
819 (2018). Low-Cloud Feedback in CAM5-CLUBB: Physical Mechanisms and Param-  
820 eter Sensitivity Analysis. *Journal of Advances in Modeling Earth Systems*, 10(11),  
821 2844–2864. doi: 10.1029/2018MS001423